Characterisation of *why1*-complemented variants and generation of *why2* mutants in barley

Inaugural dissertation

for attaining the title of Doctor (Dr. rer. nat.)

in the Faculty of Mathematics and Natural Sciences

at Heinrich Heine University Düsseldorf

submitted by

Entela Malkaj

from Mamurras, Albania

Düsseldorf, April 2026

from the Institute of Plant Biochemistry

at the Heinrich Heine University Düsseldorf

Printed with the permission of the

Faculty of Mathematics and Natural Sciences at

Heinrich Heine University Düsseldorf

Reviewers:

1. Prof. Dr. Andreas P. M. Weber
2. Prof. Dr. Karin Krupinska

Date of the oral examination: 06.07.2026

Statutory declaration

I hereby declare that I have written this dissertation independently and without unauthorized help in compliance with the principles of ”Good Research Practice”. The dissertation in its present or similar form has not been previously submitted under the same or otherwise specified institution and department name. Previous unsuccessful oral examinations have not been registered or attempted.

Düsseldorf, 28.04.2026

Entela Malkaj

”And then the day came,

when the risk

to remain tight

in a bud

was more painful

than the risk

it took

to blossom.”

—Anaïs Nin

Table of Contents

Abbreviations

ABA	abscisic acid
Amp^R	ampicillin resistance
ANAC	Arabidopsis NAM, ATAF1/2, and CUC2 transcription factor family
AOX1a	alternative oxidase 1a
APX	ascorbate peroxidase
atpF	ATP synthase subunit b
BBCH	Biologische Bundesanstalt, Bundessortenamt und Chemische Industrie
Cas9	CRISPR-associated protein 9
CAT	catalase
CCD5	carotenoid cleavage dioxygenase 5
CCD8	carotenoid cleavage dioxygenase 8
cDNA	complementary DNA
CIPK14	calcineurin B-like-interacting protein kinase 14
CLD	Compact Letter Display
CRE1/AHK4	cytokinin response 1 / Arabidopsis histidine kinase 4
CRISPR	Clustered Regularly Interspaced Short Palindromic Repeats
DAS	days after sowing
DBM	DNA-binding motif
ED	euclidean distance
EDTA	ethylenediaminetetraacetic acid
ERE	elicitor-response element
F_0	minimum fluorescence
FER1	FERRITIN 1
F_M	maximum fluorescence yield
F_V	variable fluorescence
F_V/F_M	maximum quantum efficiency of photosystem II
GA	gibberellin
GP	barley cultivar ‘Golden Promise’
gRNA	guide RNA
HA	haemagglutinin
hai	hours after inoculation/infection

hpt	hygromycin phosphotransferase
HRP	horseradish peroxidase
IgG	immunoglobulin g
LB	Luria-Bertani, Miller formulation
Lr67	Leaf rust resistance 67
M_0	primary transformed mutant plant
M_1	first generation mutant progeny
MAS	months after sowing
mtDNA	mitochondrial DNA
NCED1	9-cis-epoxycarotenoid dioxygenase 1
NEP	nuclear-encoded RNA polymerase
NMD	nonsense-mediated decay
NPR1	nonexpressor of pathogenesis-related genes 1
OTP	organelle transit peptide
PAM	protospacer-adjacent motif
PAP	3′-phosphoadenosine 5′-phosphate
PBF-2	pathogenesis-related-10a binding factor 2
PEP	plastid-encoded RNA polymerase
POP	plastid DNA polymerase
PR-10a	pathogenesis-related protein 10a
PSI	photosystem I
PSII	photosystem II
pTAC	plastid transcriptionally active chromosome
PTP	plastid transit peptide
pvAD	putative activation domain
pvCBM	putative copper-binding motif
pvNLS	putative nuclear localisation signal
RbcL	ribulose-1,5-bisphosphate carboxylase/oxygenase large subunit
RECA2	recombination protein A 2
RMSE	root mean square error
RNAi	RNA interference
RNAi-W1	RNA interference-mediated knockdown of WHIRLY1
ROS	reactive oxygen species
RuBisCo	ribulose-1,5-bisphosphate carboxylase/oxygenase
S40	senescence-associated gene 40

SA	salicylic acid
SDS	sodium dodecyl sulfate
SDS-PAGE	sodium dodecyl sulfate–polyacrylamide gel electrophoresis
SOC	super optimal broth with catabolite repression
SOD	superoxide dismutase
$Spec^R/Sm^R$	spectinomycin/streptomycin resistance
ssDNA	single-stranded DNA
Stp13	SUGAR TRANSPORT PROTEIN 13
SWC	soil water content
SWEET	SUGARS WILL EVENTUALLY BE EXPORTED TRANSPORTER
T_0	primary transgenic generation
T_1	first transgenic progeny generation
T_2	second transgenic progeny generation
T_3	third transgenic progeny generation
TBE	Tris-borate-EDTA buffer
TIDE	Tracking of Indels by DEcomposition
WAS	weeks after sowing
WT	wild type

Summary

The development and productivity of plants depend on integrating environmental cues with endogenous regulatory programmes. This integration is particularly critical in crops because abiotic and biotic stresses affect growth and yield by interfering with the functionality of energy producing organelles, i.e. mitochondria and chloroplasts. Chloroplasts and mitochondria play central roles in plants' responses to stress through retrograde signalling pathways that adjust nuclear transcription in response to organelle function. In addition to metabolite- and redox-based signals, proteins localised in organelles and the nucleus such as WHIRLY1 may act as mobile signalling components, that connect organelles and the nucleus. Transgenic barley plants with altered levels of WHIRLY1 are affected in chloroplast development, stress responses and defence signalling. For comparison, the roles of WHIRLY2 which is targeted to mitochondria remained unknown so far.

This study addresses the question, which of the multiple conserved motifs and amino acid residues of WHIRLY1 contribute to its roles in development and stress responses. Homozygous barley lines expressing WHIRLY1 variants with mutations in specific motifs and amino acid residues with proposed roles in DNA binding and redox regulation were generated. In addition, the plastid targeting peptide sequence was removed in one variant. Homozygous complemented lines were characterised under controlled light and temperature conditions, as well as under drought stress and infection with powdery mildew (*Blumeria graminis* f. sp. *hordei*). Loss of the plastid targeting peptide produced the most consistent phenotypic effects. During drought stress, plants lacking plastid-targeted WHIRLY1 exhibited a delayed decline in PSII efficiency and chlorophyll content compared with other variants and the wild type. After inoculation with powdery mildew, these plants had the highest leaf infection. These results indicate that the presence of WHIRLY1 in chloroplasts is required for appropriate responses to stress.

To functionally characterize WHIRLY2, CRISPR/Cas9 was used to generate *WHIRLY2* knockout mutants (*why2*) in the barley cultivar 'Golden Promise'. Homozygous mutants of *WHIRLY2* with a complete disruption of the gene were not obtained suggesting that complete loss of WHIRLY2 function may compromise the viability of barley plants.

Zusammenfassung

Die Entwicklung und Produktivität von Pflanzen hängt von der Integration von Umweltsignalen mit endogenen Regulationsprogrammen ab. Diese Integration ist bei Nutzpflanzen besonders wichtig, da abiotische und biotische Stressfaktoren das Wachstum und den Ertrag beeinträchtigen, indem sie die Funktionalität der energieproduzierenden Organellen, d. h. Mitochondrien und Chloroplasten, beeinträchtigen. Chloroplasten und Mitochondrien spielen eine zentrale Rolle bei der Stressreaktion von Pflanzen durch retrograde Signalwege, die die Transkription im Zellkern als Reaktion auf die Organellenfunktion regulieren. Zusätzlich zu metaboliten- und redoxbasierten Signalen können Proteine, die in Organellen und im Zellkern lokalisiert sind, wie z. B. WHIRLY1, als mobile Überträger von Organellensignalen an den Zellkern fungieren. Transgene Gerstenpflanzen mit veränderten Mengen an WHIRLY1 zeigen Veränderungen in der Chloroplastenentwicklung sowie in der Reaktion und Resilienz gegenüber Stress. Im Unterschied zu WHIRLY1 ist die Rolle von WHIRLY2, das in Mitochondrien importiert wird, noch unbekannt.

Diese Arbeit befasst sich mit dem Beitrag einzelner konservierter Motive und Aminosäurereste von WHIRLY1 auf dessen Einfluss auf die Chloroplastenentwicklung und das Verhalten gegenüber Stress. Es wurden homozygote Gerstenlinien erzeugt, die WHIRLY1-Varianten mit Mutationen in bestimmten Motiven und Aminosäureresten exprimieren, denen eine Rolle bei der DNA-Bindung und der Redoxregulation zugeschrieben wird. Darüber hinaus wurde bei einer Variante die Peptidsequenz entfernt, die für den Import in die Plastiden benötigt wird. Die homozygoten komplementierten Linien wurden unter kontrollierten Licht- und Temperaturbedingungen sowie unter Trockenstress und Infektion mit Mehltau (*Blumeria graminis* f. sp. *hordei*) charakterisiert. Der Verlust des Plastiden-Targeting-Peptids führte zu den schlüssigsten phänotypischen Effekten. Während Trockenstress zeigten Pflanzen ohne Plastiden-Targeting-Peptid vor dem WHIRLY1-Protein im Vergleich zu anderen Varianten und dem Wildtyp einen verzögerten Rückgang der PSII-Effizienz und des Chlorophyllgehalts. Nach Inokulation mit Mehltau wiesen diese Pflanzen die stärkte Infektionsrate auf. Diese Ergebnisse deuten darauf hin, dass das Vorhandensein von WHIRLY1 in Chloroplasten für eine angemessene Stressreaktion erforderlich ist.

Um WHIRLY2 funktionell zu charakterisieren, wurden mit CRISPR/Cas9 *WHIRLY2*-

Knockout-Mutanten (*why2*) in der Gerstensorte ‚Golden Promise'. erzeugt. Da keine homozygoten *WHIRLY2*- Mutanten von mit einer vollständigen Unterbrechung des Gens erhalten wurden, scheint ein vollständiger Verlust des WHIRLY2-Proteins bei Gerste auch zu einem Verlust der Lebensfähigkeit zu führen.

1 Introduction

1.1 Plant development and environment

Plant growth and performance are strongly influenced by environmental conditions that directly affect photosynthesis and chloroplast functions. Light, temperature, water availability, nutrient supply, and photoperiod determine carbon assimilation rates, thereby constraining biomass production and yield (Jarvis & Lopez-Juez, 2013; Lynch, 2022). As sessile organisms, plants must continuously adjust chloroplast activity and photosynthetic metabolism to fluctuating environmental conditions to sustain growth (Franklin, 2009).

Among these fluctuating conditions, light is the primary driver of chloroplast function, providing the energy required for photosynthetic electron transport and carbon fixation. Light availability regulates chlorophyll accumulation, photosynthetic protein abundance and thylakoid organisation, which together determine photosynthetic capacity (Pogson et al., 2015; Johnson & Wientjes, 2020). Temperature further modulates photosynthesis by affecting enzyme kinetics, membrane fluidity, and the stability of the photosynthetic apparatus. Both heat and chilling impair chloroplast performance outside the optimal range (Dusenge et al., 2019; Shi et al., 2022). Water and nutrient availability influence photosynthetic efficiency by limiting CO_2 uptake, electron transport, and metabolic fluxes, and therefore restrict carbon assimilation and biomass production (Lopez-Bucio et al., 2003; Lynch, 2022).

1.2 Chloroplast development and photosynthesis

Chloroplasts define the metabolic capacity of photosynthetic tissues by linking light energy conversion to carbon metabolism. Through the light reactions in the thylakoid membrane, photosynthetic electron transport generates ATP and NADPH that drive CO_2 fixation in the chloroplast stroma. The products of photosynthesis are subsequently channelled into central metabolic pathways, which provide carbon skeletons and reducing power required for nitrogen and sulphur assimilation, lipid and amino acid biosynthesis, and the formation of precursors for hormones and secondary metabolites (Jarvis & Lopez-Juez, 2013; Pogson et al., 2015). As a result, the establishment of functional

chloroplasts represents a critical developmental transition, that enable plant tissues to move from reliance on stored reserves to sustained photoautotrophic metabolism that supports growth, differentiation and environmental responsiveness (Dubreuil et al., 2018).

The acquisition of this metabolic capacity depends on a tightly regulated programme of chloroplast differentiation. In photosynthetic tissues, chloroplasts develop from undifferentiated proplastids through coordinated processes that include thylakoid membrane formation, pigment biosynthesis and the stepwise assembly of photosynthetic protein complexes (Waters & Langdale, 2009; Jarvis & Lopez-Juez, 2013). Chloroplast biogenesis proceeds sequentially, with structural components of the thylakoid system and core photosynthetic complexes forming before full photosynthetic efficiency is achieved. This staged progression is evident during de-etiolation, where light exposure triggers rapid thylakoid development and photosystem assembly, while optimisation of photosynthetic performance occurs later as chloroplast maturation and metabolic integration continue (Pipitone et al., 2021).

The photosynthetic apparatus is assembled through a highly coordinated biogenetic process, during which multi-subunit protein complexes are progressively integrated into the thylakoid membrane. Photosystem I (PSI) and photosystem II (PSII), the cytochrome b_6f complex, and ATP synthase comprise both plastid- and nuclear-encoded subunits, the synthesis, import, and membrane insertion of which must be precisely synchronised during chloroplast development (Waters & Langdale, 2009). Assembly proceeds in a stepwise manner. It begins with the formation of reaction-centre cores, followed by the incorporation of antenna proteins, cofactors and electron carriers. This establishes a functional photosynthetic electron-transport chain within the developing thylakoid network (Pipitone et al., 2021). The process is dependent on precise coordination between chloroplast gene expression, nuclear control and thylakoid organisation (Waters & Langdale, 2009; Pipitone et al., 2021). Disruption at any stage of this process, whether in protein synthesis, membrane biogenesis or complex assembly, compromises photosynthetic functionality.

Chloroplast development and photosynthetic function are regulated by environmental conditions, where light acts as a primary external signal. Other than serving as the energy source for photosynthesis, light controls chloroplast biogenesis by regulating the

expression and accumulation of photosynthetic proteins and pigments, and influencing thylakoid formation and photosystem assembly (Waters & Langdale, 2009; Pogson et al., 2015). Alterations in light intensity or quality therefore lead to adjustments in photosynthetic performance and are accompanied by changes in chloroplast structure, redox state and metabolic activity, all of which reflect the dynamic acclimation of chloroplasts to their prevailing light environment (Taylor et al., 2022).

Because photosynthetic electron transport is inherently light dependent, fluctuations in photosynthetic activity not only alter photosynthetic performance but also have direct consequences for the redox state of the chloroplast. When the capacity for carbon assimilation does not match the rate of light-driven electron flow, excess reducing power accumulates within the photosynthetic electron transport chain, and leads to perturbations in chloroplast redox balance and enhanced production of reactive oxygen species (ROS; Pogson et al., 2015; Taylor et al., 2022. Such redox imbalances are a common feature of chloroplasts exposed to non-optimal environmental conditions and are closely associated with changes in chloroplast function and acclimation responses.

The establishment and long-term maintenance of photosynthetic competence depend on tightly coordinated gene expression between the nuclear and plastid genomes. Most proteins required for chloroplast structure, thylakoid organisation and photosynthetic activity are encoded in the nucleus, synthesised in the cytosol, and afterward imported into the organelle (Jarvis & Lopez-Juez, 2013). At the same time, plastid gene expression remains indispensable, since the plastid genome encodes core subunits of the photosynthetic complexes as well as components of the plastid transcription and translation machinery required for chloroplast protein synthesis (Pogson et al., 2015; Zhang et al., 2023).

1.3 The plastid genome and nucleoids

Chloroplasts contain their own genome that originated from the cyanobacterial ancestor of plastids. The plastid genome encodes a limited but essential set of gene products, primarily core subunits of the photosynthetic complexes, which are indispensable for photosynthetic electron transport and energy conversion. It also encodes ribosomal RNAs, transfer RNAs, and a small number of proteins required for plastid gene expression and organelle maintenance (Bock, 2007; Stern et al., 2010). Despite its strongly

reduced gene content, plastid gene expression is essential for the establishment and maintenance of photosynthetic competence, process which necessitates precise coordination with nuclear gene expression (Woodson & Chory, 2008).

Plastid DNA is not uniformly distributed within the organelle but is organised into discrete nucleoprotein structures called nucleoids. Plastid nucleoids consist of plastid DNA associated with RNA and a diverse set of proteins involved in DNA organisation, transcription, RNA processing, and translation (Pfalz et al., 2006; Yu et al., 2014). These structures are partly analogous to bacterial nucleoids but display distinct features that reflect the integration of plastid gene expression into the eukaryotic cellular context (Sato, 2001).

The composition and organisation of plastid nucleoids are dynamic and can vary between plastids with different functional states. Proteomic analyses have shown that nucleoid-associated protein composition differs with changes in transcriptional and translational activity, including proteins involved in RNA metabolism and ribosome biogenesis (Majeran et al., 2012).

Expression of the plastid genome relies on two transcription systems: the plastid-encoded RNA polymerase (PEP), which primarily transcribes photosynthesis-related genes, and the nuclear-encoded RNA polymerase (NEP), which contributes mainly to the expression of housekeeping genes and early plastid transcription (Stern et al., 2010; Yu et al., 2014). Following transcription, plastid RNAs undergo extensive post-transcriptional processing, such as RNA editing, splicing, and maturation, before being translated by plastid ribosomes (Barkan, 2011). Efficient plastid protein synthesis is therefore dependent on the coordinated function of nucleoid-associated processes.

Although plastids retain their own genome, the majority of proteins required for plastid gene expression, nucleoid organisation, and chloroplast function are encoded in the nuclear genome and imported into the organelle after cytosolic synthesis. This requires precise coordination between nuclear and plastid gene expression to ensure proper stoichiometry of protein complexes and functional integration of plastid-encoded and nuclear-encoded components (Jarvis & Lopez-Juez, 2013; Richardson & Schnell, 2020).

1.4 Environmental challenges affecting chloroplast function

Chloroplasts act as sensors of environmental change (Pfannschmidt et al., 2020). The light reactions in the thylakoid membranes are functionally linked to the dark (carbon fixation) reactions in the stroma. Photosynthesis depends on maintaining a balance between these processes under changes in CO_2 levels, temperature, light, and water availability (Pfannschmidt et al., 2020). Environmental fluctuations that disturb this balance can change photosynthetic electron flux and the redox state of the photosynthetic components, which can act as plastid-derived signals during acclimation (Pfalz et al., 2012).

Drought can constrain photosynthesis by limiting CO_2 availability through stomatal closure, the earliest drought response and one of the main limiting factors of photosynthesis under mild to moderate drought conditions (Flexas & Medrano, 2002). Drought also affects chloroplast metabolism and can cause oxidative stress when combined with additional abiotic stress factors (Chaves et al., 2009). Reduced CO_2 availability and carbon fixation can promote imbalances in photosynthetic electron transport and accumulation of ROS in chloroplasts (Pfannschmidt et al., 2020).

Temperature stress affects chloroplast performance and the effects depend on whether temperatures exceed or fall below the physiological optimum (Dusenge et al., 2019). High temperatures destabilise thylakoid membranes and impair PSII function, leading to reduction of photosynthetic efficiency (Shi et al., 2022). Low temperatures slow enzymatic reactions and reduce metabolic rates, thus increasing susceptibility to photoinhibition even under moderate light conditions (Shi et al., 2022).

Atmospheric CO_2 is consumed in stromal carbon reactions, therefore changes in CO_2 levels affect the balance between light-driven electron transport and carbon assimilation (Pfannschmidt et al., 2020). High CO_2 levels can partially alleviate photosynthetic limitations by stimulating carbon assimilation and reducing photorespiration (Dusenge et al., 2019). However, they can also affect the respiratory metabolism and daytime carbon gain, particularly under stress conditions, which indicate complex interactions between CO_2 availability and other environmental factors (Bunce, 2021; Burgess, 2023).

Light stress occurs when the amount of absorbed light exceeds the capacity of the photosynthetic machinery to use it (Pfannschmidt et al., 2020). This excess excitation energy disturbs the balance between the light-capturing and carbon-fixing reactions of the chloroplast, alters electron flow and the internal redox state, and can generate ROS

that are potentially damaging to the cell (Pfannschmidt et al., 2020). Under prolonged or excessive light, these effects increase the risk of photoinhibition, especially at PSII (Sharma et al., 2023; Didaran et al., 2024). These light-induced changes also contribute to plastid-derived signalling that allows the chloroplast to communicate stress to the rest of the cell during acclimation (Pfannschmidt et al., 2020; Foyer & Hanke, 2022).

Chloroplast function is highly sensitive to environmental stress (Pfannschmidt et al., 2020). Drought, temperature extremes, and changes in CO_2 availability disturb electron transport, carbon assimilation, and redox balance, thereby limiting photosynthetic performance (Flexas & Medrano, 2002; Chaves et al., 2009; Dusenge et al., 2019). The combined effects of these stresses position chloroplasts as the main determinants of plant physiological responses to changing environmental conditions (Dusenge et al., 2019).

1.5 Communication between organelles and nucleus

Because environmental stress has a significant impact on chloroplast performance, there is a need for mechanisms that can communicate changes in the functional state of organelles to the nucleus. This enables a coordinated response in gene expression (Pfannschmidt et al., 2020). Anterograde pathways direct organelle biogenesis through nuclear encoded factors, whereas retrograde signalling from the chloroplasts and mitochondria enables plants to adjust nuclear transcription according to the functional state of these organelles (Chan et al., 2016; Pfannschmidt et al., 2020).

Mitochondrial retrograde regulation communicates the energetic and redox status of the organelle to the nucleus (Pfannschmidt et al., 2020). Arabidopsis NAM, ATAF1/2, and CUC2 (ANAC) transcription factors act as key regulators. Upon mitochondrial dysfunction, they translocate to the nucleus and activate mitochondrial dysfunction stimulon genes such as Alternative oxidase 1a (*AOX1a*; De Clercq et al., 2013; Ng et al., 2013. Mitochondrial retrograde signalling interacts with chloroplast-derived pathways, and together they shape nuclear responses to metabolic and environmental stress (Wang et al., 2020).

Chloroplasts play a dominant role in stress-responsive retrograde signalling. During chloroplast development, biogenic signals report the progress of plastid differentiation to the nucleus (Woodson et al., 2011). Under environmental stress, operational retrograde pathways modify nuclear gene expression to maintain chloroplast performance

(Estavillo et al., 2011; Crawford et al., 2018). These include 3'-phosphoadenosine 5'-phosphate (PAP) signalling under drought and high light (Estavillo et al., 2011), singlet-oxygen pathways mediated by EXECUTER1 and EXECUTER2 (Lee et al., 2007; Wang et al., 2016; Dogra et al., 2019; Li et al., 2023), redox-dependent responses of the photosynthetic electron transport chain (Pfannschmidt et al., 2020) and chloroplast proteostasis pathways that detect misfolded or mistargeted proteins and activate a chloroplast-specific unfolded protein response (Llamas & Pulido, 2022; Jeran et al., 2025). Collectively, these pathways link photosynthetic performance to nuclear gene expression and whole-plant acclimatisation (Dietz et al., 2016; Foyer & Hanke, 2022).

Although considerable progress has been made, many primary signals involved in operational retrograde signalling remain unidentified. In addition to metabolite-, redox- and ROS-based signals, growing evidence suggests that certain dual-localised proteins may also contribute to retrograde communication by relaying information about the organelle functional status to the nucleus (Krause et al., 2012; Krupinska et al., 2020; Pfannschmidt et al., 2020).

1.6 The WHIRLY protein family

WHIRLY1 represents a plastid-derived protein that has been involved in plastid-to-nucleus retrograde signalling and belongs to a conserved family of WHIRLY proteins in plants. Members of the WHIRLY family are present in higher plants and represent a versatile group of single-stranded nucleic acid-binding proteins whose functions vary depending on the cellular context and species (Krupinska et al., 2022; Taylor et al., 2022). Comparative genomic analyses show that most angiosperms encode two WHIRLY genes (Desveaux et al., 2005). In dicots, examples include both species with the typical two WHIRLY genes and species that encode more than two. For example, *Arabidopsis thaliana* has three WHIRLY genes (Desveaux et al., 2002; Desveaux et al., 2004; Krause et al., 2005), whereas *Solanum lycopersicum* (tomato) contains two, *WHIRLY1* and *WHIRLY2* (Akbudak & Filiz, 2019). Some dicots possess more than three WHIRLY genes. For instance, *Fragaria* spp. (strawberry) carries up to five WHIRLY genes (Hu & Shu, 2021), and the allotetraploid *Brassica napus* carries six (Wang et al., 2024). In contrast, the genomes of monocots generally encode only two proteins. Major cereals such as Triticeae (Liu et al., 2023) and *Zea mays* (maize; Prikryl et al., 2008) each encode

the WHIRLY1 and *WHIRLY2* proteins. The unicellular green alga *Chlamydomonas reinhardtii* (accession no. TC35855) also has a homologue which suggests that the family originated before the divergence of green algae and land plants (Desveaux et al., 2005).

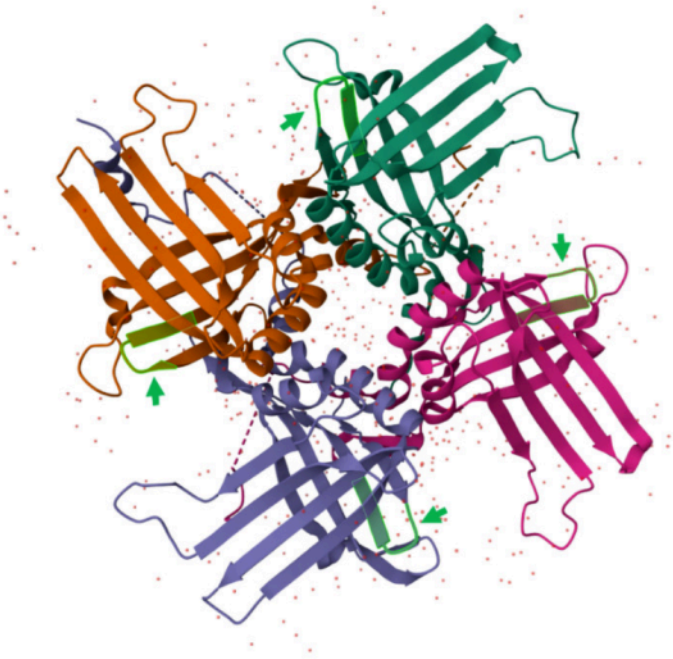

Figure 1. Crystal structure of the WHIRLY1 tetramer from potato (*Solanum tuberosum*). Each protomer is shown in a distinct colour: chain A, green; chain B, orange; chain C, lilac; and chain D, magenta. The four KGKAAL motifs, corresponding to the DNA-binding motif of WHIRLY1, are indicated by green arrows in each subunit. Structural coordinates were obtained from the RCSB Protein Data Bank (PDB ID: 1L3A), initially deposited by Desveaux et al. (2002).

The first WHIRLY protein to be identified was WHIRLY1. It was initially discovered in the nuclei of potato tubers as the 24 kDa p24 subunit of the pathogenesis-related-10a (PR-10a) binding factor 2 (PBF-2) complex, which binds the elicitor-response element (ERE) of the *PR-10a* promoter (Desveaux et al., 2000). Sequencing peptide fragments enabled the corresponding gene to be isolated. This revealed a conserved protein containing a polyglutamine-rich region typical of transcriptional activators (Desveaux et al., 2000). Structural analysis later resolved the p24 protein at 2.3 Å, showing a tetrameric assembly formed by a helix-loop-helix interface and a curved β-sheet surface that creates the characteristic WHIRLY fold (Figure 1). Gel-filtration assays demonstrated that one tetramer binds a single molecule of DNA (Desveaux et al., 2002), whereas mutational analyses identified the conserved KGKAAL motif as essential for single-stranded DNA (ssDNA) binding (Desveaux et al., 2002; Cappadocia et al., 2012). This WHIRLY domain represents the most conserved structural element of the WHIRLY family and

shows no homology to DNA-binding proteins from other kingdoms (Desveaux et al., 2005). This absence of homology suggests a unique mechanism for recognising single-stranded nucleic acids in a sequence-independent manner.

The functional importance of conserved motifs is best illustrated by the KGKAAL sequence, where research in potato and Arabidopsis has associated specific residues to higher-order assembly and genome protection. The conserved lysine (K67) within the KGKAAL DNA-binding motif (DBM) of the potato mitochondrial WHIRLY2 is essential for higher-order assembly and genome protection. WHIRLY2 tetramers assemble into 24-mers on long ssDNA via inter-tetramer interactions involving K67. Substituting this residue with alanine (K67A) abolishes 24-mer formation and cooperative binding to long ssDNA without affecting tetramer structure or binding to short ssDNA (Cappadocia et al., 2012). In Arabidopsis, mutation of the corresponding lysine (K91) in WHIRLY1 fails to rescue the DNA-damage sensitivity of *why1 why3* mutants exposed to ciprofloxacin, despite normal protein accumulation and ssDNA binding (Cappadocia et al., 2012). These findings indicate that conserved lysine-dependent oligomerisation is crucial for genome protection.

The molecular versatility of WHIRLY proteins arises from their ability to bind to ssDNA in a non-sequence-specific manner, which enables interactions with a wide range of nucleic-acid substrates. Structural modelling indicates that RNA can adopt a DNA-like conformation within the WHIRLY binding pocket, explaining the capacity of WHIRLY proteins to bind both DNA and RNA (Cappadocia et al., 2010). RNA binding is generally weaker, consistent with observations that WHIRLY proteins associate broadly with DNA but only with specific RNA subsets *in vivo* (Prikryl et al., 2008).

1.6.1 WHIRLY1

The dual-localised WHIRLY1 protein is processed in chloroplasts and later detected in the nucleus, where it modulates transcription in response to organelle status (Krupinska et al., 2020). This dual localisation led to the proposal that WHIRLY1 participates in chloroplast-to-nucleus retrograde signalling (Krause & Krupinska, 2009; Foyer et al., 2014; Krupinska et al., 2020). Among the proposed retrograde signalling mechanisms, WHIRLY1 has received particular attention because of its dual localisation and its hypothesised redox-responsive behaviour. It is suggested that WHIRLY1 oligomers dis-

sociate into monomers under chloroplast redox perturbation. They, then translocate to the nucleus and activate stress-responsive genes (Figure 2; Foyer et al., 2014). Although this model remains hypothetical and has not been experimentally validated in barley, it provides a conceptual framework for investigating which conserved WHIRLY1 motifs or amino acid residues may contribute to stress-dependent signalling.

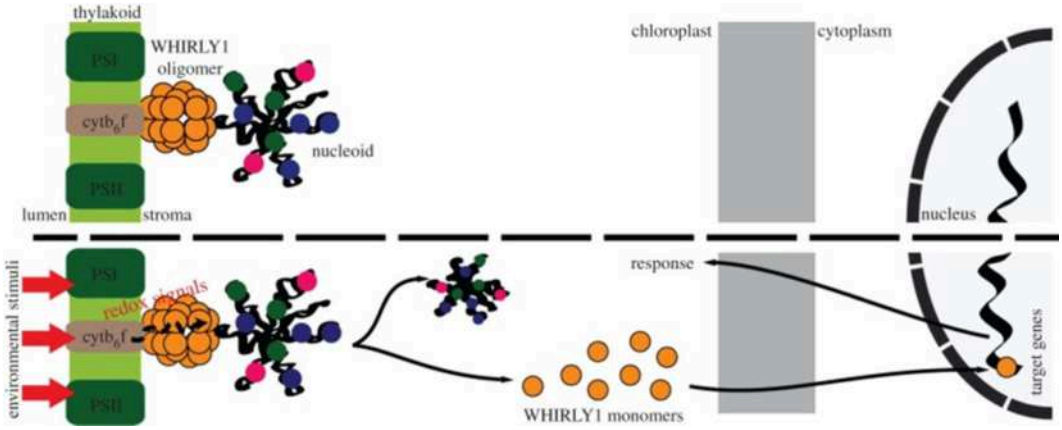

Figure 2. Schematic representation of WHIRLY1-dependent retrograde signalling from the chloroplast to the nucleus. Under normal conditions, WHIRLY1 forms 24-mer oligomers that bridge the thylakoid membranes and the chloroplast nucleoid. Environmental stimuli that alter the redox state of the photosynthetic apparatus trigger the monomerization of WHIRLY1. The monomers subsequently translocate to the nucleus, where they modulate nuclear gene expression. Reproduced from Foyer et al. (2014).

WHIRLY1 also fulfils well-characterised functions in the nucleus. In Arabidopsis, WHIRLY1 contributes to telomere-length homeostasis by inhibiting telomerase activity. Loss of WHIRLY1 results in progressive telomere elongation despite normal development (Yoo et al., 2007). In addition, WHIRLY1 in Arabidopsis enhances salicylic-acid (SA)–mediated immune responses through a pathway parallel to the nonexpressor of pathogenesis-related genes 1 (NPR1)-dependent signalling (Desveaux et al., 2004; Desveaux et al., 2005). Although Arabidopsis *why1* mutants show no visible developmental phenotypes, WHIRLY1 influences the expression of biotic- and abiotic-stress-responsive genes during early development (Nguyen, 2023). It also modulates the alternative splicing of numerous transcripts, particularly under oxidative stress (Nguyen, 2023). WHIRLY1 therefore functions as both a transcriptional and post-transcriptional regulator.

In plastids, WHIRLY1 has been shown to participate in RNA-related processes. In maize, WHIRLY1 localises to both the chloroplast stroma and thylakoid membranes, where it binds DNA and RNA and is required for proper RNA splicing and ribosome

assembly, though not for DNA replication or general transcription (Prikryl et al., 2008). Consistent with a close association with plastid gene expression machinery, proteomic analyses of plastid transcriptionally active chromosomes (pTAC) identified pTAC1 as a homolog of p24 subunit of PBF-2 (Pfalz et al., 2006). Later, pTAC1 was confirmed to correspond to WHIRLY1 (Grabowski et al., 2008). In Arabidopsis, WHIRLY1 and WHIRLY3 further contribute to plastid genome stability by preventing illegitimate recombination between short direct repeats. This is shown by the variegated leaves and rearranged plastid genomes of the double-knockout *why1 why3* mutants (Maréchal et al., 2009). Similarly, in *Oryza sativa* (rice), WHIRLY1 regulates the expression of genes involved in chloroplast and ribosome development as well as chlorophyll synthesis (Qiu et al., 2022). These functions are essential to early chloroplast development and seedling viability (Qiu et al., 2022).

As introduced in the section above, conserved motifs contribute significantly to WHIRLY1 protein function. In barley and maize, WHIRLY1 proteins, which contain an N-terminal PRAPP motif cause nucleoid compaction and growth retardation in *Escherichia coli*, whereas their Arabidopsis and potato homologs, which lack this motif, do not. Introducing the PRAPP motif into Arabidopsis WHIRLY1 is sufficient to confer nucleoid-compacting activity (Oetke et al., 2022). Although its physiological role in plastids remains unknown, the PRAPP motif is characteristic of the poaceae WHIRLY1 proteins and may influence plastid transcription and ribosome formation, given the central role of plastid nucleoids in DNA maintenance and ribosome biogenesis (Pfalz et al., 2006; Bohne, 2014; Sun et al., 2024).

The conserved cysteine at position 165 (C165) and the putative copper-binding motif (pvCBM; Figure 3) are of particular interest in the context of redox regulation. WHIRLY1 has been proposed to function analogously to NPR1 in Arabidopsis which switches between oligomeric and monomeric states in response to redox changes (Foyer et al., 2014). WHIRLY1 similarly forms tetramers that can assemble into higher-order oligomers in chloroplasts (Cappadocia et al., 2012). Changes in chloroplast redox state have been proposed to regulate oligomer dissociation and the subsequent accumulation of the WHIRLY1 monomers in the nucleus (Foyer et al., 2014). Whether C165 and pvCBM contribute to redox- or metal-dependent regulation remains to be determined.

The plastid transit peptide (PTP) of WHIRLY1 directs chloroplast targeting. It en-

ables WHIRLY1 to enter chloroplasts, where the protein supports plastid genome maintenance, RNA splicing and nucleoid organisation (Isemer et al., 2012a; Krupinska et al., 2022). Removing or inactivating the PTP abolishes these chloroplast functions and confines WHIRLY1 to the nucleus (Isemer et al., 2012a). Variation in the PTP may therefore modulate WHIRLY1 localisation and function.

1.6.2 WHIRLY2

The current understanding of WHIRLY2 and its functions is less comprehensive than that of WHIRLY1. Nevertheless, several studies have begun to elucidate its subcellular localisation and functional significance. WHIRLY2 localises primarily to mitochondria, where it associates with mitochondrial nucleoids and regulates organellar gene expression (Krause et al., 2005; Maréchal et al., 2008). Within mitochondria, WHIRLY2 contributes to nucleoid organisation and genome stability. In its absence, mitochondrial ultrastructure becomes aberrant, with fewer cristae, lower electron density, and reduced respiration (Golin et al., 2020). Arabidopsis *why2* mutants exhibit unpacked mitochondrial DNA (mtDNA), which confirms that WHIRLY2 is required for mtDNA compaction (Golin et al., 2020). Although *why2* knockouts show no visible phenotype, overexpression of *WHIRLY2* in Arabidopsis causes dwarfism, shortened siliques, and altered mitochondrial RNA profiles. These results indicate that Arabidopsis WHIRLY2 plays a role in mitochondrial RNA processing and energy regulation (Maréchal et al., 2008). Both overexpression and loss of WHIRLY2 disrupt respiration and increase mtDNA copy number more than tenfold, causing a decrease in ATP production (Cai et al., 2015). Overexpression under a pollen-specific promoter further impairs pollen-tube growth due to ROS accumulation and ATP depletion (Cai et al., 2015). These findings demonstrate that WHIRLY2 abundance must be tightly regulated, since optimal levels are essential for maintaining mitochondrial morphology, respiration, and energy homeostasis.

Under abiotic stress, WHIRLY2 supports mitochondrial stability and redox balance across species. In tomato, WHIRLY2 enhances drought tolerance by preserving mitochondrial function, reducing ROS accumulation, sustaining photosynthesis, and interacting with the mitochondrial recombinase recombination protein A 2 (RECA2; Meng et al., 2020). In Arabidopsis, WHIRLY2 promotes salt-stress tolerance by facilitating mtDNA repair and redox signalling. Its absence disrupts mitochondrion–nucleus com-

munication and compromises mitochondrial function (Negroni et al., 2024). The wheat transcription factor WHIRLY2-6A acts as a positive regulator of drought tolerance. Its overexpression in transgenic Arabidopsis results in higher chlorophyll content and improved growth under drought stress. In contrast, silencing of *WHIRLY2-6A* in wheat produces a severe wilting phenotype accompanied by elevated H_2O_2 and O_2^- levels and reduced activities of the antioxidant enzymes superoxide dismutase (SOD), catalase (CAT), and ascorbate peroxidase (APX; Yu et al., 2025). In addition to its mitochondrial role, WHIRLY2 also affects broader cellular processes. In Arabidopsis, it regulates carbon allocation by controlling starch metabolism and the expression of jasmonate-related and *SUGARS WILL EVENTUALLY BE EXPORTED TRANSPORTER* (*SWEET*), which affect senescence and seed development (Huang et al., 2020).

In summary, WHIRLY2 plays an important role in maintaining mitochondrial architecture, nucleic-acid metabolism, and stress adaptation. Its functions are conserved across multiple plant species, and precise control of its expression is essential for preserving mitochondrial integrity, energy production, and overall cellular homeostasis. Although the *WHIRLY2* gene in barley has been identified and shown to have a distinct expression profile (Grabowski, 2008), there is no published loss-of-function study of WHIRLY2 in barley and no detailed characterisation of its roles in nucleoid organisation or stress responses. Given the functional importance of WHIRLY2 in other species (Golin et al., 2020; Huang et al., 2020; Negroni et al., 2024) and its potential replacement of WHIRLY1 in the barley *why1* mutant, generating *why2* mutants in the 'Golden Promise' background is a necessary step towards understanding its contribution to plastid/mitochondrial development, organelle–nucleus communication, and stress tolerance.

1.6.3 WHIRLY proteins in barley

The barley genome encodes two WHIRLY proteins, WHIRLY1 and WHIRLY2 (Grabowski et al., 2008). Although they share conserved motifs, they differ in sequence and localisation. Immunohistochemical and immunogold analyses showed that WHIRLY1 resides in plastids and nuclei of the same cell with similar molecular mass in both compartments (Grabowski et al., 2008; Grabowski, 2008). Analogous to WHIRLY1 of Arabidopsis in transcriptionally active chromosomes (Pfalz et al., 2006) and to WHIRLY1 of

maize (Prikryl et al., 2008), barley WHIRLY1 is located in thylakoid membranes and the nucleus (Grabowski et al., 2008; Melonek et al., 2010). WHIRLY2 was initially detected only in organelles, and its presence in barley mitochondria and the nucleus still requires experimental confirmation.

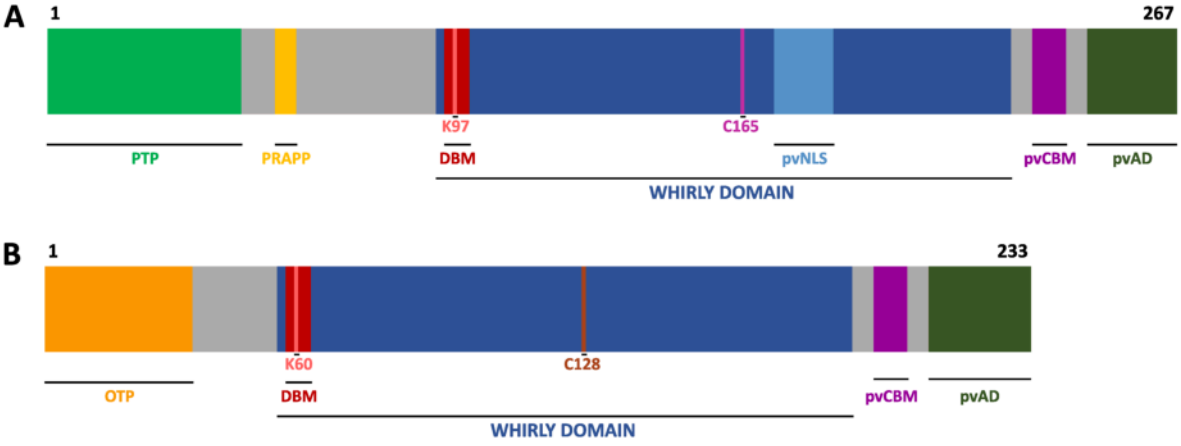

Figure 3. Schematic representation of the WHIRLY1 **(A)** and WHIRLY2 **(B)** protein of barley showing different predicted motifs and domains. The different motifs and domains are shown in different colours. PTP, plastid transit peptide; OTP, organelle transit peptide; DBM, DNA-binding motif; pvNLS, putative nuclear localisation signal; pvCBM, putative copper-binding motif; pvAD, putative activation domain. The PTP/OTP, pvNLS, and pvCBM were predicted by Krupinska et al. (2022). The putative activation domain (pvAD) was predicted by Desveaux et al. (2005). Adapted from Krupinska et al. (2022).

Expression patterns support distinct roles for the two proteins. *WHIRLY1* mRNA is most abundant at the leaf base and declines toward the tip, while protein levels peak in the middle leaf section and decrease during senescence (Grabowski et al., 2008; Krupinska et al., 2014a; Kucharewicz et al., 2017). *WHIRLY2* expression is high in meristematic tissues, declines during leaf development and increases again during senescence (Grabowski, 2008; Kucharewicz et al., 2017). Expression of the genes in response to different hormone treatments differs between WHIRLY1 and WHIRLY2. Abscisic acid (ABA) suppresses *WHIRLY1* but induces *WHIRLY2*, whereas methyl jasmonate elicits the opposite pattern (Grabowski, 2008). Both WHIRLY1 and WHIRLY2 proteins contain conserved sequence features (Figure 3) and are phosphorylated in their recombinant forms (Grabowski, 2008).

WHIRLY1 has been detected in both plastids and the nucleus, and its localisation has been discussed in the context of models proposing regulated plastid–nucleus protein relocalisation in response to cellular conditions (Krause et al., 2012). These models propose that certain plastid proteins can fulfil different functions depending on their

subcellular location, thereby linking organelle status to nuclear processes (Krause et al., 2012). In barley, although WHIRLY1 is present in chloroplasts, it does not behave as a stable component of the core plastid transcriptional machinery. Instead, experimental evidence suggests that WHIRLY1 strongly associates with RNA, particularly intron-containing transcripts, which is consistent with a role in plastid RNA metabolism (Melonek et al., 2010). At the same time, nucleic acid binding by WHIRLY1 has also been demonstrated in the nucleus, supporting a dual functional capacity depending on subcellular context (Krupinska et al., 2014b). Within this model, WHIRLY1 is proposed to have distinct functions associated with different cellular compartments (Krause et al., 2012).

Recent Clustered Regularly Interspaced Short Palindromic Repeats (CRISPR)/CRISPR-associated protein 9 (Cas9) *why1* knockout mutants showed that WHIRLY1 is not essential for chloroplast formation but is required for orderly chloroplast development. Mutants exhibit heterogeneously developed chloroplasts within cells, delayed greening and reduced photosynthetic capacity, associated with disorganised nucleoids and disturbed protein homeostasis (Krupinska et al., 2024). Loss of WHIRLY1 leads to downregulation of numerous nucleoid-associated proteins, including transcriptional components, ribosomal proteins, ATP synthase, caseinolytic protease subunits and RuBisCo, and to increased plastid DNA content and higher expression of plastid DNA polymerase (POP; Krupinska et al., 2014a; Krupinska et al., 2024). These findings suggest that WHIRLY1 contributes to the structural organisation of plastid nucleoids, which have been described as functional platforms for macromolecular assembly processes, including ribosome biogenesis (Bohne, 2014).

WHIRLY1 has been involved in the regulation of nuclear gene expression, particularly in response to stress. In barley, WHIRLY1-dependent phenotypes under nutrient limitation, high light intensity and oxidative stress are associated with impaired acclimation to environmental cues without affecting the retrograde signalling pathways that are associated with plastid protein homeostasis (Comadira et al., 2015; Kucharewicz et al., 2017; Świda-Barteczka et al., 2018; Saeid Nia et al., 2022; Krupinska et al., 2024). Consistent with this, WHIRLY1-dependent nuclear responses have been observed during biotic stress, where accumulation of WHIRLY1 in the nucleus has been found to correlate with changes in defence-related transcriptional programmes (Frank et al., 2024).

Beyond its role in stress-associated nuclear responses, WHIRLY1 has been directly associated with the regulation of senescence and hormone-dependent transcription. In barley, WHIRLY1 binds to W-box elements in the promoter of the senescence-associated gene 40 *S40*, thereby repressing its expression prior to the onset of visible senescence (Krupinska et al., 2014b). During drought, WHIRLY1 modulates ABA-related signalling by affecting gene expression and chromatin structure. Overexpression of *WHIRLY1* delays drought-induced senescence by suppressing the expression of barley genes 9-cis-epoxycarotenoid dioxygenase 1 (*NCED1*) and (*S40*) and by reducing ABA accumulation. In contrast, knockdown of *WHIRLY1* also delays senescence, but abolishes drought-induced histone acetylation at the barley *S40* gene. This indicates that balanced levels of WHIRLY1 are required for ABA-mediated gene regulation (Janack et al., 2016).

Recent work has extended the role of WHIRLY1 to include nutrient and redox homeostasis, particularly iron metabolism. Under high light conditions, RNA interference-mediated knockdown of *WHIRLY1* (RNAi-W1) barley exhibits reduced accumulation of iron-dependent proteins, including PSI and PSII subunits, nitrite reductase, cytochrome f, and Fe-superoxide dismutase, despite having a normal total iron content. This suggests that there are defects in chloroplast iron allocation and utilisation (Krupinska et al., 2025). Increased FERRITIN 1 (*FER1*) transcript and protein levels suggest the sequestration of free iron to limit oxidative damage as a compensatory response. As free iron promotes ROS formation, the absence of WHIRLY1 indirectly increases oxidative stress, necessitating ferritin-mediated detoxification (Krupinska et al., 2025). Overall, studies on barley identify WHIRLY1 as a multifunctional DNA/RNA-binding protein that modulates stress-responsive nuclear gene expression and developmental transitions rather than being a core component of plastid-derived retrograde signalling pathways.

1.7 Targeted mutagenesis in barley

Barley is one of the world's major cereal crops and a well-established genetic model for temperate small-grain species, supported by a high-quality reference genome and advanced genetic resources (Alqudah et al., 2020; Schreiber et al., 2020). Since the late 1990s, efficient *Agrobacterium tumefaciens*–mediated transformation of barley has been established, particularly using immature embryos of the spring cultivar 'Golden

Promise' (Tingay et al., 1997). Continuous optimisation of this system has enabled routine generation of stable transgenic barley lines with predictable transgene integration and inheritance, providing a robust platform for functional genomics and genome editing studies (Hensel et al., 2008; Kumlehn et al., 2009).

The CRISPR/Cas9 genome-editing technique is a precise, sequence-specific method for creating targeted mutations in plants, including cereals (Belhaj et al., 2015; Ma et al., 2016; Chen & Gao, 2020; Montecillo et al., 2020). CRISPR/Cas9 uses a guide RNA (gRNA) to direct the Cas9 nuclease to a complementary genomic sequence adjacent to a protospacer-adjacent motif (PAM). There, Cas9 introduces a double-strand break, which is predominantly repaired by error-prone non-homologous end joining. This can result in small insertions or deletions that disrupt gene function (Doudna & Charpentier, 2014; Belhaj et al., 2015; Ma et al., 2016; Chen & Gao, 2020). CRISPR/Cas9 has been widely used to generate loss-of-function alleles for yield-related, architectural, disease-resistant, and stress-tolerant traits in cereals (Ma et al., 2016; Chen & Gao, 2020; Ahmar et al., 2023).

In barley, CRISPR/Cas9 systems are typically introduced using the same *Agrobacterium*-mediated immature embryo transformation pipelines developed for classical transgenesis (Gasparis et al., 2018; Hinchliffe & Harwood, 2019). A simple and efficient CRISPR/Cas9 platform has been developed in barley. This platform uses binary vectors that carry an intron-optimised Cas9 and one or more gRNAs. These are used in combination with *Agrobacterium*-mediated transformation of immature embryos to induce heritable mutations at one or more loci (Gasparis et al., 2018). Subsequent studies have used this platform to generate knockout lines for various barley genes, confirming high mutation frequencies in primary transformants and enabling the recovery of homozygous mutants in subsequent generations (Gasparis et al., 2018; Galli et al., 2022; Garcia-Gimenez et al., 2020).

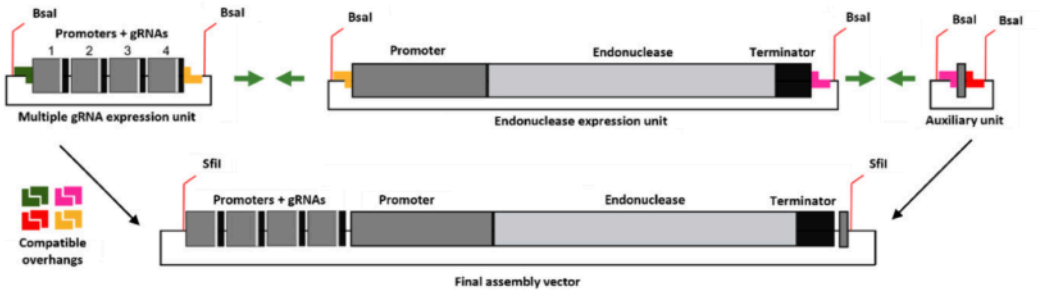

Figure 4. Assembly of the CasCADE modular vector system. The gRNA and endonuclease vectors are assembled into the final vector in a Golden Gate cloning reaction using the enzyme BsaI. The assembled expression units can be cloned into a binary vector using SfiI, which can then be used for *Agrobacterium*-mediated transformation of plants. The gRNAs shown in the image include both the target-specific spacer and the scaffold sequence. Adapted from Hoffie (2023).

In addition to the established CRISPR/Cas9 systems, new modular toolkits have been developed to increase the flexibility and efficiency of targeted mutagenesis in cereals. One such system is CasCADE (Cas9 and CRISPR Assembly for Directed Editing; Hoffie, 2023). CasCADE is a modular Golden-Gate-based cloning system that enables the assembly of CRISPR/Cas expression constructs in three sequential cloning steps (Hoffie, 2023). In the first step, the target-specific 5′ gRNA sequence is inserted into a generic gRNA module vector using the BsaI or BbsI type IIS enzyme. Each resulting module contains one gRNA. In the second step, one to four of these individual gRNA modules are assembled into a single gRNA module through a Golden-Gate reaction using another type IIS enzyme, Esp3I (Hoffie, 2023). Next, the promoter, Cas9 endonuclease and terminator modules are assembled into a complete endonuclease expression unit via a SapI-based Golden-Gate reaction (Hoffie, 2023). CasCADE provides several Cas9 variants for monocots, including maize-codon-optimised cZm-Cas9 and derivatives such as cZm-Cas9-D10A, cZm-xCas9 and cZm-Cas9-NG, as well as corresponding promoter and terminator modules (Hoffie, 2023). The final Golden-Gate step joins the assembled gRNA module, the endonuclease expression cassette and an optional auxiliary module into a functional construct using BsaI. The auxiliary module could be, for example, a multiple cloning site or a reporter module (Figure 4; Hoffie, 2023). The resulting expression unit can be transferred into a binary vector via SfiI for *Agrobacterium*-mediated plant transformation (Hoffie, 2023). The CasCADE system was validated in barley and wheat through targeted mutagenesis of the barley gene SUGAR TRANSPORT PROTEIN 13 (*Stp13*), and its ortholog in wheat, the Leaf rust resistance 67 (*Lr67*). Its modularity,

high assembly efficiency, and successful validation in barley and wheat demonstrate that the CasCADE system is well suited for targeted mutagenesis in cereals.

These developments demonstrate that combining highly optimised *Agrobacterium*-mediated transformation of immature barley embryos (particularly the 'Golden Promise' cultivar) with an expanding range of CRISPR-based genome-editing tools provides a reliable framework for generating stable gene-knockout lines in this species (Hensel et al., 2008; Bartlett et al., 2008; Marthe et al., 2015; Gasparis et al., 2018; Hinchliffe & Harwood, 2019). Modular cloning systems, such as CasCADE (Hoffie, 2023), which facilitate the assembly of multiple gRNAs and various Cas9 variants, further expand the range of methods available for targeted mutagenesis in barley. These methods provide a robust foundation for targeted reverse genetic research in barley.

1.8 Aims of the study

Despite extensive research into the role of WHIRLY1 in chloroplast development, senescence and stress responses, the molecular basis of its diverse functions remained unclear. The functional relevance of individual WHIRLY motifs and conserved residues has not been tested, and it is unclear how they contribute to the observed developmental and stress-related phenotypes.

This study uses a genetic complementation approach with modified *WHIRLY1* variants to assess the contribution of specific domains and motifs *in vivo*. Since there is no WHIRLY2 loss-of-function mutant available in barley, a targeted mutant was generated to enable analysis of its potential role in organelle function and stress responses.

The first objective of this study is to elucidate the specific contributions of individual conserved motifs and amino acid residues within the WHIRLY1 protein. The respective specific aims are as follows:

1. Establish homozygous *why1*-complemented barley lines. Homozygous lines will be established for the seven transgenic barley genotypic variants generated by complementing *why1* mutants with modified *WHIRLY1* sequences. Each transgenic line contains a defined modification in the *WHIRLY1* coding sequence, including specific deletions or amino acid substitutions. Homozygosity will be verified according to Mendelian segregation analysis, with a 3:1 phenotypic segrega-

tion ratio, assuming a single-locus transgene insertion.

2. Assess stress responses of *why1*-complemented homozygous lines with mutations in diverse motifs under controlled light and temperature conditions.

3. Assess drought stress responses in *why1*-complemented homozygous lines with mutations in diverse motifs by measurements of photosynthesis parameters and leaf lengths.

4. Determine whether and which modifications of the *WHIRLY1* gene affect the response to *Blumeria graminis* f. sp. *hordei* (*Bgh*).

Recent genetic analyses indicate that WHIRLY1 is not essential for chloroplast formation. To investigate whether WHIRLY2 is responsible for chloroplast development, the *WHIRLY2* gene will be mutated by genome editing. Accordingly, the second objective of this study is to generate a loss-of-function mutant of *WHIRLY2* (*why2*) in barley 'Golden Promise' using the CRISPR/Cas9 gene-editing system.

2 Results

2.1 Generation and characterisation of homozygous *why1*-complemented lines

The *Hordeum vulgare* L. (barley) 'Golden Promise' *why1* mutant was generated at the Leibniz Institute of Plant Genetics and Crop Plant Research (IPK) to investigate the role of the WHIRLY1 protein in abiotic and biotic stress responses. Since WHIRLY1 is a multifunctional protein (Krupinska et al., 2022), the *why1* mutant was complemented with modified *WHIRLY1* sequences carrying targeted mutations in specific conserved motifs and amino acid residues, in order to determine their individual contributions to protein function. The resulting lines are hereafter referred to as *why1*-complemented variants (Table 1).

Previous studies have investigated WHIRLY1 function using complementary approaches, but none has generated and characterised complementation lines *in planta* in barley. With the exception of the ΔPTP variant in Arabidopsis (Isemer et al., 2012a), such lines have not been produced in any other plant species. In Arabidopsis plastid localisation is required for WHIRLY1-mediated enhancement of ABA responsiveness during germination. Seedlings expressing only the nuclear isoform of WHIRLY1, i.e. a truncated version lacking the PTP, were as insensitive to ABA as the *why1* mutant (Isemer et al., 2012a). The ΔPTP variant generated in the present study was therefore expected to behave similarly to the *Arabidopsis why1* mutant. Structural and biochemical analyses showed that the conserved lysine residue within the DBM is required for oligomerisation and DNA binding in Arabidopsis, predicting that its substitution would severely impair WHIRLY1 function (Cappadocia et al., 2012). Accordingly, a strong mutant phenotype was expected for the K97A variant in barley, where the conserved lysine K97 is replaced with alanine. The PRAPP motif was identified as a determinant of nucleoid compaction in barley and maize WHIRLY1 through site-directed mutagenesis and heterologous expression in *Escherichia coli* (Oetke et al., 2022). Since correct nucleoid organisation is required for proper chloroplast development and function (Powikrowska et al., 2014), the ΔPRAPP variant was expected to display an impaired phenotype. The *in planta* consequences of PRAPP deletion in barley have not been investigated prior to this study. Similarly, the variants targeting the conserved cysteine

residue (C165A) and the computationally predicted copper-binding motif (pvCBM), motivated by the proposed redox-sensing role of WHIRLY1 involving cysteine-mediated disulfide bridge formation (Foyer et al., 2014), have not been investigated in any plant system to date. A K97AΔCBM double mutant was also included to assess potential combinatorial effects. Together with a line expressing the full-length WHIRLY1 sequence as a complementation control, these seven *why1*-complemented barley lines represent the first *in planta* investigation of WHIRLY1 functional domains.

To ensure reliable results, lines that were homozygous for the transgene were identified before phenotypic and physiological characterisation. Homozygosity was established by analysing the segregation of the hygromycin phosphotransferase (*hpt*) selectable marker in the second transgenic generation (T_2) families derived from independent first transgenic generation (T_1) plants of each *why1*-complemented variant. Based on Mendelian inheritance of a single transgene locus, it was expected that T_2 families from hemizygous T_1 parents would segregate at a ratio of 3:1 (*hpt*-positive:*hpt*-negative). The majority of T_2 families showed no significant deviation from this expected ratio (Table A1).

Based on the segregation analysis, four to six independent T_2 families per variant were selected for further propagation. Individual T_2 plants that were positive for the *hpt* selectable marker were advanced to the third transgenic generation (T_3), and the resulting T_3 families were again screened for *hpt* marker segregation. T_3 families in which all seedlings were *hpt*-positive were considered homozygous at the *hpt* locus and used for subsequent analyses.

In contrast to the other variants, homozygous lines for the ΔCBM and K97AΔCBM variants could not be obtained within the timeframe of this study due to biological and experimental constraints. For these variants, only three independent events (families) were generated per construct. This number is insufficient for a reliable assessment of the 3:1 segregation ratio (Table A1). In addition, these variants had exceptionally long generation times. As a result, although T_2 grains were successfully harvested, advancement to the T_3 generation could not be completed. Homozygous lines for the ΔCBM and K97AΔCBM variants remain to be established in future work.

In total, homozygous lines were successfully selected from five of the seven *why1*-complemented variants. Due to space limitations in the greenhouse and particularly

the long generation times, the total time required to select all the homozygous lines was approximately 2.5 years.

Table 1. List of *why1*-complemented variants, constructs, and phenotypic outcomes

Variant	Construct	Expected phenotype	Observed phenotype	Generation time[b]
Control[a]	*WHIRLY1$_{prom}$::WHIRLY1*	Green; full rescuing of the WHIRLY1 function, normal chloroplast development.	green	6 months
K97A	*WHIRLY1$_{prom}$::WHIRLY1K97A*	Green; impaired stress response due to monomer accumulation in the nucleus.	green	6 months
ΔPTP	*WHIRLY1$_{prom}$::WHIRLY1ΔPTP*	*Xantha*-to-green; without the PTP WHIRLY1 cannot localise to chloroplasts, impairing their development.	*xantha*-to-green	11 months
ΔPRAPP	*WHIRLY1$_{prom}$::WHIRLY1ΔPRAPP*	*Xantha*-to-green; reduced compaction of plastid DNA impairing chloroplast development.	green	4.5 months
C165A	*WHIRLY1$_{prom}$::WHIRLY1C165A*	Green; impaired sensing of stress-associated redox changes in the photosynthetic apparatus.	green	4.5 months
ΔCBM	*WHIRLY1$_{prom}$::WHIRLY1ΔCBM*	Green; impaired stress response since plants might not respond to SA.	*xantha*-to-green	11 months
K97AΔCBM	*WHIRLY1$_{prom}$::WHIRLY1K97AΔCBM*	Green; impaired stress response due to monomer accumulation in the nucleus and insensitivity to SA.	*xantha*-to-green	13 months

[a]Variants highlighted in green represent those successfully advanced to homozygosity. No homozygous lines could be selected from the ΔCBM and K97AΔCBM variants due to the limited number of spikes produced.
[b]Generation times represent the average duration of two successive generations required to advance plants to homozygosity.

The generation times for the different *why1*-complemented variants exceeded the three to four months typically observed for wild-type barley 'Golden Promise' (hereafter "wild type") in greenhouse conditions. This variation in generation time was not uniform across variants, and it correlated with the observed phenotype. Variants displaying a green phenotype, i.e. the control, K97A, ΔPRAPP, and C165A, completed their life cycle within 4.5 to 6 months. In contrast, *xantha*-to-green variants, i.e. ΔPTP, ΔCBM, and K97AΔCBM required substantially longer generation times of 11 to 13 months (Table 1; Figure 5). This difference was evident also at awn emergence, which occurred

approximately 2.5 months after sowing (MAS) in the green phenotype variants and after more than 8 months in the *xantha*-to-green variants. In all the variants, regardless of the time of awn emergence, grain maturity was reached approximately three months later. For comparison, in the wild type, awn emergence occurs about 50 DAS.

2.1.1 Morphological parameters

The *why1*-complemented variants were cultivated at different times and in different greenhouse chambers, resulting in variable environmental conditions that introduced confounding variables. Therefore, the interpretation of quantitative morphological traits such as plant height, spike number, or tiller number would have been unreliable. The primary objective of this part of the study was the production of homozygous lines, and the observations presented here are accordingly qualitative (Figure 5).

At 5.5 MAS, the C165A variant plants had already completed their life cycle and were ready for harvesting (Figure 5). The foliage was yellowish and the tiller number was reduced. This is consistent with the shorter generation times observed for green-phenotype variants. The other green-phenotype variants, the control, K97A, and ΔPRAPP, also completed their life cycle within a comparable timeframe (Table 1). In contrast, the K97AΔCBM variant, despite being of the same age, remained at a substantially earlier developmental stage, with green foliage and actively growing tillers.

Similarly, the ΔPTP variant had not yet reached maturity at 7 MAS and maintained a largely green, dense tiller cluster. The wild type, the *why1* mutant, and the control variant all formed comparable basal tiller clusters with multiple culms emerging from the plant base. The wild type, documented at an earlier developmental stage, displayed fewer and more widely spaced tillers (Figure 5).

Plant height also varied across genotypes. The wild type reached 89 cm at 2 MAS. Among plants documented at 5.5 months or older, the C165A variant was the tallest (70 cm), followed by the control (67 cm). The *why1* mutant was the shortest (48 cm), while the ΔPTP (59 cm) and K97AΔCBM (56 cm) variants showed intermediate heights (Figure 5).

Figure 5. Comparison of morphological parameters among representative barley genotypes. Tiller density could only be compared between plants of similar age. The heights are shown on the left-hand side of each plant. The C165A variant is shown at its harvesting time. MAS, months after sowing.

To investigate whether the *why1*-complemented variants exhibited differences in root development, roots of twelve 14-day-old seedlings from each of three families per variant were examined (Figure 6). Root length and root area were quantified using image analysis in Fiji (ImageJ 1.54p; Schneider et al., 2012).

Root length did not differ significantly between any of the variants and the wild type (Welch's ANOVA with Games-Howell post-hoc test, $\alpha = 0.05$; Figure 6B; Figure 6C). Root area, however, was significantly reduced in all three families of the ΔPTP variant (E898, E899, and E900) compared with the wild type and the remaining variants. The strongest reduction was observed in comparison to the wild type (Figure 6A; Figure 6C). No significant differences in root area were detected between the wild type and any of the other four variants (Figure A2).

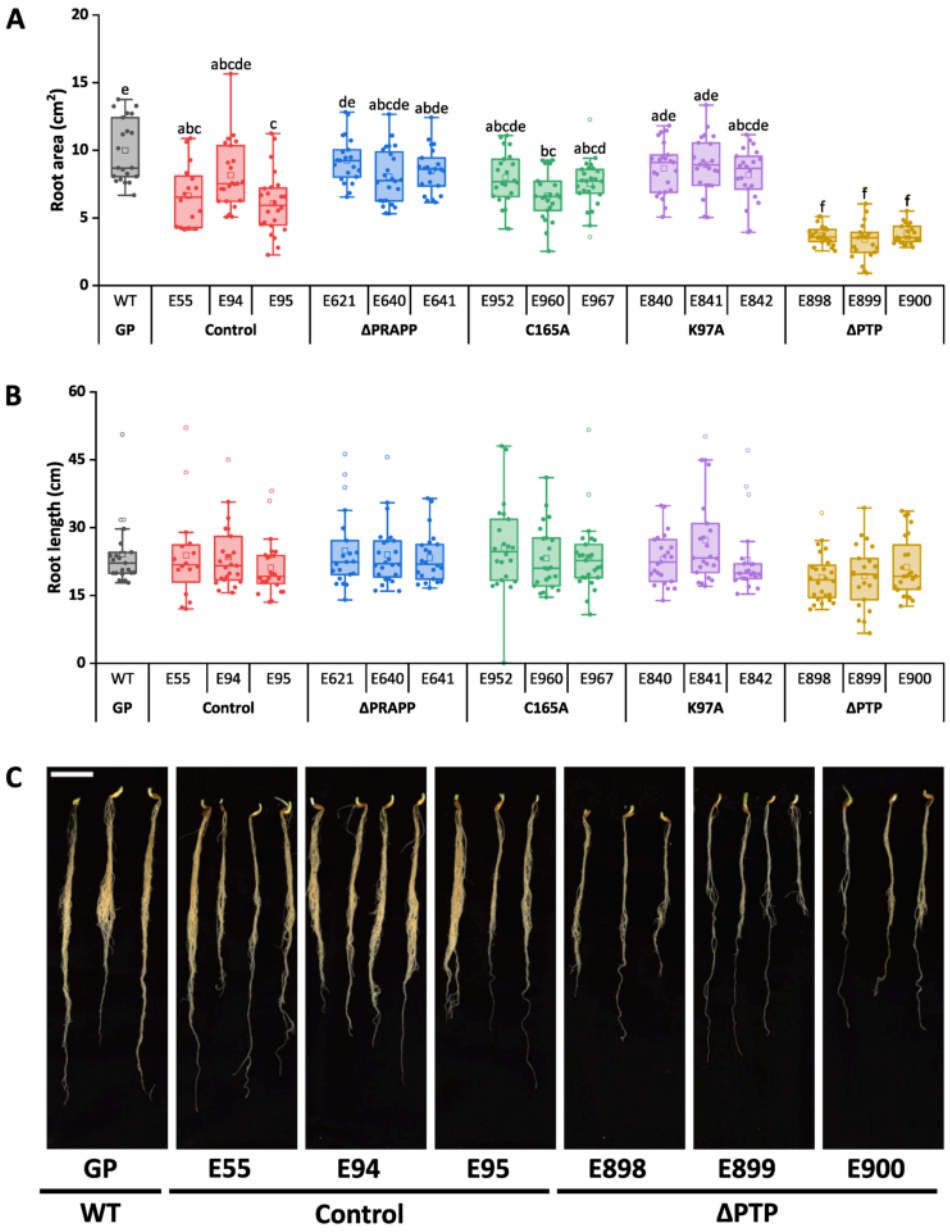

Figure 6. Root phenotype of *why1*-complemented variants under normal conditions. **(A)** Root area. **(B)** Root length. **(C)** Representative root images of the ΔPTP variant, the control variant, and the wild type. Root length and area of 14 day-old seedlings were quantified using Fiji (ImageJ 1.54p; Schneider et al., 2012). Statistical analysis was performed using Welch's ANOVA with Games-Howell post-hoc test, $\alpha = 0.05$ in IBM SPSS Statistics, version 28. Different letters indicate statistically significant differences. No statistically significant differences were detected for root length **(B)**, therefore, no letters are shown. Data were collected from 12 plants per family per experiment, with two experimental replicates. GP, Golden Promise; WT, wild type.

2.1.2 WHIRLY1 protein accumulation

To confirm expression of the modified WHIRLY1 protein in the *why1*-complemented variants, total protein extracts were analysed by SDS-PAGE and Western blotting using a WHIRLY1-specific antibody (Figure A1; see Section 4.2.10). Two immunoreactive bands

were detected across all variants, at approximately 25 kDa and 35 kDa. The 25 kDa band corresponds to the mature WHIRLY1 protein and was present in all variants, although its abundance was reduced in the ΔPTP variant. A second band at approximately 35 kDa was consistently detected in all variants. Its identity remains to be determined.

2.1.3 Physiological characterization of the *why1*-complemented lines

The homozygous *why1*-complemented variants were characterised under both abiotic and biotic stress conditions. Abiotic stresses included drought, continuous light, and high temperature. Biotic stress was assessed using powdery mildew (*Blumeria graminis* f. sp. *hordei*, *Bgh* isolate CH4.8), the most prevalent fungal pathogen of barley.

2.1.3.1 Combined exposure to continuous light and high temperature

Four of the *why1*-complemented variants, the control, ΔPRAPP, C165A, and K97A, displayed no obvious morphological differences compared to the wild type under standard greenhouse conditions. All four variants produced green leaves, developed comparable root systems, and completed their life cycle within similar generation times, with no apparent differences in overall plant architecture or early seedling development. Since these variants could not be distinguished based on morphology alone, their responses to environmental conditions known to influence chloroplast development were investigated to uncover potential functional differences. Specifically, seedlings were exposed to high temperature in combination with continuous light, conditions known to impair chloroplast development in grasses. Primary leaf length and chlorophyll content were assessed in 14 DAS seedlings under defined light and temperature conditions. Chlorophyll content was determined by imaging three representative primary leaves per plant, while primary leaf length was measured for all germinated seedlings of each family (see Section 4.2.7.1).

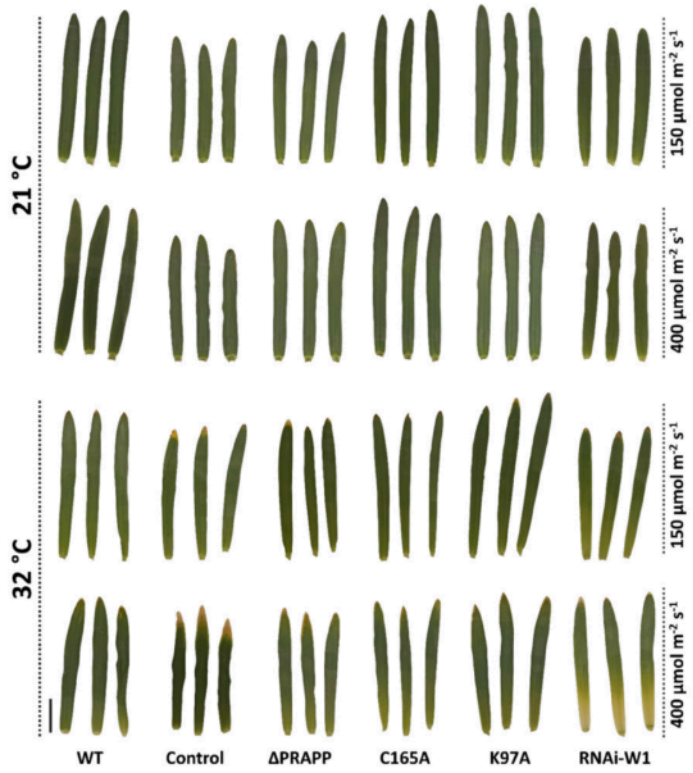

Figure 7. Primary leaves of barley plants under different temperature and continuous light conditions. The temperature conditions are shown on the left hand side of the image, whereas the continuous light conditions are shown on the right hand side of the image. Three representative primary leaves of each variant, the wild type, and RNAi-W1 plants are shown. RNAi-W1 are RNAi-mediated knockdown *WHIRLY1* plants (Melonek et al., 2010). Images were taken 14 DAS. Scale bar = 2 cm.

Seedlings were initially exposed to four defined combinations of temperature and continuous light intensity conditions: high temperature and high light (32 °C and 400 µmol m^{-2} s^{-1}), high temperature and normal light (32 °C and 150 µmol m^{-2} s^{-1}), normal temperature and high light (21 °C and 400 µmol m^{-2} s^{-1}), and normal temperature and normal light (21 °C and 150 µmol m^{-2} s^{-1}). These experiments were repeated twice, using three families from each *why1*-complemented variant and the wild type, with 12 grains sown per family. The wild type and RNAi-W1 plants (Melonek et al., 2010) served as controls. Data were collected from all germinated seedlings (see Section 4.2.7.1).

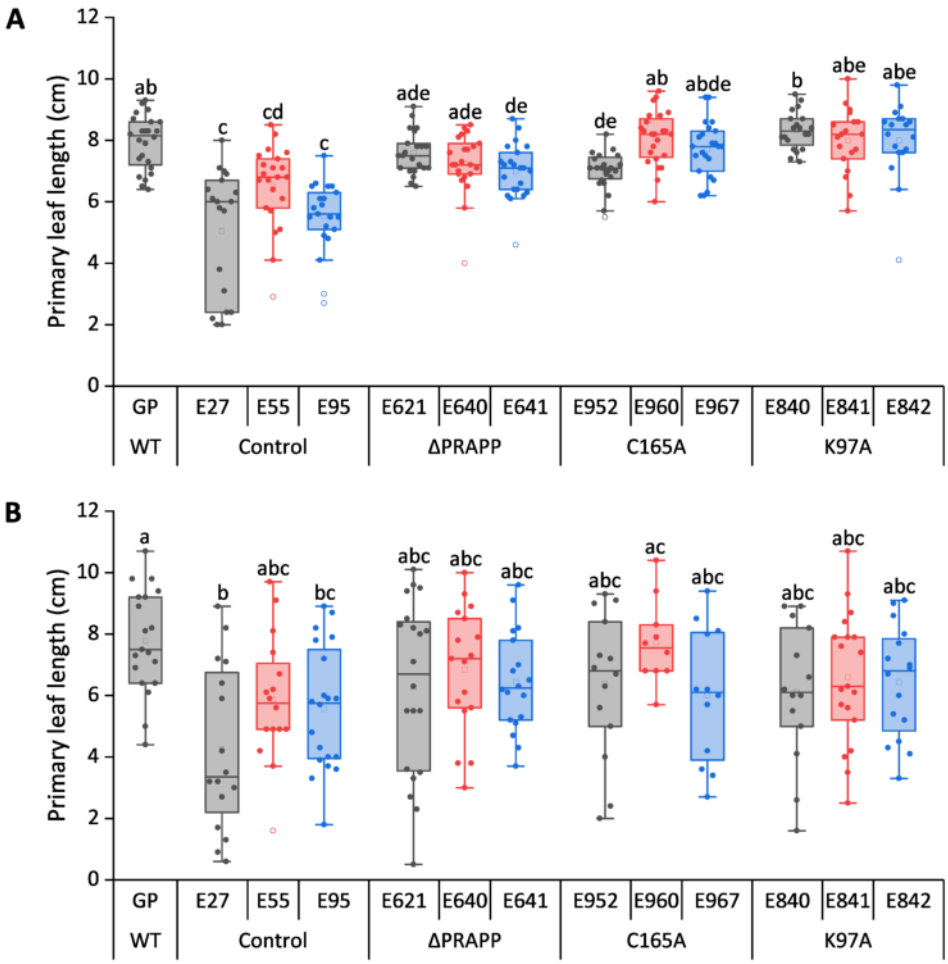

Figure 8. Response of *why1*-complemented variants to high temperature. **(A)** Primary leaf length under normal photoperiod light and temperature (21 °C) conditions. **(B)** Primary leaf length at 34 °C under continuous light. E27, E55 etc. denote individual genotypes/families of each variant. GP, cultivar 'Golden Promise'; WT, wild type. Statistical analysis was performed using Welch's ANOVA with Games–Howell post hoc test ($\alpha = 0.05$). Data were collected from 12 plants per family per experiment, and two experimental replicates.

To evaluate potential differences in chlorophyll content, images of three representative primary leaves were analysed for leaf greenness. In all growth conditions, no major differences in leaf greenness were detected either in plants within each condition or between different conditions (Figure 7). As expected, RNAi-W1 seedlings grown at 32 °C and continuous high light (400 µmol m^{-2} s^{-1}) exhibited pronounced bleaching at the basal region of the primary leaves. Seedlings of the control variant developed necrosis at the leaf tips, a phenotype which was most obvious under high-temperature and continuous high-light conditions, but still noticeable even under continuous normal light intensity (150 µmol m^{-2} s^{-1}).

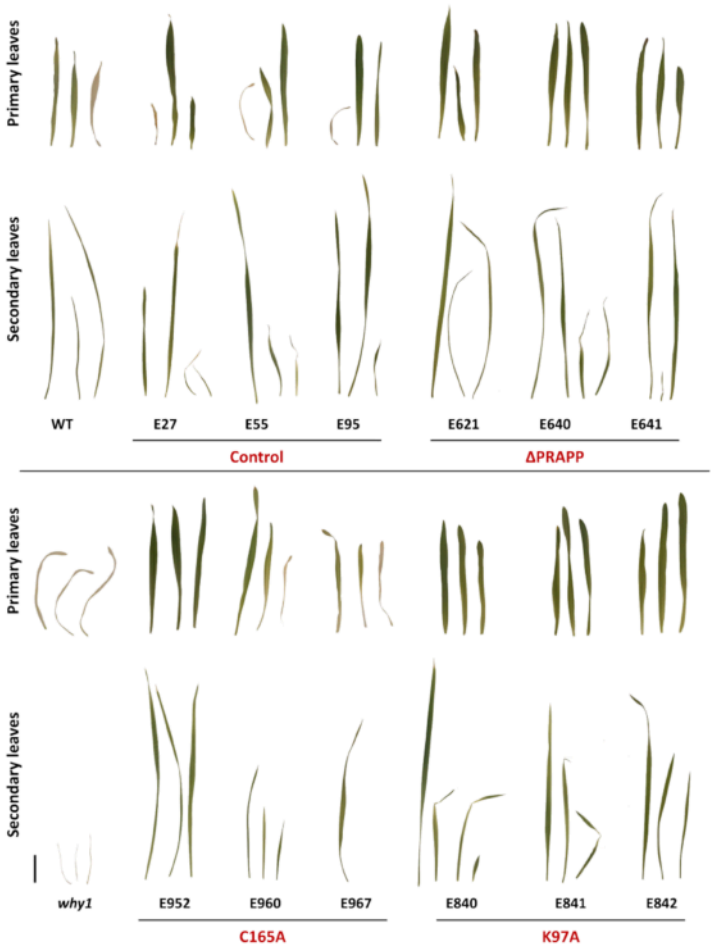

Figure 9. Primary leaf greenness of *why1*-complemented variants under continuous normal light and 34 °C. Images were taken 14 DAS. Three representative leaves of each of three families of the Control, ΔPRAPP, C165A, and K97A variants are shown, as well as three representative leaves of the wild-type plants (WT) and the *why1* barley mutant plants (Krupinska et al., 2024). Data were collected from 12 plants per family per experiment, with two experimental replicates. Scale bar on the lower left-hand side = 2 cm.

To further investigate the response of the *why1*-complemented variants to higher temperatures, an additional experiment was conducted at 34 °C with continuous light at normal light intensity (150 µmol m^{-2} s^{-1}). The control experiment was performed under normal temperature (21 °C) and photoperiod conditions (16 h light/8 h dark) with normal light intensity (150 µmol m^{-2} s^{-1}). High growth temperatures in the range of 32–34 °C are commonly used to impair chloroplast development in cereal seedlings, because they selectively prevent the accumulation of plastid 70S ribosomes (and plastid rRNA), resulting in chlorotic leaves despite only modest effects on overall leaf growth (Feierabend & Mikus, 1977; Bünger & Feierabend, 1980; Herrmann & Feierabend, 1980). For each variant, three independent families and 12 plants per family were analysed. Both experimental conditions (normal and high temperature) were assessed in

two independent replicates (see Section 4.2.7.1).

Primary leaf length was compared in all genotypes and growth conditions using Welch's ANOVA with Games–Howell post hoc test. Results were confirmed by Kruskal–Wallis test with Dunn's post hoc test (Table A2).

Under control conditions, the wild-type plants developed significantly longer primary leaves than all three control variant families, family E641 of the ΔPRAPP variant, and family E952 of the C165A variant ($\alpha = 0.05$; Figure 8A). At 34 °C, most of these differences were no longer observed. Significant reductions in primary leaf length compared to the wild type were detected only in control variant families E27 and E95. No other variants differed significantly from the wild type ($\alpha = 0.05$; Figure 8B). A direct comparison between conditions showed that primary leaf length was significantly shorter at 34 °C in family E967 of the C165A variant and all three families of the K97A variant. The remaining variants showed no significant differences between normal conditions and high temperature conditions (Figure A6; independent two-sample t-test with Welch's correction for unequal variances, $\alpha = 0.05$).

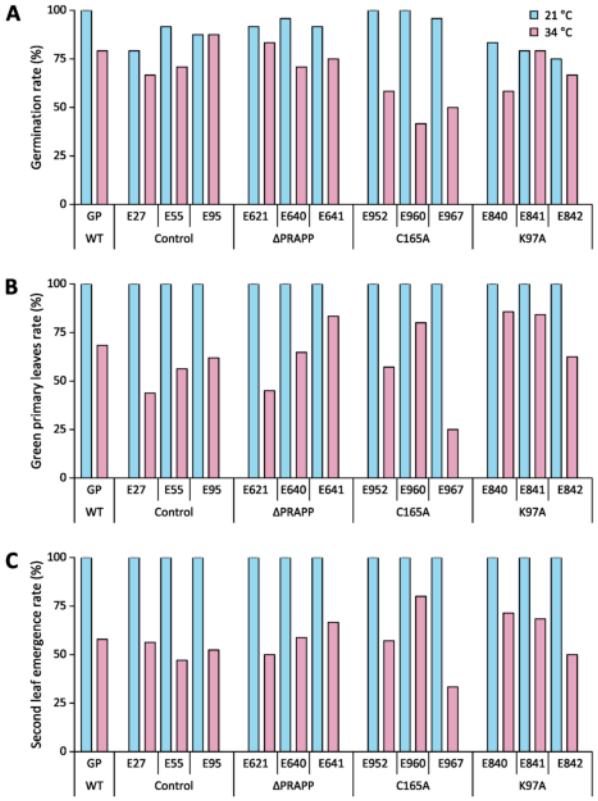

Figure 10. Effect of high temperature and continuous light on germination, second-leaf emergence, and primary leaf greenness. **(A)** Germination rate of *why1*-complemented lines. **(B)** Second leaf emergence rate. **(C)** Green primary leaves rate. Data were collected from 12 plants per family per experiment, with two experimental replicates at 14 DAS.

Primary and secondary leaf greenness was assessed from photographs of three representative leaves of each family. Growth under high temperature and continuous light was associated with reduced primary leaf greenness and impaired seedling development compared to plants grown under normal conditions (Figure 9; Figure A7). Chlorosis was observed in the primary leaves of several seedlings and, in severe cases, complete bleaching and tissue necrosis were recorded. Despite these stress symptoms, no clear differences in primary leaf greenness were evident between the wild type and the *why1*-complemented variants at 34 °C. However, K97A seedlings had a higher proportion of green non-necrotic primary leaves compared to the other *why1*-complemented variants. A similar pattern was observed for family E641 of the ΔPRAPP variant, in which 83% of primary leaves were green (Figure 10B).

In addition to these phenotypic effects, two additional observations were made in seedlings grown at 34 °C under continuous light. First, germination rates were generally lower than under normal conditions for most families. On average, only 68% of sown grains germinated at high temperature, whereas under normal conditions, more than 90% of the sown grains germinated. This effect was particularly evident in the C165A variant where germination rates approached 100% under normal conditions, but decreased to 50% or lower at 34 °C (Figure 10). Second, secondary leaf emergence was delayed in seedlings grown under continuous light and at 34 °C. Under normal growth conditions, all seedlings had developed both the second and third leaves by day 14. In contrast, at 34 °C, most seedlings had not yet formed a third leaf, and a substantial proportion lacked a fully expanded second leaf (Figure 10C). To quantify this effect, the rate of second leaf emerged was calculated as the proportion of germinated plants that had developed a second leaf.

2.1.3.2 Drought sensitivity

To assess the impact of drought on photosynthetic performance, PSII efficiency and chlorophyll content were quantified in plants exposed to water deficit starting at 11 DAS and monitored for 33 to 41 days, depending on their developmental progression (see Section 4.2.7.2). Soil water content was measured every two days before watering the plants (Figure 11C, Figure 12C, Figures A3C-A5C). Lower SWC values reflect a higher consumption of water by the plants.

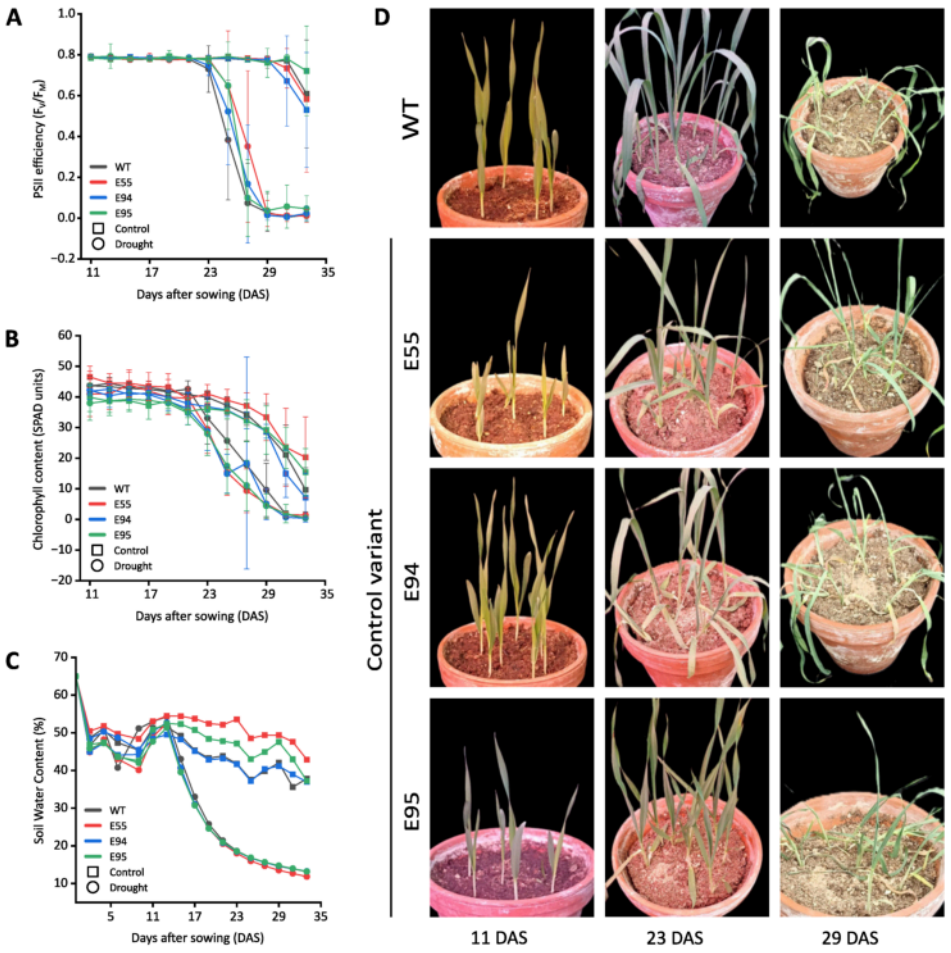

Figure 11. Response of the control variant to drought. Three independent homozygous families (E55, E94, and E95) were grown under drought and well-watered (control) conditions. **(A)** Maximum quantum efficiency of PSII (F_V/F_M), **(B)** chlorophyll content, and **(C)** soil water content were monitored over time and are shown as mean values ± standard deviation. **(D)** Representative plants grown under drought conditions are shown at three defined time points: 11 DAS, corresponding to the last day of watering; 23 DAS, corresponding to the onset of the decline in PSII efficiency in all plants; and 29 DAS, when PSII efficiency approached zero and remained unchanged thereafter. The experiment was repeated twice, using 3–7 plants per family in each repetition. Occasional instances with only three plants resulted from reduced seedling numbers due to germination failure.

Under control conditions, at 11 DAS, SWC was approximately 50% across all lines. The wild type and the green-phenotype variants had F_V/F_M values of approximately 0.79, which remained stable until 31 DAS, after which the F_V/F_M declined. Chlorophyll content in these lines declined gradually throughout the experiment. By 23 DAS, SWC had decreased to approximately 42-46%, and by 31 DAS to approximately 36%. The ΔPTP variant showed a different pattern. At 11 DAS, its F_V/F_M was approximately 0.50 and its chlorophyll content approximately 30% of the wild-type level, consistent with its *xantha*-to-green phenotype. Both values increased steadily, reaching approximately 0.78 and 63% of the wild-type level respectively by 23 DAS, and remained relatively sta-

ble until 41 DAS, the final measurement day for this line. SWC in the ΔPTP variant was consistently higher than in the other lines throughout the experiment, decreasing from approximately 52.5% at 23 DAS to approximately 50% at 31 DAS and 41% by 41 DAS (Figure 11; Figure 12; Figures A3-A5).

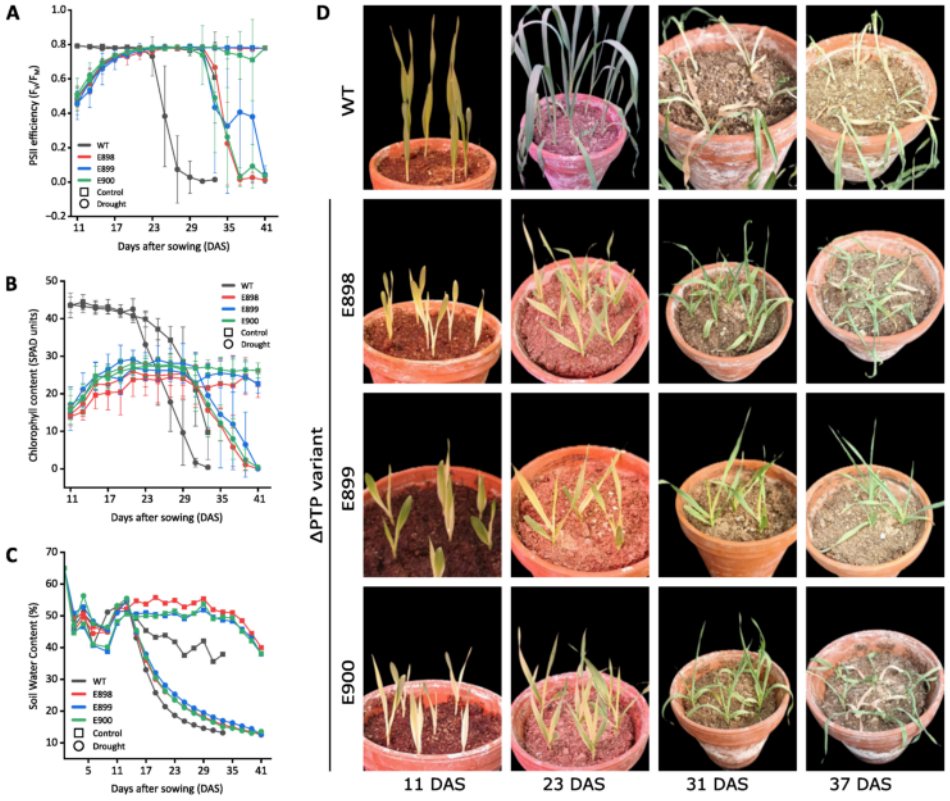

Figure 12. Response of the ΔPTP variant to drought. Three independent homozygous families (E898, E899, and E900) were grown under drought and well-watered (control) conditions. **(A)** Maximum quantum efficiency of PSII (F_V/F_M), **(B)** chlorophyll content, and **(C)** soil water content were monitored over time and are shown as mean values ± standard deviation. **(D)** Representative plants grown under drought conditions are shown at three defined time points: 11 DAS, corresponding to the last day of watering; 23 DAS, corresponding to the onset of the decline in PSII efficiency in wild-type plants; 31 DAS, corresponding to the onset of the decline in PSII efficiency in the ΔPTP plants; 37 DAS, when PSII efficiency approached zero and remained unchanged thereafter. The experiment was repeated twice, using 3–7 plants per family in each repetition. Occasional instances with only three plants resulted from reduced seedling numbers due to germination failure.

Under drought conditions, at 11 DAS, SWC was approximately 50% across all lines, comparable to control conditions. By 23 DAS, SWC had declined to approximately 19% in the wild type and the green-phenotype variants, and to approximately 24% in the ΔPTP variant. At this time point, F_V/F_M in the wild type and green-phenotype variants, which had been approximately 0.79 at 11 DAS, began to decline rapidly, reaching values close to zero by 29 DAS and remaining so until 33 DAS, the final measurement day for these lines. Chlorophyll content in these lines decreased slowly until 21 DAS, then de-

clined rapidly, reaching values close to zero by 33 DAS. SWC continued to fall, reaching approximately 14% by 23 DAS and approximately 13% by 33 DAS. In the ΔPTP variant, F_V/F_M was approximately 0.50 at 11 DAS and increased to approximately 0.78 by 23 DAS. Chlorophyll content followed a similar trajectory, rising from approximately 30% to 65% of the wild-type level by 21 DAS. Both parameters remained relatively stable until 31 DAS, after which they declined rapidly, reaching values close to zero by 37-41 DAS. SWC in the ΔPTP variant was again higher than in the other lines, at approximately 17.5% at 23 DAS, declining to approximately 13% by 41 DAS (Figure 11; Figure 12; Figures A3-A5).

Table 2. Quantification of drought-induced changes in photosynthesis-related parameters using Euclidean distance and root mean square error

		PSII efficiency				Chlorophyll content				Soil water content			
		Normal conditions		Drought conditions		Normal conditions		Drought conditions		Normal conditions		Drought conditions	
Line	Family	ED[a]	RMSE[a]	ED	RMSE	ED	RMSE	ED	RMSE	ED	RMSE	ED	RMSE
WT	GP[a]	0.000[b]	0.000	0.000	0.000	0.000	0.000	0.000	0.000	0.000	0.000	0.000	0.000
Control	E55	0.050	0.014	0.386	0.112	12.943	3.736	15.433	4.455	29.410	7.133	13.743	3.333
	E94	0.127	0.037	0.170	0.049	9.407	2.716	14.897	4.300	7.282	1.766	10.812	2.622
	E95	0.115	0.033	0.278	0.080	14.240	4.111	17.909	5.170	16.838	4.084	13.089	3.174
ΔPRAPP	E621	0.333	0.096	0.368	0.106	9.975	2.879	23.566	6.803	12.998	3.152	15.417	3.739
	E640	0.218	0.063	0.057	0.017	4.744	1.370	23.417	6.760	7.760	1.882	10.716	2.599
	E641	0.029	0.008	0.070	0.020	3.792	1.095	14.074	4.063	9.063	2.198	10.298	2.498
C165A	E952	0.154	0.045	0.162	0.047	18.717	5.403	5.764	1.664	7.250	1.758	7.544	1.830
	E960	0.165	0.048	0.570	0.165	22.848	6.596	15.895	4.588	14.692	3.563	10.274	2.492
	E967	0.129	0.037	0.139	0.040	14.436	4.167	14.260	4.116	14.844	3.600	13.211	3.204
K97A	E840	0.069	0.020	0.058	0.017	10.458	3.019	14.963	4.319	7.862	1.907	16.498	4.001
	E841	0.062	0.018	0.125	0.036	11.475	3.313	12.317	3.556	11.231	2.724	10.664	2.586
	E842	0.078	0.022	0.291	0.084	7.646	2.207	3.992	1.152	8.325	2.019	12.672	3.073
ΔPTP	E898	0.428	0.124	1.556	0.449	65.276	18.843	63.021	18.193	39.936	9.686	14.384	3.489
	E899	0.474	0.137	1.477	0.426	57.077	16.477	60.785	17.547	31.365	7.607	19.422	4.711
	E900	0.412	0.119	1.452	0.419	56.835	16.407	59.359	17.135	31.958	7.751	15.570	3.776

[a]GP, cultivar Golden Promise; ED, Euclidean distance; RMSE, root mean square error
[b]Colour formatting is done with blue showing the highest values and red showing the lowest values.

To quantitatively assess differences between the five *why1*-complemented variants and the wild type, Euclidean distances (ED) and root mean square error (RMSE) were

calculated for the PSII efficiency, chlorophyll content, and soil water content. This analysis revealed a clear and consistent pattern. The largest deviations occurred between the wild type and the ΔPTP variant under both control and drought conditions. A similar pattern was found for chlorophyll content. Four of the *why1*-complemented variants exhibited comparable tendencies, whereas the ΔPTP variant deviated significantly. As with PSII efficiency, the most pronounced differences in chlorophyll content were again detected between the wild type and the ΔPTP variant (Table 2).

The consistently higher SWC values in the ΔPTP variant under both conditions suggested reduced water consumption, which could be related to differences in leaf size. To assess this, primary leaf length was measured was measured using ImageJ at 11 DAS, the first day of measurements. The final primary leaf length of the ΔPTP variant (n = 66) was approximately 73% of the wild-type length (n = 20). To confirm that this length did not increase in the following days, measurements were also taken at 13 DAS and 15 DAS, showing that the lengths of both the ΔPTP variant and the wild type remained unchanged. These results confirmed that ΔPTP primary leaves are indeed shorter than those of the wild type.

2.1.3.3 Microscopic quantification of powdery mildew infection

The response of *why1*-complemented transgenic variants to powdery mildew was quantified using the machine-learning-assisted phenotyping platform BluVision Micro. Five transgenic variants and the wild type were inoculated with *Blumeria graminis* f. sp. *hordei* (*Bgh*) isolate CH4.8, and fungal development was assessed 48 hours after inoculation. Colony number and median colony area were quantified by automated image analysis (see Section 4.2.8).

The number of *Bgh* CH4.8 colonies was significantly higher in all three families of the ΔPTP variant compared to the wild type and the remaining *why1*-complemented variants (Figure 13A, Figure 13C). Mean colony numbers in the ΔPTP families ranged from 83.0 (E899) to 102.1 (E898), compared to 23.4 in the wild type and means ranging from 19.5 to 44.2 in the remaining variants.

Median colony area showed a less consistent pattern than colony number. The full statistical groupings are shown in Figure 13B. The biggest difference was observed in the E900 family of the ΔPTP variant, which had a significantly larger median colony area

than the wild type and several other families of different variants.

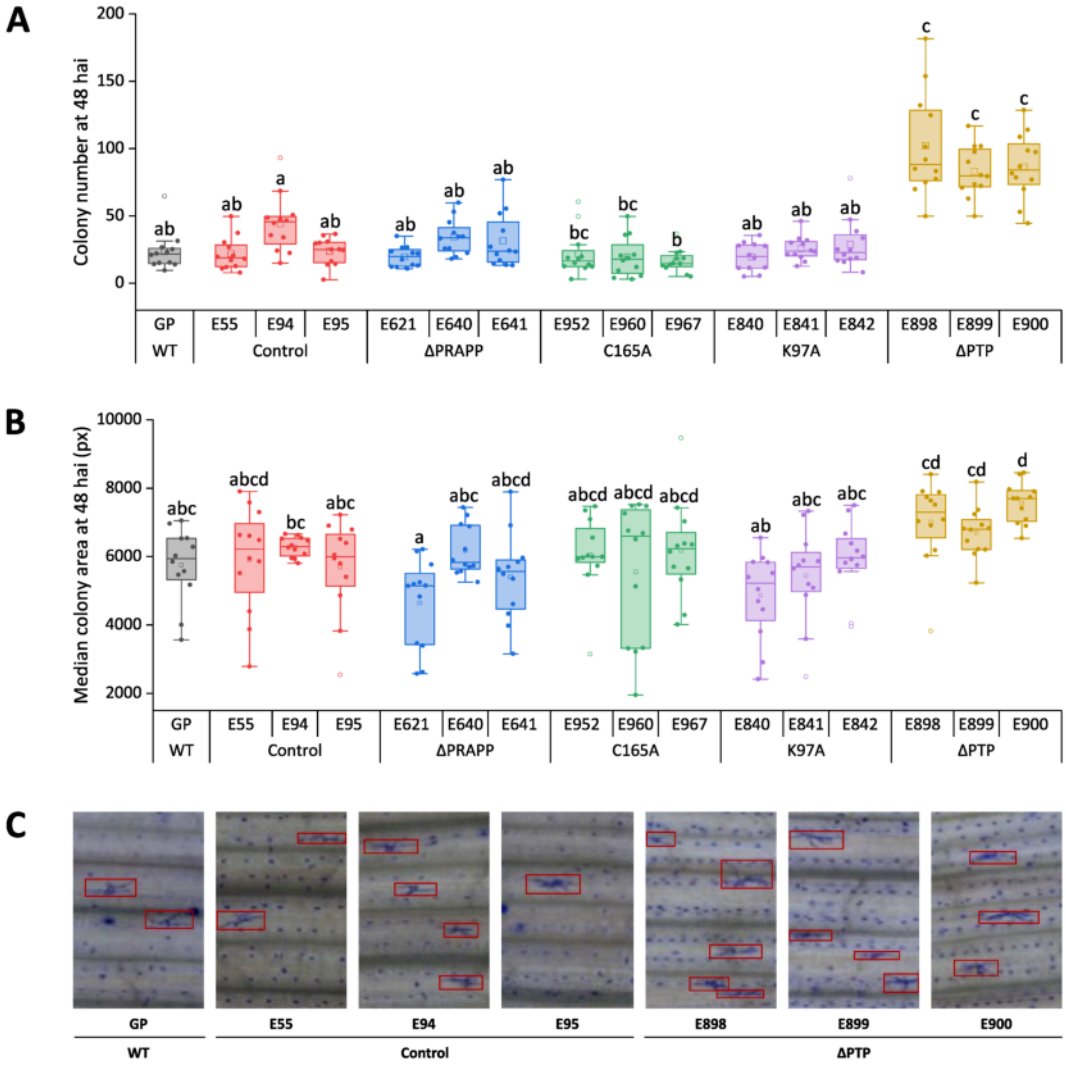

Figure 13. Response of *why1*-complemented variants to *Blumeria graminis* f. sp. *hordei* (*Bgh* isolate CH4.8) at 48 hours after inoculation (hai). **(A)** Colony number. **(B)** Median colony size. **(C)** Representative images of the wild type, Control line, and ΔPTP line. The measured colonies are shown in red boxes. Statistical analysis was conducted using Welch's ANOVA followed by the Games-Howell post hoc test ($\alpha = 0.05$) in IBM SPSS Statistics, version 28.

2.2 Establishing *why2* knockout mutant in *Hordeum vulgare* 'Golden Promise'

Generating a *why2* knockout mutant in barley is of particular interest, given that the biological function of the WHIRLY2 protein remains poorly understood in grasses. To date, *why2* knockout mutants have only been reported in *Arabidopsis thaliana*, a species that encodes three WHIRLY proteins. In *Arabidopsis*, functional redundancy exists as WHIRLY3 can compensate for the loss of WHIRLY1 and WHIRLY2 (Golin et al., 2020).

By contrast, barley contains only two WHIRLY proteins, WHIRLY1 and WHIRLY2. This suggests reduced functional redundancy and potentially more pronounced phenotypic consequences upon loss of WHIRLY2.

Table 3. gRNA spacer sequences targeting the *WHIRLY2* gene

Label	Ordered gRNA spacer	Sequence in *WHIRLY2*
gRNA 1	gTCAAAGATGCTCTCTGGAG[a]	TCAAAGATGCTCTCTGGAG
gRNA 2	aCTTCCCGGCAGTTGGACAA[b]	TCTTCCCGGCAGTTGGACAA
gRNA 3	ATCCATTATCACTGCCAAG[c]	TATCCATTATCACTGCCAAG
gRNA 4	GCACATCATGGGCTGGGACC	GCACATCATGGGCTGGGACC

[a]The gRNA 1 sequence identified by CRISPOR (Haeussler et al., 2016; Concordet & Haeussler, 2018) as a good guide starts with a thymine (T). Since we know that guides are more efficient when they start with a guanine, it was added to the beginning of the gRNA spacer sequence when ordering it.
[b]For guide efficiency reasons, the first thymine was replaced with adenine.
[c]For guide efficiency reasons, the first thymine was removed so that the guide starts with adenine.

The WHIRLY2 function has mainly been addressed using overexpression or knockdown approaches (Meng et al., 2020; Taylor et al., 2022). In barley, previous attempts to downregulate *WHIRLY2* expression using RNA interference were unsuccessful, preventing functional analysis of this protein. Therefore, targeted gene knockout using the CRISPR/Cas gene-editing system was employed to generate *why2* mutant lines, allowing direct assessment of WHIRLY2 function in barley.

To this end, four gRNA spacer sequences were designed to target the second, fourth, sixth, and eighth exon of the *WHIRLY2* gene (Table 3; Figure 14). Individual gRNA expression modules were assembled for each target site and subsequently combined with a Cas9 expression cassette and a placeholder (dummy) module to generate a higher-order construct using a manual modular assembly system optimised for RNA-guided Cas endonucleases in monocots (Hoffie, 2023; see Section 4.2.4). The resulting construct was then introduced into a binary vector suitable for *Agrobacterium*-mediated stable transformation (Figure 14B, Figure 14C).

To identify optimal CRISPR gRNA sequences for targeting the *WHIRLY2* gene in barley 'Golden Promise', candidate guides were selected using the CRISPOR web tool (Haeussler et al., 2016; Concordet & Haeussler, 2018). In addition, the secondary structure of each guide in combination with the scaffold sequence was predicted using the RNAfold web server (Hofacker et al., 1994; Lorenz et al., 2011) to assess guide accessibility and structural compatibility.

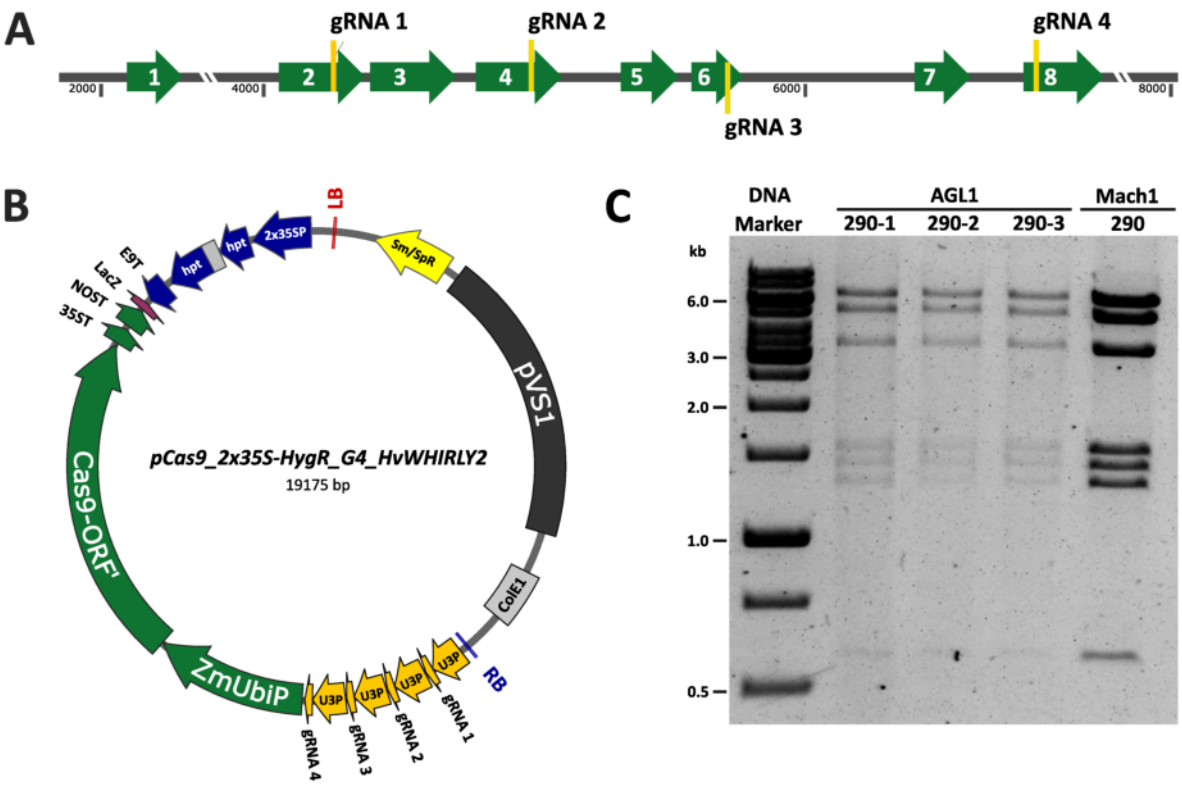

Figure 14. Schematic representation and validation of the final construct used for transformation. **(A)** Targeting sites of the Cas9 on the *WHIRLY2* gene of barley. In green numbered arrows are shown the exons; in yellow are shown the targeting sites of each gRNA. The lengths of exons shown in the image are in real scale. **(B)** gRNA-Cas9 construct used for the *Agrobacterium*-mediated transformation of the immature barley embryos. **(C)** Restriction digest analysis of three AGL1 colonies carrying the final construct. The Mach1 colony was used as positive control. AGL1, *Agrobacterium tumefaciens* AGL1; Mach1, *Escherichia coli* Mach1; kb, kilobase pairs; 290, vector number of the final gRNA-Cas9 construct used for stable transformation.

To evaluate the specificity of the four designed gRNAs targeting *WHIRLY2*, an *in silico* off-target analysis was performed using CRISPOR (Haeussler et al., 2016; Concordet & Haeussler, 2018). Potential off-target sites were identified by screening the barley reference genome GCA_902500625.1 for sequences with high similarity to each gRNA, allowing for mismatches. No perfect off-target matches were detected outside the *WHIRLY2* locus, indicating high target specificity (Table A3). Accordingly, the selected gRNAs are unlikely to induce unintended genomic modifications.

For stable transformation, immature barley embryos were used as explants (Hensel et al., 2008; Marthe et al., 2015). Plants regenerated from tissue culture (hereafter referred to as "regenerants") were transferred to greenhouse conditions optimised for barley approximately three months after transformation (Figure 15). The regenerants were subsequently screened for mutations and for the presence of the Cas9 expression cassette. Screening was performed using PCR and Sanger sequencing of PCR amplicons

(Table A4).

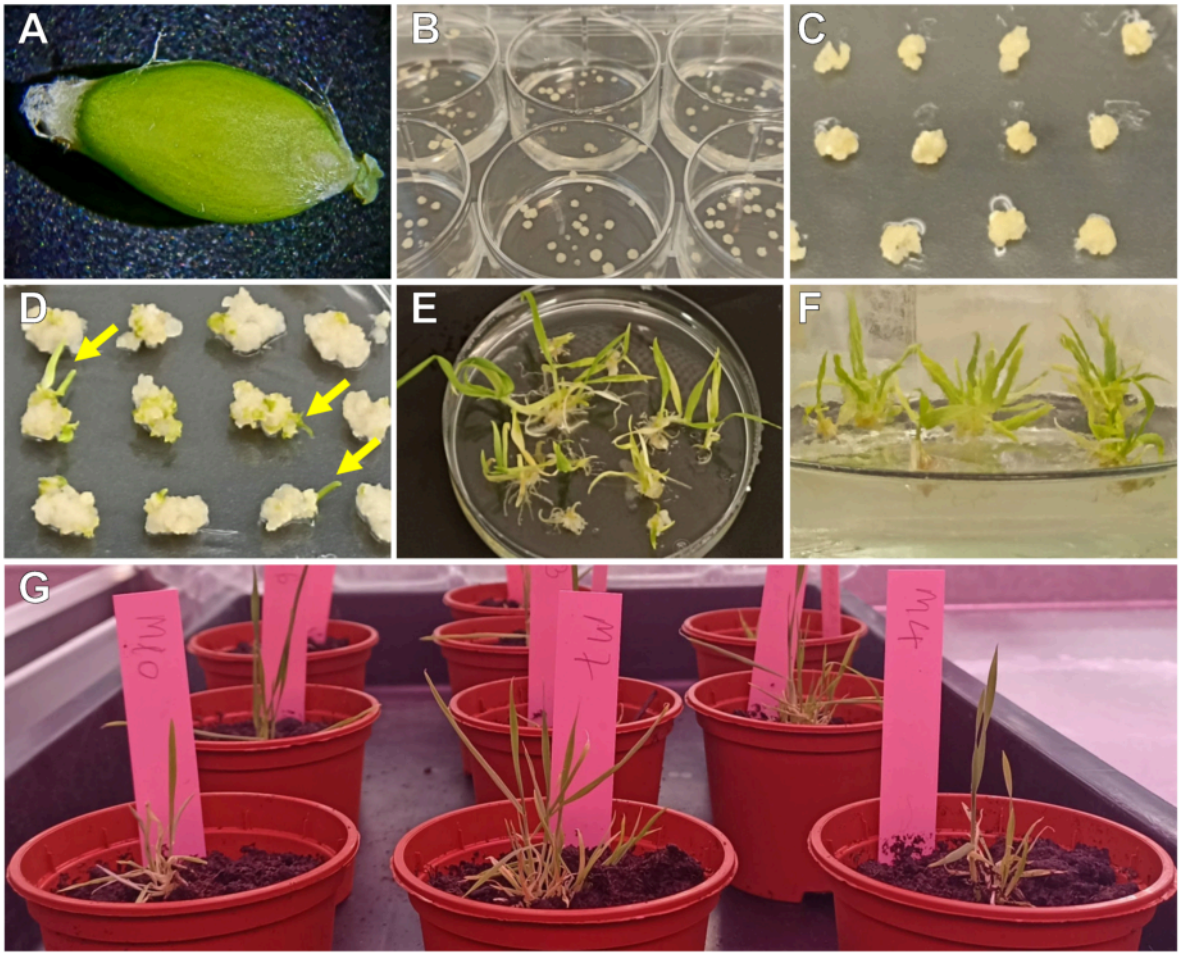

Figure 15. Visualisation of the different stages of stable transformation of cultivar 'Golden Promise'. Immature embryos were transformed with the gRNA-Cas9 construct designed to target different exons of the *WHIRLY2* gene. **(A)** Immature caryopsis. **(B)** Isolated embryos in co-cultivation medium 2 days post inoculation (dpi). **(C)** Calli on callus induction medium 2 weeks post inoculation (wpi). **(D)** Calli with embryogenic structures (indicated by yellow arrows) on regeneration medium (6 wpi). **(E)** and **(F)** Regenerants on regeneration medium 3 months post inoculation (mpi). **(G)** Regenerants transferred to soil in the greenhouse (3.5 mpi).

All genotyped *why2* mutant plants, including heterozygous and homozygous individuals, exhibited normal greenness and were visually indistinguishable from the wild-type plants under the growth conditions used (Figure A8). A small number of regenerants did not survive and, therefore, their genotype and potential mutation status could not be established (Figure 17).

The *why2* mutant plants reached harvest maturity approximately 4 months after being transferred to greenhouse conditions. The number of spikes varied between 25 and 75 per plant. However, many spikes were small, poorly developed and without grains.

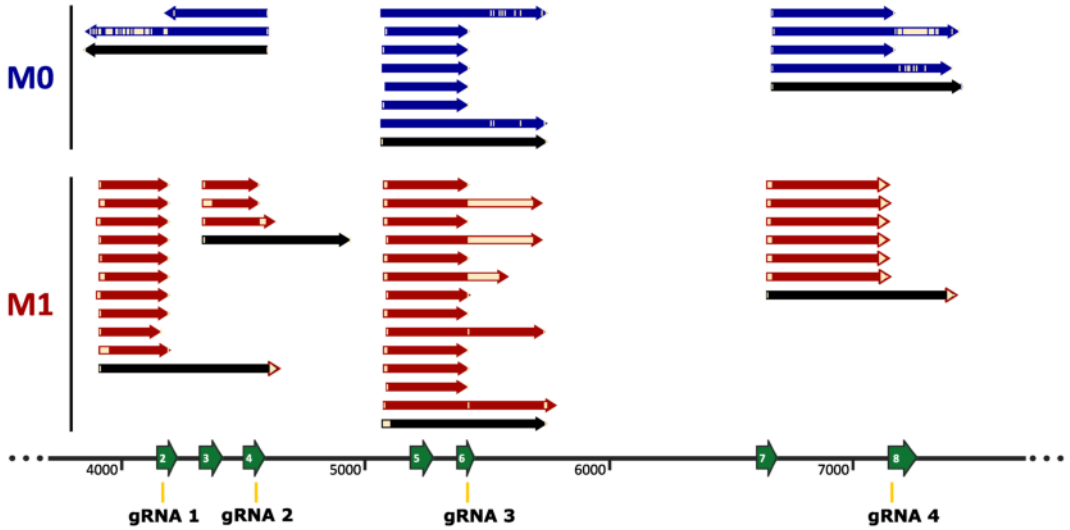

Figure 16. Sequencing analysis of M_0 and M_1 *why2* mutants. The M_0 mutants are shown in blue. The M_1 mutants are shown in red. The wild-type sequence is shown in black. Exons are shown in green. M_0, primary transformed mutant. M_1, first progeny generation mutant. The direction of the sequences is dependent on the primer used for sequencing. The lengths of exons and amplicons are in real scale.

For sequence analysis, primers were designed for each gRNA target site within the *WHIRLY2* gene (Table 7) and PCR amplicons were analysed via Sanger sequencing (Microsynth AG, Switzerland). Of the 51 regenerants, 31 carried the Cas9 expression cassette. Targeted mutagenesis was detected in 13 regenerants. These regenerants represent the primary transformed mutants (M_0). Eleven of the M_0 plants carried small insertions or deletions (indels) in a single exon, one carried mutations in two distinct exons, whereas one regenerant had mutations in the intron region. Mutations were identified in the second, sixth, and eighth exons, corresponding to target sites of gRNA 1, 3, and 4, respectively. No mutations were detected in the fourth exon, which was targeted by gRNA 2 (Figure 16A; Table 4).

Genome editing events were characterised using the Tracking of Indels by DEcomposition (TIDE) method (Brinkman et al., 2014). A single-nucleotide deletion was the most frequently observed mutation, and overall editing efficiencies ranged from 14.5% to over 90% (Table 4). With the exception of plant 32, which carried heterozygous biallelic mutations, all edited plants were heterozygous. In plant 32, one allele carried a single-nucleotide deletion, while the second allele carried a 42-nucleotide deletion extending from the exon into the upstream intron. This resulted in the predicted loss of 31 nucleotides from the second exon. Despite these mutations, no visible phenotypic differences were observed between the unedited and edited mutant plants, irrespective of

mutation type or zygosity (Figure 17).

Table 4. Sequencing analysis of the M_0 and M_1 *why2* knockout mutant plants using TIDE[a]

Generation	Exon	Plant number	Total efficiency (%)	R^2	Mutation type	Indel frequency (%)	p-value	Indel size range
M_0 plants	2	19	52.0	0.97	−1	46.3	0	50
		32	**90.4**	**0.90**	**−1** **−42**	**34.2** **48.2**	**1.10E-226** **0**	50
	6	3	14.5	0.90	−1 −6	4.0 7.8	8.10E-05 1.50E-14	50
		4	45.4	0.95	−1 −6	20.2 16.5	5.50E-294 4.40E-202	50
		5	60.5	0.94	−1 −6	28.4 24.1	0 0	50
		21	39.8	0.95	−1	30.7	0	50
		36	47.9	0.94	+1G	40.2	0	50
		38	49.9	0.92	−2	40.3	0	50
		40	15.7	0.92	−6	13.2	7.10E-47	50
	8	8	51.6	0.92	−1	40.0	1.40E-196	40
		14	31.3	0.57	ns	ns	ns	40
		21	64.2	0.90	−2 +1G	38.4 16.4	1.30E-222 4.10E-43	40
		29	34.1	0.92	+1A	19.2	5.20E-48	40
M_1 plants	2	19-55	52.4	0.95	−1	46.2	0	50
		19-56	52.9	0.95	−1	44.1	0	50
		19-57	53.3	0.95	−1	47.3	0	50
		19-60	52.6	0.95	−1	46.4	0	50
		19-61	51.2	0.95	−1	43.5	0	50
		19-70	53.3	0.96	−1	47.1	0	50
		19-72	51.1	0.95	−1	45.5	0	50
		19-74	51.4	0.95	−1	44.9	0	50
		32-100	**54.2**	**0.91**	**−41**	**48.0**	**0**	50
		5-224	37.3	0.96	+1C	31.4	0	30
	4	21-148	28.8	0.98	+1T	28.7	0	50
		5-224	75.2	0.97	−1 −15	20.8 53.3	0 0	30
		4-235	68.0	0.89	−1 −15	19.4 46.6	2.10E-246 0	40
	6	21-131	38.0	0.95	−1	29.2	0	50
		21-134	37.8	0.95	−1	29.1	0	50

Continued on next page

Table continued from previous page

Generation	Exon	Plant number	Total efficiency (%)	R^2	Mutation type	Indel frequency (%)	p-value	Indel size range
M_1 plants	6	21-138	51.9	0.94	−1	43.6	0	50
		21-148	37.8	0.95	−1	29.1	0	50
		38-161	49.0	0.95	−2	43.7	0	50
		5-222	28.0	0.95	+1G	20.2	3E-228	50
		5-224	32.3	0.93	−3	24.1	0	50
		4-227[b]	**92.9**	**0.93**	**−1** **−6**	**43.3** **42.0**	**0** **0**	**50**
		4-228	**95.2**	**0.95**	**−6**	**90.1**	**0**	**50**
		4-235	**92.1**	**0.92**	**−1** **−6**	**42.9** **42.3**	**0** **0**	**40**
		4-237	**93.3**	**0.93**	**−1** **−6**	**43.4** **43.5**	**0** **0**	**50**
		4-238	**92.7**	**0.93**	**−1** **−6**	**43.2** **43.3**	**0** **0**	**50**
		4-240	**95.6**	**0.96**	**−6**	**90.8**	**0**	**50**
	8	21-131	66.1	0.86	−2 +1G	39.4 15.4	1.40E-163 5.30E-27	40
		21-134	46.1	0.87	−2 +1G	18.6 15.5	1.20E-38 6.50E-28	40
		21-138	64.6	0.87	−2 +1G	17.8 34.8	1.20E-38 4.30E-146	40
		21-140	47.5	0.87	−2	36.7	1.10E-120	40
		21-147	63.4	0.87	−2	51.5	2.80E-206	40
		21-148	48.2	0.87	−2 +1G	18.9 17.1	2.80E-42 1.50E-35	40
		5-224	40.0	0.88	−1	25.6	1.40E-98	30

[a]The TIDE method was used to characterize the mutations induced in the *WHIRLY2* gene (Brinkman et al., 2014).
[b]In bold black are shown heterozygous biallelic plants. In bold green are shown the homozygous plants. The first number in the M_1 plant label shows the M_0 parent plant number, e.g.: 4-227 shows M_1 plant 227, progeny of M_0 plant 4.

To identify homozygous *why2* mutant plants, 24 grains were sown from each of five mutant M_0 individuals. These were plant 19 and 32 carrying indels in the second exon, plants 5 and 38 carrying indels in the sixth exon, and plant 21 carrying mutations in both the sixth and eighth exons (Table 4). Leaf material from the resulting T_1 seedlings was collected for screening of the Cas9 expression cassette and for sequencing of PCR amplicons corresponding to each targeted site, following the same approach as for the M_0 parent plants (Table A5).

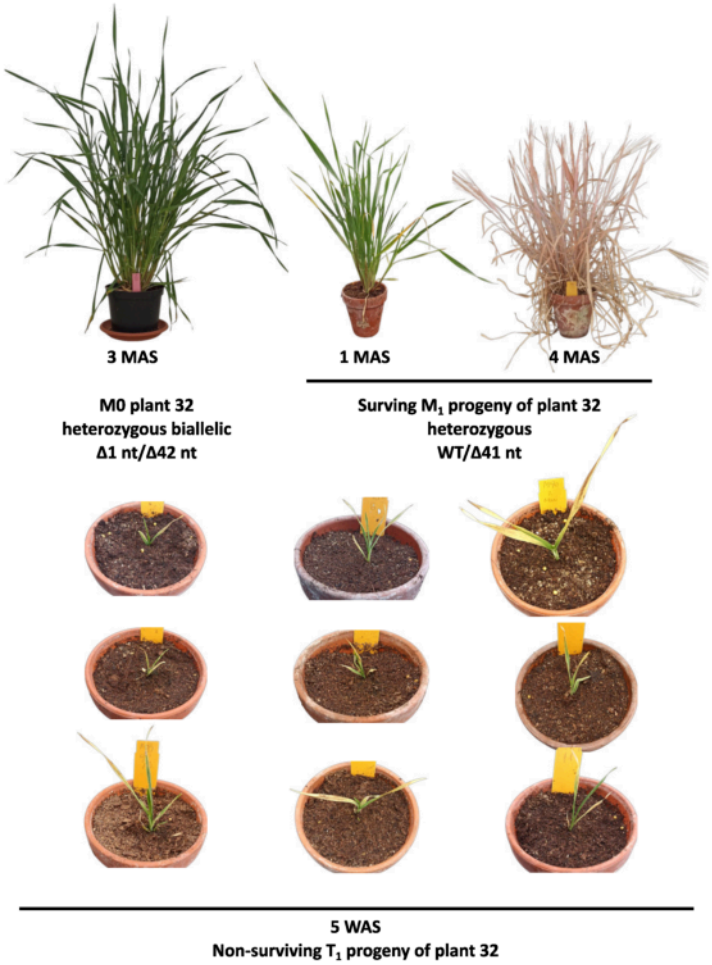

Figure 17. Progeny of the heterozygous biallelic M_0 plant 32. Out of 24 progeny, only one Cas9-free mutant plant survived, nine could not survive and died between 6 and 8 weeks after sowing, five were Cas9-positive and were not sequenced, eight carried no mutations, and one did not germinate. Only the surviving M_1 mutant and the non-surviving T_1 progeny are shown. WAS, weeks after sowing; MAS, months after sowing.

In total, 120 T_1 progeny were analysed, corresponding to 24 grains sown from each of the five M_0 plants. Seedlings that retained the Cas9 expression cassette were excluded from further analysis and were not sequenced. All remaining plants were analysed for indels across all targeted exons. In most cases, the first generation mutant progeny (M_1) exhibited the same indels as their respective M_0 parent plants. One exception was plant 21-148 (progeny of M_0 plant 21; Table 4), which additionally carried a mutation in the fourth exon targeted by gRNA 2 (Figure 16B).

Of the 120 T_1 progeny derived from the five M_0 plants, 21 seedlings exhibited delayed growth compared with the remaining individuals and died after 6 to 8 weeks after being transferred to soil. This phenotype was hypothesised to be associated with homozygous mutations. To avoid compromising plant development and to obtain suf-

ficient leaf material for sequencing, these plants were allowed to grow further before proceeding with sampling. However, the affected seedlings developed severe necrosis and premature senescence and died five to six weeks after sowing. Although limited leaf material was collected, genomic DNA isolation was unsuccessful and sequence analysis was not possible.

Table 5. Mutations at the cDNA and deduced protein sequence of the M_0 and M_1 *why2* mutant plants[a]

Nr.	Label	cDNA level mutation	Deduced protein sequence	Affected protein region
1	cDNA_WHIRLY2	702 nucleotides	233 amino acids	Unaltered reference protein
2	cDNA_2-1g[b]	c.75del	p.(W25*)	Organelle transit peptide, no WHIRLY domain
3	cDNA_2-42	c.43_74del	p.(R15Efs*18)	Organelle transit peptide, no WHIRLY domain
4	cDNA_2+1c	c.74_75insC	p.(W25Cfs*19)	Organelle transit peptide, no WHIRLY domain
5	cDNA_4-1a	c.291del	p.(Q98Kfs*22)	WHIRLY domain mutated and truncated
6	cDNA_4-15	c.277_291del	p.(F93_G97del)	WHIRLY domain 5 amino acids shorter
7	cDNA_4+1t	c.291_292insT	p.(Q98Sfs*18)	WHIRLY domain mutated and truncated
8	cDNA_6-1g	c.461del	p.(G154Afs*10)	WHIRLY domain mutated and truncated
9	cDNA_6-2gg	c.460_461del	p.(G154Qfs*2)	WHIRLY domain truncated
10	cDNA_6-3	c.460_462del	p.(G154del)	WHIRLY domain without G154
11	cDNA_6-6	c.460_465del	p.(G154_S155del)	WHIRLY domain without G154 and S155
12	cDNA_6+1g	c.461_462insG	p.(S155Qfs*2)	WHIRLY domain mutated and truncated
13	cDNA_8-1g	c.607del	p.(D203Tfs*?)	pvCBM mutated and nonstop mutation
14	cDNA_8-2gg	c.606_607del	p.(W202*)	pvCBM truncated
15	cDNA_8+1a	c.608_609insA	p.(D203Efs*16)	pvCBM truncated
16	cDNA_8+1g	c.607_608insG	p.(D203Gfs*16)	pvCBM truncated

[a]Alterations at the complementary DNA (cDNA) and protein level in different *why2* knockout mutants were described according to the Human Genome Variation Society (HGVS) recommendations for the description of sequence variants (Den Dunnen et al., 2016).
[b]Labels follow this format: cDNA_affected exon number ± number of nucleotides deleted (-) or inserted (+), with specific nucleotides indicated for one- or two-nucleotide indels.

The highest number of plants that did not survive belonged to the heterozygous biallelic M_0 plant 32. Among its 24 progeny, nine failed to survive, one did not germinate, five plants still carried the Cas9 expression cassette and were therefore excluded from further analysis, and eight were Cas9-free but showed no detectable mutations. Only one single Cas9-free individual, M_1 plant 32-100, carried a mutation consisting of a 41-nucleotide deletion spanning intron 1 and exon 2. Similar to the M_0 parent plant

32, this deletion is predicted to remove 31 nucleotides from the second exon.

To further identify viable homozygous mutants, progeny from additional M_0 plants 3, 4, 5, and 40 were selected for sequencing. These plants carried single- and six-nucleotide deletions, and it was hypothesized that homozygous individuals with in-frame six-nucleotide deletions might be viable. The viability of homozygous frameshift mutations was uncertain.

Sequencing analysis revealed that 23 progeny from these M_0 plants carried indels in one or more targeted exons (Table A5). For instance, plant 5-222 carried heterozygous mutations only in the fourth exon, whereas plant 5-224 carried heterozygous mutations in all four targeted exons. Most of the mutations were heterozygous. However, two plants, 4-228 and 4-240, were confirmed by Sanger sequencing and TIDE analysis as homozygous knockouts with in-frame six-nucleotide deletions. In addition, plants 4-227, 4-235, 4-237, and 4-238 were identified as heterozygous biallelic mutants, carrying both single- and six-nucleotide deletions in each of their alleles. TIDE analysis predicted editing efficiencies exceeding 92% for all of the sequenced homozygous M_1 plants (Brinkman et al., 2014). Homozygous and homozygous diallelic genotypes were further confirmed by manual inspection of Sanger chromatograms (Table 4).

The predicted consequences of these mutations at the protein level depend on their position within the *WHIRLY2* coding sequence. As expected, frameshift mutations in the second exon result in more severe effects. Indels at this position, introduced by gRNA 1, resulted in nonsense mutations and premature stop codons in both affected plants which lead to severely truncated proteins. Translation is interrupted within the organelle transit peptide (amino acids 1-35; mutations 2 to 4 in Table 5; Figure 18).

Mutations in the fourth exon targeted by gRNA 2 were detected in only three M_1 plants: 21-148, 5-224, and 4-235 (mutation 5 to 7 in Table 5). Each plant carried a distinct mutation affecting the WHIRLY domain. Two plants harboured frameshift mutations caused by either a single-nucleotide deletion or insertion, both of which introduced premature stop codons and resulted in truncation of the WHIRLY domain. In contrast, the third plant carried an in-frame 15-nucleotide deletion, leading to a WHIRLY domain shortened by five amino acids (Figure 18).

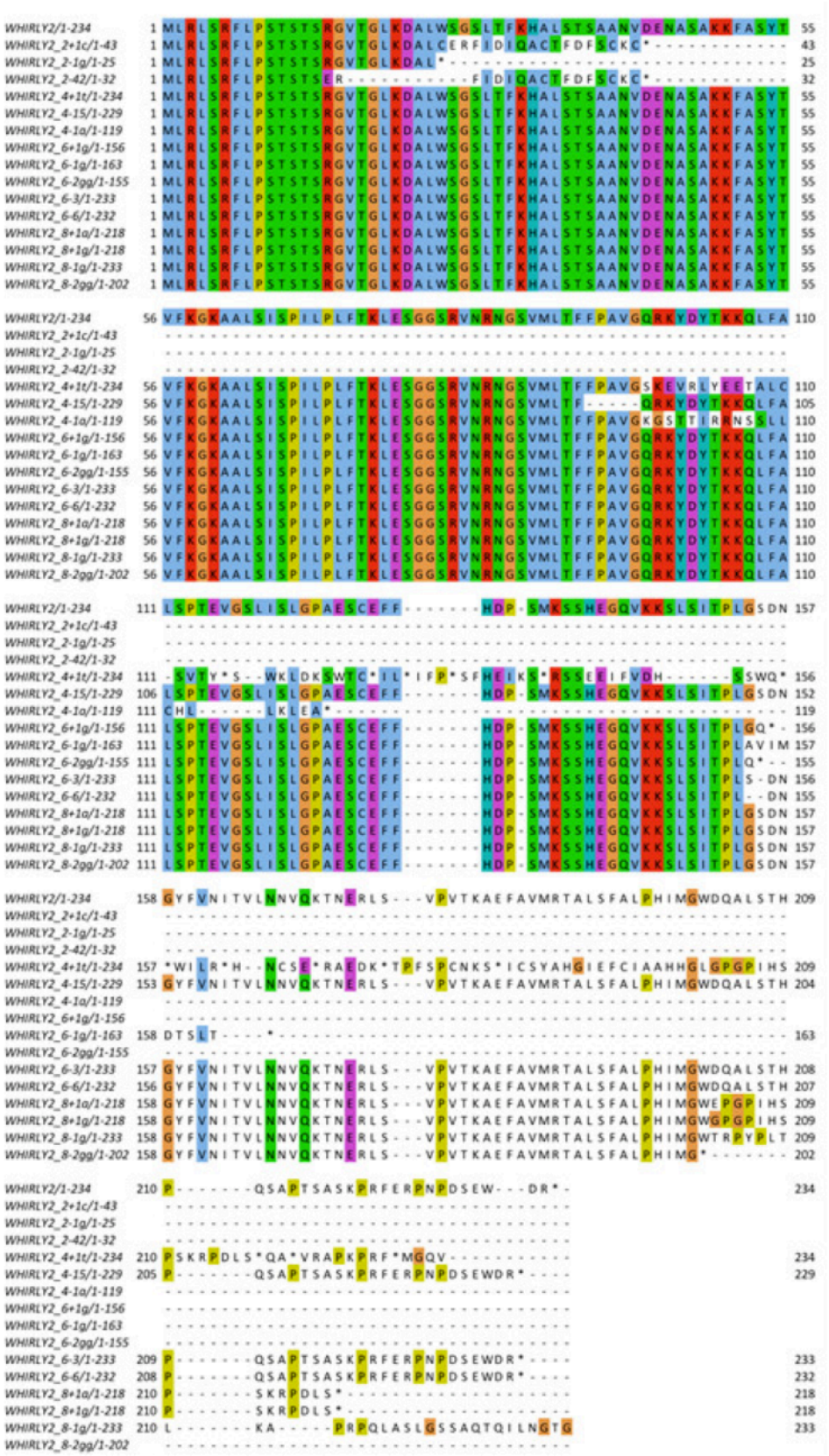

Figure 18. Deduced protein sequence alignments of *why2* mutant plants. Alignment was done with Clustal Omega (Madeira et al., 2024) and visualisation with Jalview 2.11.5.1. Amino acid colouring follows the Clustal scheme.

Several mutant plants carried nonsense mutations in the sixth exon targeted by gRNA 3 (mutations 8 to 12 in Table 5). In all cases, frameshift mutations introduced premature stop codons, truncating the predicted protein within the WHIRLY domain (amino acids 56–191), downstream the KGKAAL DBM. The DBM itself remained intact. In addition, a six-nucleotide deletion was detected in the sixth exon in several plants. This in-frame deletion resulted in the loss of two amino acids within the WHIRLY domain (mutation 11 in Table 5). As a result, the WHIRLY domain is slightly shorter, but all the rest of the WHIRLY2 protein is predicted to remain unaffected.

Some mutant plants carried nonsense mutations in the eighth exon, targeted by gRNA 4 (mutations 13 to 16 in Table 5). These mutations resulted from single-nucleotide insertions or deletions and introduced premature stop codons within the copper binding motif (amino acids 197–204). One particular single-nucleotide deletion resulted in a nonstop mutation, which may lead to the production of a misfolded or dysfunctional protein.

The *why2* mutants 228 and 240 are homozygous for the same six-nucleotide in-frame deletion (c.460_465del; p.G154_S155del) within the WHIRLY domain. As this deletion does not disrupt the reading frame, the WHIRLY2 protein is expected to be produced. The protein structures of wild-type WHIRLY2 and the *why2* in-frame homozygous mutants (mutants 228 and 240) were predicted using AlphaFold-Multimer v3. The resulting models display extended regions lacking defined secondary structure, corresponding to intrinsically disordered regions where no confident structural prediction could be obtained (Figure 19A; Figure 19B).

The two amino acids targeted for deletion are highlighted in red and are located within a loop region connecting two β-strands. This loop is spatially distant from the ssDNA-binding site identified in the WHIRLY structure (Cappadocia et al., 2010; PDB ID: 3N1K), suggesting that the deletions are unlikely to directly impair ssDNA binding. Consistent with this, AlphaFold-Multimer v3 predicts no effect of the deletions on the overall tetrameric structure of WHIRLY2, in agreement with their location in a flexible loop region.

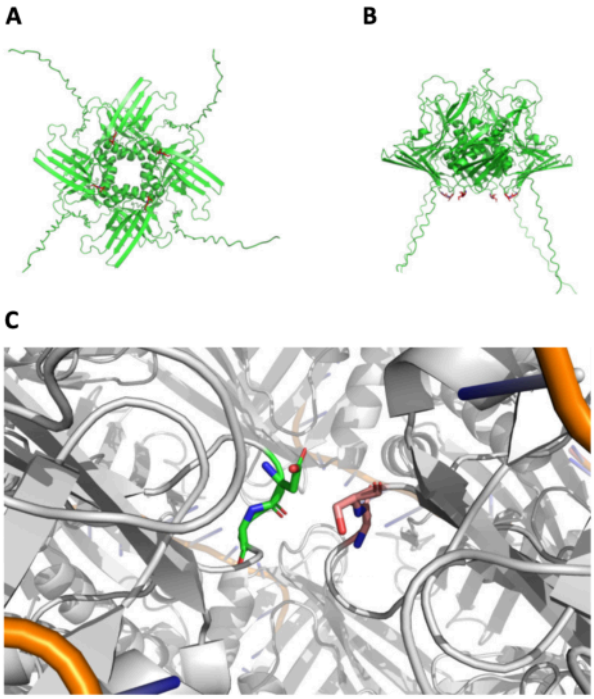

Figure 19. Structural modelling of WHIRLY2 and the predicted impact of in-frame deletions. **(A)** Top view and **(B)** side view of the AlphaFold-Multimer v3–predicted tetrameric structure of wild-type WHIRLY2. Regions lacking confident structural prediction are shown as extended strands and represent intrinsically disordered regions. The two amino acids targeted for deletion are highlighted in red and are located in a loop region connecting two β-strands. **(C)** Structural context of the deleted residues within the WHIRLY 24-mer assembly (based on PDB ID: 3N1I). The deleted residues (shown in red in A and B and in pink in **(C)** are positioned at an interface that allows interactions with a neighbouring chain from a symmetry-related tetramer (green). This neighbouring chain is part of the wild-type 24-mer assembly and does not represent a mutant-specific interaction.

However, when considering the higher-order 24-mer assembly of WHIRLY (PDB ID: 3N1I), the deleted residues are positioned at an interface that allows potential interactions with a neighbouring chain from a symmetry-related tetramer (Figure 19C). Based on this structural context, we hypothesize that the deletions may interfere with the formation or stability of the 24-mer complex, rather than affecting tetramer assembly or ssDNA binding directly.

3 Discussion

WHIRLY proteins are multifunctional single-stranded nucleic-acid binding factors that contribute to organellar genome maintenance and coordinate stress-related signalling between organelles and the nucleus (Cappadocia et al., 2010; Krupinska et al., 2022; Taylor et al., 2022). In barley, WHIRLY1 is dually localised to chloroplasts and nuclei and influences chloroplast development, nucleoid-associated processes, and nuclear stress-related gene regulation, thus linking organelle function with defence and acclimation responses (Desveaux et al., 2004; Grabowski et al., 2008; Melonek et al., 2010; Krupinska et al., 2014b; Krupinska et al., 2014a, 2019; Frank et al., 2024).

Despite this progress, it was unclear how individual conserved WHIRLY1 motifs and residues contribute to these functions *in vivo*. In addition, barley encodes a second WHIRLY protein, WHIRLY2, with an expression profile that differs from that of WHIRLY1. Until now, there are no studies that have addressed its role in barley development and stress responses using *why2* mutants.

This study investigated the functional contribution of conserved motifs and residues of the WHIRLY1 protein by analysing *why1*-complemented barley variants under controlled abiotic and biotic conditions and establishes CRISPR/Cas9-generated *why2* mutants in the barley 'Golden Promise' background which can serve as a foundation for targeted functional studies of WHIRLY2 in barley.

3.1 Plastid localisation of WHIRLY1 is essential for chloroplast development and stress responses

Under normal and stress conditions, the ΔPTP variant displayed a *xantha*-to-green phenotype similar to that of the *why1* mutant. As in the case of the *why1* mutant (Krupinska et al., 2024), the ΔPTP plants had leaves that eventually became green as leaves of the wild type, but its generation time was much longer.

WHIRLY proteins are nuclear-encoded proteins whose targeting properties depend on organelle targeting sequences (Krupinska et al., 2022). The PTP of WHIRLY1 promotes selective import into plastids, as demonstrated by *in vitro* import assays in Arabidopsis (Krause et al., 2005). In Arabidopsis, WHIRLY1 lacking the PTP accumulates exclusively in the nucleus, whereas the full-length protein localises to both the

nucleus and the plastid (Isemer et al., 2012a). In the mesophyll cells of barley leaves, WHIRLY1 is detected in both plastids and nuclei within the same cell (Grabowski et al., 2008; Krupinska et al., 2022), confirming the presence of both a native nuclear and plastid WHIRLY1. In regard to the subcellular localisation of the WHIRLY1ΔPTP protein, which was not tested in the present work, it is likely that removing the PTP prevents the plastid import of WHIRLY1, based on established mechanisms of protein import into chloroplasts (Nakai, 2018; Richardson & Schnell, 2020). In fact, western blot analysis showed that the WHIRLY1 protein abundance was reduced in the ΔPTP variant (Figure A1). Nuclear-encoded organellar precursors that fail to be imported are often ubiquitinated and degraded by the cytosolic ubiquitin–26S proteasome system to prevent cytosolic accumulation of unimported plastid-targeted proteins (Lee et al., 2009; Lee et al., 2013).

Plastid-localised WHIRLY1 supports proper chloroplast development (Krupinska et al., 2024). In WHIRLY1-deficient plants (RNAi-W1 and *why1* mutants), plastid WHIRLY1 levels are reduced or absent, resulting in enlarged nucleoids, delayed chloroplast development, and alterations in the plastid proteome (Krupinska et al., 2014a, 2019; Krupinska et al., 2024). WHIRLY1 deficiency also impairs the coordinated assembly of plastid- and nucleus-encoded photosynthetic proteins (Krupinska et al., 2019, 2019). Thus, the absence of plastid WHIRLY1 in the ΔPTP variant is likely to affect nucleoid organisation and delay the establishment of the photosynthetic machinery. In addition, WHIRLY1 has been found to associate with intron-containing plastid RNAs (Melonek et al., 2010), which suggests a role in post-transcriptional regulation beyond its function as a DNA-binding protein. Specifically, knockdown of *WHIRLY1* in barley leads to impaired splicing of *atpF* transcripts. Unspliced precursor transcripts overaccumulate, whereas the abundance of spliced *atpF* RNA is reduced (Melonek et al., 2010). This finding is consistent with results from maize, where *why1* mutants show a decreased ratio of spliced to unspliced *atpF* transcripts (Prikryl et al., 2008). A lack of plastid WHIRLY1 would therefore result in impaired splicing of plastid transcripts. This would affect the synthesis of photosynthetic proteins such as the ATP synthase subunit encoded by *atpF*, and would contribute to the delayed chloroplast development observed as the delayed greening phenotype in the ΔPTP variant.

Similarly to the barley *why1* mutant, the ΔPTP families showed a significant reduc-

tion in chlorophyll accumulation and in primary leaves. In the *why1* mutant, primary leaves contained less chlorophyll than the wild-type leaves throughout development. At 11 DAS, chlorophyll content was more than twofold higher in the wild type, and even at 21 DAS the chlorophyll content of mutant leaves remained clearly below wild-type levels (Krupinska et al., 2024). Chlorophyll in the *why1* mutant continued to increase until 20 DAS, whereas in the wild type it had already reached its maximum by 8 DAS. Plants of the ΔPTP variant showed a similar slow greening phenotype. At 11 DAS their leaves have about 30% of the wild-type level and and at 21 DAS it reached approximately 63–65% of the wild-type level. The continued increase until 21 DAS indicates a delay in chlorophyll accumulation relative to leaf development. Primary leaves of the ΔPTP families were also shorter than those of the wild type, as in the *why1* mutant. In the *why1* mutant, primary leaves reached only 65–75% of wild-type final length (Krupinska et al., 2024). In the ΔPTP families, primary leaf length was approximately 73% of the wild-type length under similar conditions. This reduction in leaf length in the ΔPTP lines should, however, be interpreted cautiously. Unlike the *why1* mutant, which lacks WHIRLY1 entirely, the ΔPTP variant may produce a truncated WHIRLY1 protein lacking the PTP sequence. This protein would be unable to enter the chloroplast. Chloroplast import is thought to be a prerequisite for subsequent nuclear localisation in the wild type (Krause & Krupinska, 2009; Isemer et al., 2012b), and therefore the subcellular localisation of the truncated protein in the ΔPTP variant remains unclear. The observed phenotype may reflect not only the absence of WHIRLY1 from plastids, but also the effects of a truncated WHIRLY1 that has not undergone chloroplast processing. Such a protein could differ functionally from the mature form present in the nucleus of wild-type plants.

In addition to differences in greenness and primary leaf length, the ΔPTP plants had significantly smaller root surface area compared to the wild type and the other *why1*-complemented variants under normal greenhouse conditions, whereas root length showed no significant differences. The impact on root morphology indicates that impaired plastid targeting of *WHIRLY1* might affect processes beyond chloroplast development in leaves. It has been found that barley growth depends on WHIRLY1 abundance. By using independent *WHIRLY1* overexpression lines with about 10-fold or 50-fold higher levels of WHIRLY1 protein, it was shown that lines with higher accu-

mulation exhibited stronger growth reduction, lower photosynthetic performance, as well as hormone changes such as lower levels of cytokinins, and higher levels of jasmonic acid (Frank et al., 2024). These findings indicate that the presence of WHIRLY1 in chloroplasts is required for normal plant growth and development. If the absence of PTP leads to a lack of WHIRLY1 in plastids, this could also affect plant growth in general and root growth in particular. One potential indirect route is a reduced supply of photosynthesis-derived sugars from the shoot. The transport of sugars via the phloem into the root and photosynthate from the cotyledons are necessary for root growth during the early stages of development (Kircher & Schopfer, 2012; Wang et al., 2018). This means that a shoot defect that reduces carbon assimilation or export would limit the availability of carbohydrates to the roots. In Arabidopsis, plastid-localised WHIRLY1 contributes to ABA responsiveness during germination (Isemer et al., 2012a). Because ABA regulates both seed germination and root growth (Liang et al., 2025b), altered ABA sensitivity could influence early root development as well. Moreover, deficiencies in plastid translation or photosynthesis have been shown to impair root growth (Nakata et al., 2018; Duan et al., 2021).

Under drought stress, the ΔPTP variant maintained a high PSII efficiency and chlorophyll content for longer than the wild type and the other *why1*-complemented variants, despite similar soil water loss. It is possible that the ΔPTP plants are unable to perceive or respond to drought stress, which would explain why PSII efficiency and chlorophyll content remained high despite similar soil water loss. This interpretation is supported by the observation that under well-watered conditions, no differences in PSII efficiency or chlorophyll content were detected between the ΔPTP variant, the wild type, and the green-phenotype variants suggesting that the effect is specific to the stress response rather than a consequence of delayed chloroplast development. The same was found for the foliage leaves of the *why1* mutant, which, under normal conditions, showed no significant differences in PSII efficiency in comparison to the wild type (Krupinska et al., 2024). Therefore, the sustained photosynthetic performance of the ΔPTP variant under drought most likely reflects an impaired ability to induce the stress and senescence response, rather than a consequence of its *xantha*-to-green phenotype. A mechanistically plausible explanation is that the lack of plastid-targeted WHIRLY1 impairs both the sensing of stress and the communication of the stress situation to the nucleus. As

a result, the associated nuclear transcriptional and epigenetic programmes that drive drought-induced senescence and photosynthetic downregulation are not activated. In fact, the behaviour of ΔPTP plants under drought conditions is similar to the previously reported senescence-related phenotypes observed in barley lines with modified *WHIRLY1* expression. In barley *WHIRLY1* knockdown lines under drought stress, the induction of senescence- and drought-associated genes and the decline in chlorophyll levels are delayed in comparison to the wild-type plants. In addition, a delay in the induction of nuclear genes related to drought and senescence as well as in histone acetylation changes were also reported (Janack et al., 2016). Similarly, *WHIRLY1* overexpression delayed the drought-induced onset of senescence and resulted afterwards in higher PSII efficiency and chlorophyll content than the wild type. This correlated with suppressed drought induction of ABA biosynthesis genes such as *NCED1*, carotenoid cleavage dioxygenase 5 (*CCD5*), and carotenoid cleavage dioxygenase 8 (*CCD8*) and the ABA-responsive senescence gene *S40*, as well as with lower ABA accumulation. Accordingly, reduced levels of the euchromatic marks H3K4me3 and H3K9ac at the promoter-proximal regions and around the transcriptional start site of *NCED1* and *S40* genes were observed (Manh et al., 2023). Taken together, these findings suggest that WHIRLY1 plays a broader role in stress sensing and communication between chloroplasts and the nucleus, as the delayed senescence response in *WHIRLY1* knockdown plants has also been observed under high light stress independently of drought (Kucharewicz et al., 2017).

The ΔPTP seedlings were smaller than those of the wild type. However, this size phenotype is unlikely to be caused by impaired PSII function as in the *WHIRLY1* overexpression lines (Frank et al., 2024), because the PSII efficiency of ΔPTP plants remains at wild-type levels until day 33, when senescence begins in the wild type. Instead, the smaller seedling size can be more likely associated with the root phenotype described above, i.e. fewer lateral roots and unchanged root length. The root system architecture is impaired which could cause a decrease of the absorptive surface area and potentially the whole-plant sink strength leading to limited shoot biomass accumulation even when PSII efficiency is still normal. After the onset of senescence under control conditions, PSII efficiency declines in the wild type but remains stable in the ΔPTP variant at least until 41 DAS (Figure 12), which suggests delayed senescence in the ΔPTP variant and

not a permanent difference in photosynthetic capacity.

Taken together, the studies on barley drought resistance demonstrate that the plastid localisation of WHIRLY1 is indispensable for a proper drought stress response. The ΔPTP phenotype observed in the present study indicates that it is not merely the abundance of WHIRLY1 but its specific localisation to chloroplasts that is the critical factor.

The importance of plastid-localised WHIRLY1 has also been demonstrated in other plant species. In Arabidopsis, loss of plastid WHIRLY proteins results in chloroplast genome instability and increased illegitimate recombination. This indicates a crucial role of these proteins in plastid DNA maintenance (Cappadocia et al., 2010; Lepage et al., 2013). In maize, complete loss of WHIRLY1 is required for chloroplast ribosome accumulation and plastid RNA metabolism, and maize *why1* mutants exhibit severe defects in chloroplast development (Prikryl et al., 2008), though it should be noted that these phenotypes reflect the absence of WHIRLY1 from both plastids and the nucleus rather than a specific loss of plastid targeting. Research comparing the full-length WHIRLY1 protein of Arabidopsis, which accumulates in both plastids and the nucleus, with a WHIRLY1 that accumulates only in the nucleus (as is hypothesised for WHIRLY1ΔPTP) found that the latter could not restore ABA responsiveness (Isemer et al., 2012a). Since the synthesis of ABA starts in plastids and ABA is an upstream regulator of drought-induced stress responses (Estrada-Melo et al., 2015), these results support the idea that plastid-targeted WHIRLY1 can modulate drought-associated gene reprogramming in the nucleus.

Other than modulating drought-associated gene reprogramming, plastid-targeted WHIRLY1 might also contribute to defence mechanisms during the early stages of pathogen infection. Upon powdery mildew inoculation, the ΔPTP plants were the only variant that showed increased susceptibility to this pathogen. This result is not unexpected given previous findings where WHIRLY1 abundance was shown to modulate powdery mildew susceptibility. In *WHIRLY1* overexpression lines, fungal colony formation was decreased, whereas in RNAi-W1 barley lines, as in the ΔPTP variant, it was increased (Frank et al., 2024).

Although the number of established colonies was higher, there were no differences in colony size among the *why1*-complemented variants and the wild type at 48 hai. Two possible explanations are that the differences in colony size may not yet be significant

enough to be detected at this early time point (Orton & Brown, 2016; Lück et al., 2025), or that, once established, the fungal colonies grow at similar rates in all variants (Godfrey et al., 2010; Lück et al., 2025).

The ΔPTP phenotypes under normal and stress conditions support a model in which plastid-localised WHIRLY1 contributes to coordinating chloroplast function with nuclear stress responses. WHIRLY1 has been detected in both chloroplasts and nuclei (Grabowski et al., 2008) and experiments in which an haemagglutinin (HA)-tagged version of Arabidopsis *WHIRLY1* was expressed from the plastid genome of tobacco demonstrated that a plastid-synthesised WHIRLY1 protein can be translocated from chloroplasts to the nucleus (Isemer et al., 2012b). Furthermore, phosphorylation of WHIRLY1 by Calcineurin B-Like-Interacting Protein Kinase 14 (CIPK14) promotes its accumulation in the nucleus and alters its plastid–nuclear distribution (Ren et al., 2017), demonstrating that this process is regulated. Since plastids generate retrograde signals that influence nuclear gene expression (Estavillo et al., 2011; Woodson et al., 2011), a mechanistic possibility consistent with the above findings is that WHIRLY1 participates in plastid-to-nucleus communication. Plastid-localised WHIRLY1 could either undergo modification within chloroplasts prior to relocation to the nucleus, or associate with plastid-derived nucleic acids or other molecules and thus contribute to the transmission of plastid status to the nucleus. Deletion of the plastid transit peptide in the ΔPTP construct would prevent chloroplast import and therefore eliminate any plastid-dependent processing or plastid-associated interactions occurring before nuclear localisation. As a result, ΔPTP phenotypes may reflect not only loss of WHIRLY1 function within chloroplasts but also the absence of a plastid-dependent modification required for the function of WHIRLY1 in the nucleus. The use of a *why1* knockout background for the generation of the *why1*-complemented variants ensured that the observed ΔPTP phenotypes reflect the functional properties of the modified WHIRLY1ΔPTP protein itself without contribution from the endogenous WHIRLY1. Direct experimental evidence whether WHIRLY1 carries or transmits a plastid-derived signal in this manner is currently lacking. To address this, it would be necessary to determine the subcellular distribution of WHIRLY1, assess chloroplast redox status and reactive oxygen species levels, and analyse downstream nuclear responses, such as stress-responsive microRNAs and changes in hormone signalling.

The other *why1*-complemented variants, the ΔPRAPP, K97A, C165A and control variants, displayed normal greening and were indistinguishable from the wild type under normal greenhouse conditions. Similarly, under drought stress, these variants followed the wild-type pattern of declining PSII efficiency and chlorophyll content, and when infected with powdery mildew, colony number was not significantly different from the wild type. These findings indicate that the PRAPP motif and the conserved residues K97 and C165 are not required for chloroplast development, stress responses under drought conditions, as well as for early resistance to powdery mildew. Instead, they may contribute to molecular processes that do not result in visible developmental or physiological changes.

In addition to the stress assays that have been discussed so far, the *why1*-complemented variants also differed in terms of generation times (Table 1). The green phenotype variants reached maturity within 4.5 to 6 months, whereas the wild type required only 3 to 4 months to mature under the same greenhouse conditions. For comparison, the three *xantha*-to-green variants, the ΔPTP investigated here, as well as the ΔCBM and K97AΔCBM that could not be advanced to homozygosity within the duration of this work, exhibited a significant delay in maturation. All three of them had generation times of 11 to 13 months, i.e. two or more years are needed to obtain homozygous lines from these variants. The *xantha*-to-green variants showed a significant delay in awn emergence (BBCH 49; Lancashire et al., 1991) compared to the green variants and the wild type, whereas the period from awn emergence to grain maturity was similar among all *why1*-complemented variants at approximately three months. This similarity suggests that the phenotypic differences among them occurred before awn emergence rather than during grain filling and ripening. However, this period was substantially longer than in the wild type, where grain maturity is typically reached within 10 to 30 days of awn emergence, which shows that development after awn emergence was also delayed in the variants relative to the wild type. These significant differences in generation time could be attributed to the crucial role that chloroplasts have in photosynthetic carbon assimilation and energy production. Chloroplast development requires proper plastid gene expression (Pfalz et al., 2006). Since this process is linked to plastid-to-nucleus retrograde signalling, any disruption in it may also alter developmental progression through changes in nuclear gene expression (Estavillo et al., 2011; Woodson et

al., 2013). WHIRLY1 has been shown to contribute to plastid nucleoid organisation and plastid gene expression (Melonek et al., 2010; Krupinska et al., 2014a). Therefore the lack of plastid WHIRLY1 in the ΔPTP variant could explain the delayed development of fully functional chloroplasts and the longer generation time. The developmental delay and *xantha*-to-green phenotype of the ΔCBM and K97AΔCBM variants suggest that the putative CBM motif may also play a role in chloroplast development, though its contribution remains unclear without further investigation of the homozygous lines.

3.2 Specific WHIRLY1 motifs modulate early developmental stages under combined high temperature and continuous light

The absence of a significant difference in primary leaf length under both normal and the combined high temperature and continuous light conditions suggests that this trait is unlikely to be determined by the motifs and residues modified in the WHIRLY1 protein. However, a comparison of the lengths of the primary leaves of each *why1*-complemented variant at high temperature and continuous light conditions with the primary leaf lengths at normal conditions, showed that all three K97A families and one C165A family had significantly shorter primary leaves at high temperature and continuous light conditions. These results suggest that both K97 and C165 are important for leaf growth under stress conditions.

The conserved lysine residue, part of the DBM (K97 in barley WHIRLY1, analogous to K91 in Arabidopsis WHIRLY1 and K67 to potato WHIRLY2), is critical for the DNA repair function of WHIRLY proteins (Cappadocia et al., 2010; Cappadocia et al., 2012). Structural studies in potato showed that K67 of the WHIRLY2 protein is required for higher-order assembly of WHIRLY tetramers into 24-mers upon binding long ssDNA without major changes of the tetrameric protein structure or short ssDNA binding (Cappadocia et al., 2012). Mutation of this residue in Arabidopsis WHIRLY1 (K91) interfered with the repair of DNA double-strand breaks (Cappadocia et al., 2012). The substitution of K97 with alanine could disrupt WHIRLY1's ability to form higher-order complexes on ssDNA and thereby its role in DNA double-strand break repair. Under continuous light and high temperature, chloroplasts are expected to experience increased photooxidative stress (Sun et al., 2016; Wang et al., 2018; Liang et al., 2025a) that po-

tentially could induce DNA lesions. WHIRLY1K97A may fail to prevent microhomology-mediated rearrangements, leading to an unstable plastid genome. Plastid genome instability and impaired chloroplast function can further enhance ROS accumulation and the activation of retrograde stress signalling (Lepage et al., 2013). This can induce the expression of defence genes and shift metabolism towards stress tolerance as in the *WHIRLY1* overexpression lines that upregulate defence at the expense of growth (Frank et al., 2024). In the K97A variant, DNA damage under stress could similarly affect retrograde signalling, leading to limited cell proliferation or hormone levels. This, in turn, could result in shorter leaves.

WHIRLY1 also affects nuclear regulation of chloroplast development (Krupinska et al., 2022). RNAi-W1 barley leaves showed different levels of transcription factors involved in chloroplast development and cell morphogenesis and fewer chloroplast proteins (Karpinska et al., 2022). If K97A changes would affect WHIRLY1 activity or stability, this could reduce the efficiency of plastid gene expression via PEP/NEP-dependent transcription, RNA metabolism, or nucleoid organisation, leading to a lower photosynthetic efficiency, thus limiting the resources needed for leaf growth.

Continuous light can induce chlorosis and impair photosynthetic performance (Velez-Ramirez et al., 2014; Liang et al., 2025a). High temperature, on the other hand, can destabilise thylakoid membranes and protein complexes, and accelerate chloroplast turnover (Wang et al., 2018). A dysfunctional WHIRLY1 under these stress conditions could compromise the chloroplast's capacity to preserve plastid genome integrity.

Another phenotype observed at high temperature and continuous light conditions was a reduced germination rate that varied from 41.6% to 87.5%, for all the variants despite prior cold stratification being applied to the grains. Cold stratification is known to accelerate germination by lowering seed ABA levels and increase gibberellin (GA)-synthesis genes (Gubler et al., 2008; Tuan et al., 2018). If these cold pre-treated grains are then exposed to stress conditions, stratification may provide some protection by activating stress responses, however, it could not fully counteract the effects of high temperature (Ullah et al., 2022) and continuous light (Roth-Bejerano et al., 2008; Gubler et al., 2008) on barley germination. There are studies showing that continuous blue light (Hoang et al., 2014) and continuous far-red light (Burger, 1965) inhibit barley germination under the different temperatures tested. However, in these studies, the highest

temperatures tested were 30 °C and 25 °C respectively, and barley grains were not cold stratified. The lower germination rates observed here most likely reflect the combined inhibitory effects of high temperature and continuous light, which cold stratification alone could not fully counteract.

Germination is impaired by both substitutions, but to different extents and under different conditions. C165A caused the most significant reduction at high temperature, with germination decreasing from 98% under normal conditions to approximately 50% at 34 °C. In contrast, K97A showed the lowest germination among all the variants under control conditions (79%) and the second-lowest under high temperature (68%; Figure 10). This suggests distinct functional roles for the two conserved residues. The most straightforward interpretation of the K97A substitution is that it affects higher-order protein assembly, since the equivalent lysine residue in Arabidopsis WHIRLY1 has been shown to be necessary for forming 24-mer complexes (Cappadocia et al., 2012). The stronger phenotype of C165A at high temperatures is more difficult to attribute to a simple structural defect and might be better explained by a role in stress-responsive regulation. It has been proposed that the conserved cysteine may participate in redox-dependent changes in the oligomerisation state of WHIRLY1 (Foyer et al., 2014), though this remains hypothetical. One possibility is that C165 contributes to stress-sensitive protein interactions that become less stable at high temperatures. However, the present data do not reveal whether the C165A effect is caused by changes in redox responsiveness, protein stability, or another aspect of WHIRLY1 function.

Overall, the germination phenotypes suggest that both residues are crucial for the positive impact of WHIRLY1 on germination but are unlikely to act via the same mechanism. In Arabidopsis, a truncated WHIRLY1 lacking the plastid transit peptide, which accumulates exclusively in the nucleus, cannot restore ABA responsiveness during germination in *why1* mutants, whereas the full-length protein present in both plastids and nucleus can (Isemer et al., 2012a). If, as hypothesised, the WHIRLY1ΔPTP protein in barley is similarly unable to enter plastids, the germination phenotypes of K97A and C165A may reflect impairment of specific aspects of plastid WHIRLY1 function that are required for ABA-dependent germination responses depending on whether stress is applied.

High temperature and continuous light stress also caused a delay in the emergence

of secondary leaves in all of the investigated variants as well as the wild type. This indicates that this response reflects a general effect of the growth conditions rather than a genotype-specific phenotype. Both, high temperature and continuous light are known to affect plant development. Temperature influences plant development in a stage-dependent manner (Granier et al., 2002), and continuous light can cause physiological stress (Velez-Ramirez et al., 2014; Sun et al., 2016; Wang et al., 2018; Liang et al., 2025a). Even though barley WHIRLY1 has been associated with early leaf development and coordination of plastid and nuclear gene expression (Krupinska et al., 2019; Karpinska et al., 2022; Saeid Nia et al., 2022), and WHIRLY1 deficiency affects light-dependent developmental responses, such as senescence progression and acclimation to high light (Kucharewicz et al., 2017; Saeid Nia et al., 2022), the delay in all plant lines including the wild type, suggests that WHIRLY1 is not a major determinant of leaf emergence under these conditions.

3.3 CRISPR/Cas9 editing of *WHIRLY2* and phenotypic consequences

This study established the first targeted genetic modifications of *WHIRLY2* in barley using CRISPR/Cas9 gene-editing technology. The resulting mutant lines carried either frameshift mutations predicted to disrupt protein function or in-frame deletions within the WHIRLY domain of the WHIRLY2 protein. Cas9-free T_1 plants carrying stable mutations (M_1 plants) were selected for phenotypic and genotypic analysis. Frameshift mutations were found only in heterozygous state in the genotyped mutants from multiple independent M_0 events. One Cas9-positive M_0 plant carried heterozygous biallelic frameshift mutations, with each allele carrying a different mutation. Homozygous in-frame or frameshift mutants could not be obtained from M_0 plants. In the next generation, M_1 mutants carrying homozygous in-frame deletions and heterozygous biallelic mutations were obtained. In the latter, one allele carried a premature stop codon caused by a single-nucleotide deletion, while the other carried an in-frame deletion of two amino acids. The inability to obtain biallelic frameshift Cas9-free mutants in this generation, whether homozygous or heterozygous, suggests that complete loss of WHIRLY2 function may compromise plant viability during early development.

Under normal greenhouse growth conditions, all genotyped *why2* mutants were indistinguishable from the wild type with respect to greenness and overall vegetative

morphology. The genotyped mutants are therefore unlikely to represent complete loss of WHIRLY2 function, which may explain the absence of a visible phenotype. Whether WHIRLY2 is required for normal vegetative growth under these conditions cannot be determined from the current mutant lines. The lack of a vegetative phenotype in *why2* mutants has also been observed in Arabidopsis. Loss-of-function Arabidopsis *why2* lines display disorganised mitochondrial nucleoids and reduced cristae density (Golin et al., 2020) but develop normally under normal conditions (Maréchal et al., 2008; Golin et al., 2020). Such findings suggest that changes in mitochondrial structure do not always lead to visible defects during vegetative growth. Instead, phenotypic consequences become apparent under conditions of high mitochondrial demand (Golin et al., 2020). Overexpression studies further illustrate that WHIRLY2 abundance affects mitochondrial function (Maréchal et al., 2008; Cai et al., 2015).

The predicted severity of the effect of the mutations depends on their position within the *WHIRLY2* gene. Frameshift mutations in the second exon are predicted to introduce premature stop codons truncated within the organelle transit peptide, upstream of the WHIRLY domain (Figure 3B). If the mRNA resulting from the transcription of the *WHIRLY2* carrying these premature stop codons can escape degradation by the nonsense-mediated decay mechanism (Urquidi Camacho et al., 2020; Bagherian et al., 2025) this could lead to the synthesis of a very short truncated protein. However, in the majority of cases nonsense-mediated decay (NMD) reduced the abundance of aberrant transcripts and thus limits the synthesis of truncated proteins (Urquidi Camacho et al., 2020; Krzyszton et al., 2025). In contrast, frameshift mutations occurring in the fourth, sixth, or eighth exon after glycine in position 154 (G154) located within the WHIRLY domain do not disrupt the conserved DNA-binding motif and may retain partial structural or functional properties if the truncated protein is synthesised. In plants, transcripts containing premature stops are targeted by NMD when they contain a strong plant NMD signal, especially a long 3' UTR or a 3' UTR intron located more than 50 nt downstream of the stop codon. In Arabidopsis, long 3' UTRs that trigger NMD are generally longer than 350 nt, although there are exceptions, and the efficiency of intron-based NMD increases with the distance between the stop codon and the downstream intron (Kalyna et al., 2012; Nyiko et al., 2013). Transcripts containing premature stop codons have been able to escape degradation and yield truncated proteins (Kralova et al., 2024).

For instance, an Arabidopsis study on the cytokinin receptor Cytokinin Response 1 / Arabidopsis Histidine Kinase 4 (CRE1/AHK4) showed that an intron-retention isoform introducing a premature stop codon was translated *in planta* into a truncated receptor that lacks the C-terminal receiver domain. A premature stop codon in the second exon would be expected to leave a longer downstream region and therefore a longer 3' UTR and splice junctions than a premature stop codon in the fourth, sixth, or eighth exon. This is consistent with the observation that the non-surviving T_1 regenerants were predominantly progeny of the M_0 mutants carrying frameshift mutations in the second exon. However, the association between frameshift mutations in the second exon and non-survival of the progeny does not prove causality.

In contrast to the phenotypes described above, a subset of T_1 progeny from four independent M_0 plants was characterised by delayed germination, reduced plant size, severe necrosis, and premature senescence. Unlike the *why2* mutants described above, which were genotyped and confirmed to carry mutations, these plants died before genotyping was possible, leaving their genetic status unresolved. Whether this phenotype resulted from *WHIRLY2* mutations or was a consequence of factors such as somaclonal variation or segregation distortion remains unclear. Given the role of WHIRLY2 in mitochondrial genome maintenance (Maréchal et al., 2008), biallelic loss-of-function mutations could impair early development. However, without genotypic confirmation, a causal relationship cannot be established. Interestingly, a phenotype similar to that of the non-surviving regenerants, smaller plants and accelerated leaf senescence, was also observed in the *WHIRLY2* overexpression lines in Arabidopsis (Maréchal et al., 2008). This similarity in phenotypes, observed under both reduced and increased WHIRLY2 levels, suggests that mitochondrial function is sensitive to WHIRLY2 abundance. In the overexpression lines, mtDNA abundance and mtDNA-encoded transcript levels were reduced, leading to decreased activity of respiratory chain complexes containing mtDNA-encoded subunits. The lack of a vegetative phenotype in the Arabidopsis *why2* mutants was attributed to a third WHIRLY protein, WHIRLY3, which is dually targeted to both chloroplasts and mitochondria. In mitochondria, WHIRLY3 is thought to compensate for the absence of WHIRLY2 only in the vegetative parts of the plant (Golin et al., 2020). Barley does not have a WHIRLY3 homolog. Therefore, the consequences of WHIRLY2 loss may be more severe in barley than in Arabidopsis. The Arabidopsis *why2* mutants

were also characterised by impaired germination, which suggests that early development may be sensitive to the absence of the WHIRLY2 protein. The delayed germination, necrosis, and premature senescence observed in the non-surviving regenerants support the hypothesis that they carried biallelic *WHIRLY2* loss-of-function mutations. These findings suggest that WHIRLY2 plays a more critical role in maintaining the stability of the mitochondrial genome during the early stages of barley development than it does in Arabidopsis. This could reflect differences between species in the ability of mitochondrial DNA repair pathways to compensate for the absence of WHIRLY2.

The most direct evidence of a link between biallelic frameshift mutations and non-survival of progeny comes from plant 32, which was the only M_0 plant to carry heterozygous biallelic frameshift mutations, with a different mutation in each allele (see Table 4). Of the 24 progeny of plant 32, nine died between six and eight weeks after sowing, and only one Cas9-free heterozygous mutant survived (Figure 17; Table A4; Table A5). Eight progeny carried no mutations, which confirms that some gametes transmitted a wild-type allele. The M_0 plant 32 itself showed no visible phenotype. This can be attributed to somatic mosaicism, a well-documented consequence of CRISPR/Cas9 editing in primary transformants, where the genotype identified in leaf tissue may not reflect the germline genotype uniformly. In such plants, editing occurs after cell lineages are already established, and different cell populations therefore carry different genotypes (Jang et al., 2016; Impens et al., 2022). The high proportion of non-surviving progeny from plant 32, compared to non-surviving progeny from heterozygous M_0 parents, is consistent with a higher probability of inheriting two non-functional alleles from a parent carrying frameshift mutations in both alleles.

In contrast to frameshift mutations, plants carrying the biallelic in-frame mutation p.G154_S155 deletion in the WHIRLY domain (corresponding to the sixth exon of *WHIRLY2*) remained viable and displayed no visible developmental phenotype under standard growth conditions. Structural modelling using AlphaFold-Multimer v3 predicted that the deleted residues were located within a surface-exposed loop of the WHIRLY domain and did not disrupt the core fold or tetramer assembly. WHIRLY proteins function as oligomeric DNA-binding complexes that are involved in nucleoid organisation (Cappadocia et al., 2010; Cappadocia et al., 2012). Therefore, maintaining the core structure and predicted DNA-binding surfaces of WHIRLY2 is expected to

preserve at least some of its mitochondrial genome maintenance activity. Modifications in surface-exposed regions may affect higher-order assembly or protein-protein interactions. However, structural modelling is only predictive, therefore experimental analyses will be necessary to determine whether the two-amino acid deletion affects WHIRLY2 function. Assays examining oligomer formation, DNA-binding affinity, and protein-protein interactions could clarify whether the mutation affects mitochondrial genome maintenance, under stress conditions or at specific developmental stages.

3.4 Distinct roles of WHIRLY1 and WHIRLY2 in barley

The results of this study help to clarify the roles of WHIRLY1 and WHIRLY2 in barley. WHIRLY1 which is required for normal chloroplast development and overall plant development, contributes to drought responses and early resistance to powdery mildew. These functions depend on its correct plastid targeting. The analysis of WHIRLY1 variant lines indicates that not all conserved motifs and residues contribute equally to development and stress responses. Deletion of the PTP caused a delayed chloroplast development and stress responses that differed from the wild type and the rest of the investigated variants. The presence of WHIRLY1 in plastids is important for its activity not only in the plastids but also in the nucleus. By contrast, substitutions in conserved residues such as K97 and C165 did not compromise normal development apart from a modest delay in maturation compared to the wild type. Their effects became apparent only under specific conditions, such as combined high temperature and continuous light stress. In addition, the generation time is longer in the absence of WHIRLY1 and in *why1*-complemented variants than in the wild type, and was most severely affected in the *xantha*-to-green variants. Plastid targeting therefore may be a crucial requirement for WHIRLY1 function, whereas the conserved residues modulate stress-associated responses rather than contribute to chloroplast development.

In contrast, the *why2* mutant lines did not display obvious vegetative differences from the wild type under standard growth conditions. Although WHIRLY2 has been associated with the maintenance of the mitochondrial genome in other species (Maréchal et al., 2008; Golin et al., 2020), confirmed biallelic *WHIRLY2* loss-of-function mutants could not be obtained in this study, which suggests that complete loss of WHIRLY2 function may compromise plant viability. As a result, the lack of a visible phenotype in

the surviving mutant lines should be interpreted cautiously.

Overall, the data support a functional divergence between WHIRLY family members in barley. WHIRLY1 plays a dominant role in chloroplast development and stress regulation. WHIRLY2 is likely involved in mitochondrial processes, but its contribution may be more evident under stress conditions, during early development, or during phases when the metabolic demand is high. Future work that enables recovery and validation of biallelic frameshift mutants of *WHIRLY2*, should clarify whether such mutants exist. In addition, appropriate tissue-culture controls are essential in order to distinguish the effects of CRISPR/Cas9-induced *WHIRLY2* mutations from the variation introduced during transformation and regeneration. These controls could include wild-type plants that have been regenerated using the same tissue-culture procedure, as well as plants that have been transformed using an empty vector.

3.5 Conclusions and outlook

This study analysed the functional relevance of conserved WHIRLY1 motifs and amino acid residues and generated targeted CRISPR/Cas9 *WHIRLY2* mutants in barley.

The most consistent phenotype was observed in the ΔPTP variant. Deletion of the plastid transit peptide resulted in delayed greening during early development, reduced root area under greenhouse conditions, a delayed decline in PSII efficiency and chlorophyll content during drought, and increased colony numbers after infection with powdery mildew. These findings suggest that the PTP and therefore, the plastid targeting of WHIRLY1, are required for proper chloroplast development and stress responses in barley. In contrast, the K97A, C165A and ΔPRAPP variants did not show any developmental differences from the wild type under normal conditions. Under high temperature and continuous light, however, specific motif-dependent effects were observed, including shorter primary leaves and reduced germination. These results suggest that the conserved residues K97 and C165 might play a role in stress sensitivity during early development, but are not important for chloroplast development.

Frameshift *WHIRLY2* mutations were detected in the M_0 generation in heterozygous states, either monoallelic, where only one allele carried a mutation or biallelic, where both alleles carried different mutations. Homozygous plants carried only in-frame deletions. All confirmed Cas9-free mutants obtained in this study were green and in-

distinguishable from the wild type under the conditions tested. In-frame deletions of *WHIRLY2* do not cause obvious vegetative phenotypes under normal greenhouse conditions. Nevertheless, since biallelic frameshift mutants could not be recovered, the possibility that complete disruption of *WHIRLY2* gene may affect plant survival cannot be excluded.

Several questions remain open. First of all, the subcellular localisation of the WHIRLY1ΔPTP protein needs to be immunologically tested on plastid and nucleus fractions. Although some observations suggest that the ΔPTP variant resembles the *why1* mutant, the difference in generation time indicates potential functional divergence. A comparison of plastid and nuclear transcript profiles among the wild type, *why1* mutant, and ΔPTP variant would therefore help determine whether WHIRLY1 can influence nuclear gene expression independently of its plastid localization. Second, the stress-dependent molecular mechanisms downstream of WHIRLY1 were not examined. Using the *why1* mutant and the wild type as controls, measurements of plastid and nuclear transcript profiles, chloroplast redox state, hormone levels (such as ABA and SA), and stress-responsive gene expression would help determine whether the presence of WHIRLY1 in plastids is associated with differences in the timing of drought-associated responses and the activation of defence processes that restrict fungal entry and establishment. Finally, the *why2* mutants require comprehensive investigations under abiotic and biotic stress conditions. Since biallelic frameshift mutations were not obtained despite extensive screening of M_0 lines and their progeny, further screening could help determine whether complete loss-of-function *why2* mutants are obtainable and whether such loss of function affects barley viability. In addition, detailed mitochondrial analyses should include assessment of mitochondrial nucleoid organisation, mtDNA copy number and recombination patterns, mitochondrial gene expression, respiratory complex activity, oxygen consumption rates, mitochondrial ultrastructure. Such assays would clarify whether CRISPR/Cas9-induced WHIRLY2 mutations impair mitochondrial genome stability, respiration, or early developmental processes. However, these effects would be expected only if the mutations lead to a reduction of WHIRLY2, which should be verified by assessing WHIRLY2 protein abundance using a specific antibody.

By establishing the importance of plastid targeting for WHIRLY1 function, identify-

ing residue-specific effects under stress conditions, and generating targeted *why2* mutants, this study provides a foundation for further investigation of WHIRLY protein function in barley.

4 Materials and Methods

4.1 Materials

4.1.1 Reagents, enzymes, kits, and antibodies

The PCR reagents used in this work were provided by Promega GmbH, Walldorf, Germany. Type IIP and IIS restriction enzymes, ligases, and their respective buffers were provided by the New England Biolabs GmbH (NEB), Frankfurt am Main, Germany and Thermo Fisher Scientific Inc., Waltham, MA, USA. The plasmid miniprep kits were provided by Macherey-Nagel GmbH & Co. KG, Düren, Germany and Thermo Fisher Scientific Inc., Waltham, MA, USA. Kits and other reagents used for protein analysis were provided by Bio-Rad Laboratories GmbH, Feldkirchen, Germany and EMD Millipore Corporation, Burlington, MA, USA. The antibodies were provided by Agrisera AB, Vännäs, Sweden and Thermo Fisher Scientific Inc., Waltham, MA, USA.

4.1.2 Microorganisms

The *Escherichia coli* strain Mach1 chemically competent cells (F– φ80 lacZΔM15 ΔlacX74 hsdR(rK–, mK+) ΔrecA1398 endA1 tonA, (Thermo Fisher Scientific Inc., Waltham, MA, USA) were used for the cloning of the CRISPR/Cas9 construct. The *Agrobacterium tumefaciens* (syn. *Rhizobium radiobacter*) strain AGL1 (AGL0 recA::bla pTiBo542ΔT Mop+ CbR) were used for the cloning of the CRISPR/Cas9 construct and for the stable transformation of immature barley embryos. *Blumeria graminis* f. sp. *hordei* isolate CH4.8 (*Bgh* CH4.8) was used for the powdery mildew assay of the *why1*-complemented variants.

4.1.3 Vectors

In Table 6 are listed all the vectors generated in this work. The backbone vectors and the pre-assembled vector CPGE_VEC00084, which provided the Cas9 expression cassette, and CPGE_VEC00089, which served as an auxiliary module containing a multiple cloning site, were generated by Hoffie (2023). CPGE_VEC000113 was cloned at the DNA Cloning Service e.K., Hamburg (dna-cloning.com).

Table 6. Expression-competent vectors generated for targeting the *WHIRLY2* gene

Vector name	Backbone	Insert(s)	Pol III promoter driving gRNA	Pol II promoter driving Cas9	Cas9 variant	Plant selection cassette	Bacterial selection marker	Terminator(s)	Vector role
CPGE_VEC00284	CPGE_VEC00058	gRNA expression unit 1	*OsU3*	–	–	–	*AmpR (bla)*	*U3* terminator (poly-T)	gRNA expression module; cloning intermediate
CPGE_VEC00285	CPGE_VEC00059	gRNA expression unit 2	*OsU3*	–	–	–	*AmpR (bla)*	*U3* terminator (poly-T)	gRNA expression module; cloning intermediate
CPGE_VEC00286	CPGE_VEC00060	gRNA expression unit 3	*OsU3*	–	–	–	*AmpR (bla)*	*U3* terminator (poly-T)	gRNA expression module; cloning intermediate
CPGE_VEC00287	CPGE_VEC00061	gRNA expression unit 4	*OsU3*	–	–	–	*AmpR (bla)*	*U3* terminator (poly-T)	gRNA expression module; cloning intermediate
CPGE_VEC00288	CPGE_VEC00070	Multi-gRNA expression unit	*OsU3*	–	–	–	*SpecR/SmR (aadA)*	*U3* terminator (poly-T)	Multi-gRNA expression module; cloning intermediate
CPGE_VEC00289	CPGE_VEC00072	Cas9 expression unit; multi-gRNA expression unit	*OsU3*	*ZmUbi1*	*Sp*Cas9 (maize codon-optimised)	–	*AmpR (bla)*	gRNA: *U3* terminator (poly-T); Cas9: *nos*, *35S*	Expression-competent assembly intermediate
CPGE_VEC00290	CPGE_VEC00113	Cas9 expression unit; multi-gRNA expression unit	*OsU3*	*ZmUbi1*	*Sp*Cas9 (maize codon-optimised)	2×35S::*hpt* (*HygR*)	*SpecR/SmR (aadA)*	gRNA: *U3* terminator (poly-T); Cas9: *nos*, *35S*; Plant selection marker: *Rbcs*-E9	Final expression vector

4.1.4 Primers

The primers used in this work are listed in Table 7. Primers were designed using the PCR Primer Design tool (Eurofins Genomics Europe Shared Services GmbH, Ebersberg, Germany). The gRNA spacer oligonucleotides were selected using the CRISPOR web tool (Haeussler et al., 2016; Concordet & Haeussler, 2018). They were synthesised by Biolegio BV (Zaltbommel, the Netherlands).

Table 7. Primers used in this study

Name	Type[a]	Nucleotide sequence (5' → 3')	Target/Binding site	Purpose of use
CPGE_PRM00045	Fwd	GGAGAGGACACGCTGAAATC	CaMV 35S enhanced promoter	PCR genotyping *why1*-complemented mutants
CPGE_PRM00047	Rev	GTGTCGTCCATCACAGTTTG	*hpt* gene	PCR genotyping *why1*-complemented mutants
CPGE_PRM00001	Fwd	TTTAGCCCTGCCTTCATACG	ZmUbi1 promoter	PCR genotyping of CRISPR/Cas9-edited regenerants
CPGE_PRM00011	Rev	TTAATCATGTGGGCCAGAGC	Cas9 gene	PCR genotyping of CRISPR/Cas9-edited regenerants
CPGE_PRM00009	Fwd	GCTCACATGTTCTTTCCTGCG	Vector backbones of all levels	PCR genotyping and sequencing of CRISPR/Cas9 constructs
CPGE_PRM00010	Rev	CACCTGACGTCTAAGAAACC	Vector backbones of all levels	PCR genotyping and sequencing of CRISPR/Cas9 constructs
PBC_PRM00142	Fwd	GGCATGCACATACAAATGGA	ZmUbi1 promoter	PCR genotyping of CRISPR/Cas9 constructs
CPGE_PRM00237	Fwd	TGGCGTCAAAGATGCTCTCTGGAG[b]	gRNA spacer 1 forward	Cloning of gRNA1 level 0 construct
CPGE_PRM00238	Rev	AAACCTCCAGAGAGCATCTTTGAC	gRNA spacer 1 reverse	Cloning of gRNA1 level 0 construct
CPGE_PRM00239	Fwd	TGGCACTTCCCGGCAGTTGGACAA	gRNA spacer 2 forward	Cloning of gRNA2 level 0 construct
CPGE_PRM00240	Rev	AAACTTGTCCAACTGCCGGGAAGT	gRNA spacer 2 reverse	Cloning of gRNA2 level 0 construct
CPGE_PRM00241	Fwd	TGGCATCCATTATCACTGCCAAG	gRNA spacer 3 forward	Cloning of gRNA3 level 0 construct
CPGE_PRM00242	Rev	AAACCTTGGCAGTGATAATGGAT	gRNA spacer 3 reverse	Cloning of gRNA3 level 0 construct
CPGE_PRM00243	Fwd	TGGCGCACATCATGGGCTGGGACC	gRNA spacer 4 forward	Cloning of gRNA4 level 0 construct

Continued on next page

Table continued from previous page

Name	Type[a]	Nucleotide sequence (5' → 3')	Target/Binding site	Purpose of use
CPGE_PRM00244	Rev	AAACGGTCCCAGCCCATGATGTGC	gRNA spacer 4 reverse	Cloning of gRNA4 level 0 construct
CPGE_PRM00245	Fwd	CTTTGACTTGTTCTCGCCC	*WHIRLY2* genomic locus, upstream of gRNA spacer 1	PCR genotyping and sequencing of CRISPR/Cas9-edited regenerants
CPGE_PRM00246	Rev	CTGCTTGTGACCAGTTTCC	*WHIRLY2* genomic locus, downstream of gRNA spacer 1	PCR genotyping and sequencing of CRISPR/Cas9-edited regenerants
CPGE_PRM00247	Fwd	ACAGCCTGCTACATGCTTC	*WHIRLY2* genomic locus, upstream of gRNA spacer 2	PCR genotyping and sequencing of CRISPR/Cas9-edited regenerants
CPGE_PRM00248	Rev	AACCTTCCTTCCCTCTTGAC	*WHIRLY2* genomic locus, downstream of gRNA spacer 2	PCR genotyping and sequencing of CRISPR/Cas9-edited regenerants
CPGE_PRM00249	Fwd	ACAGCCTAACAGTGAAGACC	*WHIRLY2* genomic locus, upstream of gRNA spacer 3	PCR genotyping and sequencing of CRISPR/Cas9-edited regenerants
CPGE_PRM00250	Rev	TTAACCACACATGCACACC	*WHIRLY2* genomic locus, downstream of gRNA spacer 3	PCR genotyping and sequencing of CRISPR/Cas9-edited regenerants
CPGE_PRM00251	Fwd	GCAGAAGACAAATGAACGCC	*WHIRLY2* genomic locus, upstream of gRNA spacer 4	PCR genotyping and sequencing of CRISPR/Cas9-edited regenerants
CPGE_PRM00252	Rev	GAACAGACACGAGAGAAACAC	*WHIRLY2* genomic locus, downstream of gRNA spacer 4	PCR genotyping and sequencing of CRISPR/Cas9-edited regenerants

[a]Fwd, Forward; Rev, Reverse.

[b]Adapter sequences are underlined.

4.1.5 Plant material

In this work, barley *Hordeum vulgare* L. 'Golden Promise' referred to as the "wild type" was used as a control. Immature barley embryos used for the *Agrobacterium*-mediated stable transformation also originate from the wild type. T_1 grains of the *why1*-complemented variants, homozygous grains of RNAi-W1 (Melonek et al., 2010), and of the *why1* barley knockout mutant (Krupinska et al., 2024) were obtained from

the group of Prof. Dr. Karin Krupinska (Plant Cell Biology, Christian Albrecht University of Kiel). The T_3 homozygous grains of the *why1*-complemented variants and the *why2* mutants were generated during this work. All mutant lines used here, except the *why1*-complemented variants, were generated in the 'Golden Promise' background. The *why1*-complemented variants were generated in the *why1* mutant background.

4.2 Methods

4.2.1 Greenhouse cultivation of barley plants

Barley *H. vulgare* L. 'Golden Promise' wild type, *why1*-complemented variants, and/or *why1* knockout mutants and RNAi-W1 were used in all assays. Before sowing, barley grains were stratified at 4 °C overnight. Only for homozygosity selection of the *why1*-complemented variants and the CRISPR/Cas9 regenerants and their progeny, the grains (and regenerants) were first sown in Floragard Floraton 3 soil (Floragard Vertriebs GmbH, Oldenburg, Germany) and cultivated for two weeks and afterwards, transferred to Einheitserde ED73 (Einheitserde Werkverband e.V., Sinntal-Altengronau, Germany) supplemented with 7% (v/v) sand and 4 g l^{-1} Osmocote® Exact Standard 3-4 M (ICL Group Ltd., Heerlen, The Netherlands). Plants were grown in this substrate until maturity. For the drought assay, after stratification, the grains were sown in 500 g of Einheitserde ED73 (Einheitserde Werkverband e.V., Sinntal-Altengronau, Germany) without additional supplementation. For the root assay, grains were sown in vermiculite supplemented with Hoagland's nutrient solution containing ferric ethylenediaminetetraacetic acid (EDTA) for two weeks (5 mM KNO_3, 5 mM $Ca(NO_3)_2$, 1 mM KH_2PO_4 (pH 6.0), 1 mM $MgSO_4$, 10 µM $MnCl_2 \cdot 4H_2O$, 1 µM $ZnSO_4 \cdot 7H_2O$, 0.5 µM $CuSO_4$, 30 µM H_3BO_3, 1 µM $Na_2MoO_4 \cdot 2H_2O$, 0.5 µM $Co(NO_3)_2 \cdot 6H_2O$, 27 µM ferric EDTA). Plants were grown in greenhouse chambers under controlled conditions. Day and night heating temperatures were set to 18 °C and 16 °C, respectively. Day and night ventilation temperatures were maintained at 21 °C and 19 °C, respectively. Plants were grown under a 16-h light / 8-h dark photoperiod with a light intensity of 350 µmol m^{-2} s^{-1}.

4.2.2 Climate chamber cultivation of barley plants

Experiments combining different temperature and light conditions were conducted in type L2 growth chambers (Poly Klima GmbH, Freising, Germany). Grains were cold stratified for 3 days at 6 °C in darkness before transfer to Einheitserde ED73 (Einheitserde Werkverband e.V., Sinntal-Altengronau, Germany) or vermiculite supplemented with Hoagland's nutrient solution (described in Section 4.2.1). Growth conditions related to the specific conditions of temperature and light are described in Section 4.2.7.1.

4.2.3 Generation and selection of homozygous *why1*-complemented lines

Segregation of the hygromycin phosphotransferase (*hpt*) selectable marker, which confers resistance to hygromycin B, was analysed in progeny derived from independently regenerated primary transformants (T_0). Mendelian inheritance of a single transgene locus was assumed, corresponding to an expected segregation ratio of 3:1. For each of seven independent constructs, spikes harvested from 12–14 independent T_0 plants were used to generate first transgenic generation T_1 families, where each family represents the selfed progeny of a single T_0 plant. For segregation analysis, 11 T_1 grains per family were sown. After 14 days of growth, leaf material was collected from individual T_1 seedlings' leaves, genomic DNA was isolated and the presence or absence of the *hpt* gene was determined by PCR (see Section 4.2.5) using *hpt*-specific primers (Table 7). Each T_1 family was assessed for the number of *hpt*-positive and *hpt*-negative seedlings and evaluated against the expected 3:1 segregation ratio. Because family sizes were small (typically 11–12 seedlings, occasionally fewer due to failed germination), deviation from the expected segregation ratio was tested using an exact binomial test. For comparison, chi-squared (χ^2) values were additionally calculated (Table A1). Only T_1 families exhibiting segregation consistent with single-locus Mendelian inheritance were advanced. From each such family, four to six T_1 plants were selected and grown to maturity. All remaining plants from these families, as well as all families that did not conform to the expected segregation ratio, were discarded. Grains harvested from each kept T_1 plant were kept separate and constituted T_2 grain families. For each *why1*-complemented variant, four to six independent T_2 families were analysed. From each T_2 family, 12 T_2 grains were sown and screened at 14 days for the presence of *hpt* by

PCR as described in Section 4.2.5.2. T_2 families in which all tested seedlings were *hpt*-positive were classified as homozygous for the *hpt* transgene. All other T_2 families were discarded. From each homozygous T_2 family, four to six T_2 plants were grown to maturity. The T_3 grains harvested from these plants were considered homozygous and were used for characterisation experiments under normal or stress conditions.

4.2.4 Generation of *why2* CRISPR/Cas9 mutants

WHIRLY2 knockout mutants (*why2*) were generated in the barley *Hordeum vulgare* L. 'Golden Promise' background using the CRISPR/Cas9 gene-editing system.

4.2.4.1 Design of guide RNA spacer oligonucleotides

Guide RNAs (gRNAs) targeting *WHIRLY2* were designed based on the *H. vulgare* reference genome (GCA_902500625). Candidate target sites were selected using the CRISPOR online tool (Haeussler et al., 2016; Concordet & Haeussler, 2018) with the SpCas9 NGG protospacer adjacent motif. Guide RNAs with high predicted on-target activity and low off-target potential were selected. The potential off-target sites of the selected gRNAs were then assessed *in silico* using the same tool, based on the same reference genome (Table A3). To ensure compatibility with the standard gRNA scaffold, the secondary structure of the selected gRNAs was evaluated using RNAfold (Hofacker et al., 1994; Lorenz et al., 2011). Based on these results, four guides, gRNA1, gRNA2, gRNA3, and gRNA4, were selected to target the second, fourth, sixth, and eighth exons of the *WHIRLY2* gene, respectively. Next, adapters suitable for Golden Gate cloning according to the method described in Hoffie (2023) were added: TGGC for the forward gRNA spacer oligonucleotides and AAAC for the reverse gRNA spacer oligonucleotides (Table 7).

4.2.4.2 Assembly of CRISPR/Cas9 constructs

A modular Golden Gate-based CRISPR/Cas9 vector system for monocot plants, following the CasCADE system described by Hoffie (2023), was used to assemble a CRISPR/Cas9 plasmid construct targeting the barley *WHIRLY2* gene. Cloning was performed in successive assembly levels (Level 0–II), followed by integration into a binary vector suitable for

Agrobacterium-mediated transformation of immature barley embryos. Annealing of the gRNA spacer nucleotides was done by mixing 5 µl of the forward and 5 µl of the reverse oligonucleotide (Table 3). The mixture was incubated at 95 °C for 5 min. Afterwards, the oligonucleotides were hybridised at room temperature for 20 min.

Level 0 assembly. Each of the four annealed gRNA spacer oligonucleotides was assembled into each of the four respective generic gRNA module vectors (Table 6). Cut-ligation reactions were performed in a total volume of 10 µl using 15 ng of the respective destination vectors CPGE_VEC0058, CPGE_VEC0059, CPGE_VEC0060, and CPGE_VEC0061 (vectors pIK1–pIK4 in Hoffie 2023), 1.5 µl 10 µM annealed gRNA spacer oligonucleotides, 1x CutSmart® Buffer (New England Biolabs, NEB; Cat. No. B7204), 0.5 µl of 10 mM ATP (NEB; Cat. No. P0756), 10 units of BsaI-HF (NEB; Cat. No. R3535), and 200 units of T4 DNA Ligase (NEB; Cat. No. M0202). Reactions were incubated in an Eppendorf Mastercycler® nexus X2 (Eppendorf AG, Hamburg, Germany) using alternating cycles of 37 °C for 5 min and 22 °C for 10 min, repeated 10 times, followed by a final incubation at 37 °C for 30 min and enzyme inactivation at 75 °C for 15 min. The resulting ligation products were transformed into chemically competent *Escherichia coli* Mach1(Thermo Fisher Scientific Inc., Waltham, MA, USA) by heat shock according to the manufacturer's instructions, following the method originally described by "Studies on transformation of *Escherichia coli* with plasmids" (1983). Transformants were selected on Luria-Bertani, Miller formulation (LB; Sambrook et al., 1989) agar (10 g l^{-1} tryptone, 5 g l^{-1} yeast extract, 10 g l^{-1} NaCl, 15 g l^{-1} agar), with 100 µg ml^{-1} carbenicillin. For colony PCR, individual colonies were picked directly from the selective agar plates and used as template DNA. The colony PCR conditions are described in Section 4.2.5.2, with modifications in the annealing temperatures adjusted to the primer pair used. The correct clones were propagated in LB liquid culture with 100 µg ml^{-1} carbenicillin, and the plasmid DNA was isolated using the NucleoSpin Plasmid Mini Kit (Macherey-Nagel GmbH & Co. KG, Düren, Germany) according to the manufacturer's instructions. The sequence integrity of the gRNA cassettes was then confirmed by Sanger sequencing (Microsynth AG, Balgach, Switzerland). The verified constructs for gRNA modules 1 to 4 were designated CPGE_VEC00284, CPGE_VEC00285, CPGE_VEC00286 and CPGE_VEC00287, respectively.

Level I assembly. The four individual Level 0 gRNA modules, CPGE_VEC00284,

CPGE_VEC00285, CPGE_VEC00286 and CPGE_VEC00287, were assembled into a multi-gRNA expression unit using the generic gRNA assembly vector CPGE_VEC00070, which allows the combination of up to four gRNA expression units via Esp3I-compatible overhangs (Table 6). Cut-ligation reaction conditions and cycling parameters were identical to those used for Level 0 assembly, except that 5 units of Esp3I (NEB; Cat. No. R0734) were used. The molar insert-to-vector ratio was approximately 10:1. Ligation products were transformed into *E. coli* Mach1 cells as described for level 0 assembly and selected on LB agar containing spectinomycin (100 µg ml^{-1}). Correct assembly was assessed by colony PCR using the appropriate primers (Table 7). The correct clones were propagated in LB liquid culture with spectinomycin (100 µg ml^{-1}). Plasmid DNA was isolated as described for level 0 assembly and analysed by restriction digestion. The digestion reaction was performed in a 10 µl volume using 1× rCutSmart Buffer (NEB; Cat. no. B6004), 4 units of EcoRI-HF (NEB; Cat. no. R3101), 4 units of BamHI-HF (NEB; Cat. No. R3136), and 4 units of PvuI-HF (NEB; Cat. no. R3150), with 200 ng of plasmid DNA. Reactions were incubated under conditions recommended by the manufacturer. Sequence integrity was confirmed by Sanger sequencing (Microsynth AG, Balgach, Switzerland). The verified multiplex gRNA construct was designated CPGE_VEC00288.

Level II assembly. To assemble the complete gRNA/Cas9 expression unit, the multiplex gRNA cassette CPGE_VEC00288 was combined with a preassembled Cas9 expression module, CPGE_VEC00084, and an auxiliary module containing a multiple cloning site, CPGE_VEC00089, in the transformation vector CPGE_VEC00072 (Table 6). Assembly reactions were carried out using BsaI-mediated cut–ligation, as described in the level 0 assembly. Reaction mixtures contained approximately 75 ng of CPGE_VEC00072 and 80-90 ng of each insert vector, corresponding to an overall insert-to-vector ratio of approximately 3:1. Ligation products were transformed into *E. coli* Mach1 cells as previously described and selected on LB agar containing carbenicillin (100 µg ml^{-1}). Correct assembly was assessed by colony PCR, and the correct clones were propagated in liquid culture with carbenicillin (100 µg ml^{-1}). Plasmid DNA was isolated as previously described and analysed by restriction digestion. Digestion reactions were performed as described in level I assembly with only EcoRI-HF (NEB; Cat. no. R3101) and BamHI-HF (NEB; Cat. No. R3136). Sequence integrity was confirmed by Sanger sequencing (Microsynth AG, Balgach, Switzerland). The verified gRNA/Cas9 construct was designated

CPGE_VEC00289.

Final assembly. For plant transformation, the fully assembled gRNA/Cas9 expression unit CPGE_VEC00289 was transferred into the binary destination vector CPGE_VEC00113 (Table 6) by SfiI-mediated digestion followed by ligation. Both vectors were digested separately using SfiI FastDigest (Thermo Fisher Scientific; Cat. No. FD1824) in FastDigest buffer at 50 °C for 2 h, using approximately 1 µg plasmid DNA per reaction. Digested fragments were ligated at an approximate insert-to-vector ratio of 10:1 using 400 units T4 DNA ligase (NEB; Cat. No. M0202) and 1x T4 DNA ligase reaction buffer (NEB; Cat. No. B0202) in a 10 µl reaction. Ligation reactions were transformed into *Escherichia coli* Mach1 cells as previously described and selected on LB agar containing spectinomycin (100 µg ml^{-1}). Correct assembly of the final construct CPGE_VEC00290 was confirmed by restriction digestion as described for level I assembly using 4 units of EcoRI-HF (NEB; Cat. No. R3101) and 4 units of NotI-HF (NEB; Cat. No. R3189). The resulting binary construct was introduced into *Agrobacterium tumefaciens* (syn. *Rhizobium radiobacter*) strain AGL1 by electroporation. In pre-chilled electroporation cuvettes, 100 ng of the plasmid DNA was mixed with 50 µl of electrocompetent AGL1 cells. Electroporation was performed using an Eppendorf electroporator 2510 device (Eppendorf AG, Hamburg, Germany) set to 2.4 kV. Immediately afterwards, 500 µl Super Optimal broth with Catabolite repression (SOC) medium (20 g l^{-1} tryptone, 10 g l_{-1} yeast extract, 17 mM NaCl, 2.5 mM KCl, and 10 mM $MgCl_2$) was added, and cells were allowed to recover for 3 h at 28 °C and 180 rpm. Transformed cells were plated on MG/L agar medium (Tingay et al., 1997; 5 g l^{-1} mannitol, 1 g l^{-1} L-glutamic acid, 0.25 g l^{-1} KH_2PO_4, 0.10 g l^{-1} NaCl, 0.10 g l^{-1} $MgSO_4 \cdot 7H_2O$, 1 ng ml^{-1} biotin, 5 g l^{-1} tryptone, 2.5 g l^{-1} yeast extract, biotin 1 µg l^{-1}, pH 7.0, 15 g l^{-1} agar), containing 100 µg ml^{-1} carbenicillin, 50 µg ml^{-1} rifampicin, and 100 µg ml^{-1} spectinomycin, and incubated at 28 °C for 48 h. Single colonies were used to inoculate 5 ml MG/L liquid cultures and were grown for 48 h at 28 °C prior to plasmid isolation. Plasmid DNA isolation was performed using the GeneJET™ Plasmid Miniprep Kit (Thermo Fisher Scientific Inc., Waltham, MA, USA) according to the manufacturer's instructions. Correct assembly of the binary construct CPGE_VEC00290 was confirmed by restriction digestion as described above.

4.2.4.3 Transformation of barley and plant regeneration

Immature barley embryos were transformed via *Agrobacterium* with CPGE_VEC00290 according to the protocol described by Marthe et al. (2015), with modifications as described below.

Preparation of the cocultivation medium. The K micro (1000×) stock was prepared as follows: per 100 ml, 0.84 g $MnSO_4 \cdot H_2O$, 0.31 g H_3BO_3, 0.72 g $ZnSO_4 \cdot 7H_2O$, 12 mg $Na_2MoO_4 \cdot 2H_2O$, 2.5 mg $CuSO_4 \cdot 5H_2O$, 2.4 mg $CoCl_2 \cdot 6H_2O$ and 17 mg KI were used.

Plant acclimatisation. Regenerants were transferred to 9 cm-diameter pots under greenhouse conditions, as described in Section 4.2.1.

4.2.5 Genotyping

4.2.5.1 Genomic DNA isolation

Genomic DNA was isolated from barley wild-type, transgenic, and mutant leaf tissue using a modified protocol from Edwards et al. (1991). Leaf material was harvested using sterile scissors and forceps and transferred to 2.0 ml reaction tubes containing two metal beads (Ø 4 mm). Samples were immediately frozen in liquid nitrogen and either stored at −80 °C or processed immediately. Frozen tissue was homogenised using a Mixer Mill MM 400 (Retsch GmbH, Haan, Germany) at 30 Hz for 2 min in pre-cooled holders. Next, 400 µl extraction buffer (250 mM Tris-HCl, pH 7.5, 250 mM NaCl, 25 mM EDTA at pH 8.0, 5 g l^{-1} SDS) was added, and samples were mixed thoroughly by vortexing. Samples were kept on ice until all extracts were prepared. Protein and polysaccharide precipitation was induced by the addition of 150 µl 3 m potassium acetate (pH 5.5), followed by gentle inversion. After centrifugation for 5 min at maximum speed at room temperature, the supernatant was transferred to a fresh 1.5 ml tube. Genomic DNA was precipitated by adding 550 µl ice-cold 100% isopropanol, mixing by inversion, and centrifugation for 5 min at maximum speed. The resulting pellet was washed with 300 µl 70% (v/v) ethanol, centrifuged again for 5 min, and air-dried at room temperature for 10–15 min. DNA was resuspended in 50 µl sterile deionised water. DNA samples were used for PCR-based genotyping, typically using 1 µl template per 25 µl reaction.

4.2.5.2 PCR amplification and gel electrophoresis

PCR reactions were carried out in a total volume of 10 µl containing 1× Green GoTaq Reaction Buffer, 2 mM $MgCl_2$, 0.2 mM dNTPs, 0.25 µM of each primer, and 0.5 units GoTaq® G2 DNA Polymerase (Promega GmbH, Walldorf, Germany) and 10-50 ng of template DNA. The primers used are listed in Table 7. PCR amplification was performed using the following thermal cycling conditions: initial denaturation at 95 °C for 5 min, followed by 30 to 32 cycles of denaturation at 95 °C for 30 s, annealing at 58-62 °C depending on the primers used for 20 s, and extension at 72 °C for 60 s, with a final extension at 72 °C for 5-7 min. PCR amplification was conducted on an Eppendorf Mastercycler® nexus X2 (Eppendorf AG, Hamburg, Germany). The PCR products were analysed by gel electrophoresis in 1% agarose in 0.5x Tris-borate-EDTA (TBE) buffer at 140 V or 150 V for 20-25 min.

4.2.6 Molecular characterisation of *why2* mutants

4.2.6.1 Sequence analysis

Genomic DNA was isolated as described in Section 4.2.5.1 using primers specific to the guides, with annealing temperatures adjusted to the primers and extension time adjusted to the expected amplicon length. Mutations were confirmed by Sanger sequencing (Microsynth AG, Glabach, Switzerland) and by the Tracking of Indels by DEcomposition (TIDE) method (Brinkman et al., 2014).

4.2.6.2 Prediction of protein sequence changes

The predicted effects of CRISPR/Cas9-induced mutations on the WHIRLY2 protein were analysed *in silico*. Edited *WHIRLY2* cDNA sequences were reconstructed based on the sequencing results, with insertions or deletions introduced at the predicted Cas9 cleavage site, three base pairs upstream of the NGG PAM. To evaluate changes to the protein sequence, the modified cDNA sequences were then translated into protein sequences using SnapGene software (version 8.2.1; www.snapgene.com), aligned to the wild-type WHIRLY2 protein sequence with the EMBL-EBI Clustal Omega tool (Madeira et al., 2024) and visualised with Jalview (version 2.11.5.1; Waterhouse et al., 2009).

4.2.6.3 Structural modelling

Structural modelling and analysis of wild-type WHIRLY2 and the *why2* in-frame homozygous deletion mutants (mutants 4-228 and 4-240) were performed by Prof. Dr. Holger Gohlke of the Institute for Pharmaceutical and Medicinal Chemistry, Heinrich Heine University Düsseldorf, using AlphaFold-Multimer v3. The predicted tetrameric structures were analysed to determine the structural context of the deleted amino acids and their potential impact on WHIRLY2 assembly. Regions with low prediction confidence, represented as extended or unstructured segments in the models, were interpreted as intrinsically disordered regions. The positions of the deleted residues were assessed relative to the ssDNA-binding site based on published WHIRLY structural data (PDB ID: 3N1K). In addition, the deleted residues were examined in the context of the published WHIRLY 24-mer assembly (PDB ID: 3N1I) to evaluate potential interactions with neighbouring chains from symmetry-related tetramers.

4.2.7 Abiotic stress treatments

4.2.7.1 High-temperature and continuous-light treatment

Twelve barley grains each of wild-type plants, *why1* mutants (Krupinska et al., 2024), RNAi-W1 lines (Melonek et al., 2010), and four *why1*-complemented variants (control, ΔPRAPP, C165A, and K97A) were used per experiment. Experiments were conducted under controlled conditions in growth chambers (see Section 4.2.2). Grains were sown randomly to minimise positional effects, and trays with the germinated seedlings were rotated almost daily throughout the duration of the experiments. All experiments were conducted in two independent biological replicates, and measurements were carried out 14 days after sowing (DAS) while plants remained under their respective growth conditions. For experiments combining temperatures of 21 °C or 32 °C and continuous light intensities of 150 or 400 µmol m^{-2} s^{-1}, grains were sown in ED73 soil, and after the cold stratification, seedlings were transferred for 3 days to 21 °C under continuous light at 400 µmol m^{-2} s^{-1}. Afterwards, they were placed under the abovementioned combinations of temperature and continuous light conditions. The relative humidity was maintained at 70%. In a second experimental group, grains were sown in vermiculite mixed with Hoagland's nutrient solution. Following the cold stratification, seedlings

were grown at 34 °C, continuous light intensity of 150 µmol m^{-2} s^{-1}, and 70% relative humidity. Control growth conditions were 16 h of 150 µmol m^{-2} s^{-1} light intensity at 21 °C and 8 h darkness at 18 °C. The relative humidity was maintained at 65%. All germinated seedlings were included in the analyses. The length of primary leaves was measured while leaves remained attached to the plant. For documentation, three primary and three secondary leaves per family, representing the average leaf length, were selected for photography and qualitative assessment of leaf length and greenness. Germination rate, second-leaf emergence rate, and the proportion of green versus bleached primary leaves were determined by visual assessment and calculated as proportions of the total number of germinated seedlings.

4.2.7.2 Drought stress

Seven wild-type grains of barley, as well as homozygous grains from each of three families of each of the five *why1*-complemented variants (control, ΔPRAPP, C165A, K97A and ΔPTP), were used for the drought stress assay. The experiments were conducted in two independent biological replicates. The grains were sown in terracotta pots containing 500 g of ED73 soil and placed in greenhouse conditions (see Section 4.2.1). The pots were then watered with 0.2 litres of water to establish an initial SWC of 65%. Until 11 days after sowing (DAS), the SWC of all plants was maintained at 65% by watering as required. Drought stress was applied at 11 DAS by withholding water, while control plants continued to be watered to compensate for water loss. From 11 DAS onwards, PSII efficiency and chlorophyll content were measured in primary leaves every two days until values approached zero. SWC was recorded on the same measurement days. For plants under control conditions, SWC measurements were taken before watering. Pots were rotated on each measurement day to minimise positional effects.

4.2.8 Biotic stress treatment

The response of homozygous *why1*-complemented variants to powdery mildew was analysed using *Blumeria graminis* f. sp. *hordei* (*Bgh*) isolate CH4.8. Powdery mildew assays were performed in the group of Dr. Dimitar Douchkov (Biotrophy and Immunity, Leibniz Institute of Plant Genetics and Crop Plant Research, IPK, Gatersleben, Germany)

according to the method described in Lück et al. (2025). Briefly, leaf segments from 14-day-old plants were inoculated with *Bgh* CH4.8, and fungal development was assessed 48 hours after inoculation. Colony number and median colony area were quantified using automated image analysis. The experiment was conducted in three independent biological repetitions with four technical replicates per family of variant.

4.2.9 Physiological measurements

4.2.9.1 Photosystem II efficiency measurements

The DUAL-PAM/F (Heinz Walz GmbH, Effeltrich, Germany) was used to measure photosystem II (PSII) efficiency in the primary leaves of plants under both control and drought conditions. Before measurements, the plants were left in darkness for 10 minutes to allow for dark adaptation. The DUAL-PAM/F applies a saturating light pulse and calculates the maximum PSII efficiency as F_V/F_M. F_M represents the maximum fluorescence yield, whereas F_V represents the variable fluorescence ($F_V = F_M - F_0$), and F_0 represents the minimum fluorescence measured in the dark-adapted state.

4.2.9.2 Relative chlorophyll content measurements

The relative chlorophyll content of all primary leaves in both control and drought treatments was measured using a SPAD-502 instrument (Soil Plant Analysis Development, Konica Minolta Sensing Europe B.V., Munich, Germany). Measurements were taken at the base, middle and tip of each leaf, and the average value was used. Chlorophyll content is expressed in SPAD units.

4.2.10 Protein analysis

4.2.10.1 Protein isolation

Proteins from leaf tissue were extracted using an extraction buffer containing 1.6% (w/v) SDS, 1 M urea, and 50 mM Tris/HCl (pH 7.6). Leaf material was frozen in liquid nitrogen and homogenised using mortar and pestle. Samples were incubated at 70 °C for 20 min. Insoluble material was removed by centrifugation at 16100 × g for 20 min.

4.2.10.2 Protein quantification

Protein concentrations were determined using the Bio-Rad® DC Protein Assay (Bio-Rad Laboratories, Inc., Hercules, CA, USA) according to the manufacturer's instructions.

4.2.10.3 SDS-PAGE and immunoblotting

Equal amounts of protein from *why1*-complemented lines were separated by SDS-PAGE using hand-cast 12% TGX Stain-Free™ polyacrylamide gels (Bio-Rad Laboratories GmbH, Feldkirchen, Germany) and a standard Tris-glycine-SDS buffer system. Following electrophoresis, proteins were transferred onto PVDF membranes (Immun-Blot® PVDF Membrane, Bio-Rad Laboratories GmbH, Feldkirchen, Germany) using a semi-dry blotting system (Pierce™ Power Blotter, Thermo Fisher Scientific Inc., Waltham, MA, USA) and applying the three-buffer transfer system described by "Electroblotting of multiple gels: a simple apparatus without buffer tank for rapid transfer of proteins from polycrylamide to nitrocellulose" (1984). Membranes were incubated with primary antibodies recognising WHIRLY1 (goat polyclonal anti-WHIRLY1, Agrisera, product no. AS16 3953) or RuBisCo large subunit (RbcL; rabbit polyclonal anti-RbcL, Agrisera, product no. AS03 037), using dilutions recommended by the manufacturer. After washing, membranes were incubated with a single horseradish peroxidase (HRP)-conjugated secondary antibody, donkey anti-goat IgG (H+L; Thermo Fisher Scientific, product no. A15999). Immunoreactive proteins were detected using Immobilon® Western Chemiluminescent HRP Substrate (EMD Millipore Corporation) according to the manufacturer's instructions, and chemiluminescent signal was imaged with a ChemiDoc™ MP Imaging System (Bio-Rad Laboratories GmbH, Feldkirchen, Germany). Western blot band intensities were quantified by densitometric analysis using GelAnalyzer 23.1.1 (http://www.gelanalyzer.com).

4.2.11 Statistical analysis

All data were tested for normal distribution using the Shapiro-Wilk test and for homogeneity of variance using Levene's test in SPSS (version 28; IBM SPSS Statistics). Differences among genotypes were analysed using Welch's ANOVA followed by the Games-Howell post hoc test in SPSS (version 28; IBM SPSS Statistics). Nonparametric analy-

ses were conducted using the Kruskal-Wallis test followed by Dunn's post hoc test with Bonferroni correction in R (version 4.5.1; R Core Team, 2025). To visualise statistically significant differences among genotypes, compact letter displays (CLDs) were generated in R (version 4.5.1; R Core Team, 2025) and are shown in the respective figures as lowercase letters. All statistical tests were performed at a significance level of $\alpha = 0.05$. Graphical visualisation of the data was conducted in OriginPro (version 2023b; OriginLab Corporation).

References

Ahmar, S., Hensel, G., & Gruszka, D. (2023). CRISPR/Cas9-mediated genome editing techniques and new breeding strategies in cereals - current status, improvements, and perspectives. *Biotechnology Advances*, *69*, 108248. https://doi.org/10.1016/j.biotechadv.2023.108248

Akbudak, M. A., & Filiz, E. (2019). Whirly (Why) transcription factors in tomato (*Solanum lycopersicum* L.): Genome-wide identification and transcriptional profiling under drought and salt stresses. *Molecular Biology Reports*, *46*, 4139–4150. https://doi.org/10.1007/s11033-019-04863-y

Alqudah, A. M., Sallam, A., Stephen Baenziger, P., & Borner, A. (2020). GWAS: Fast-forwarding gene identification and characterization in temperate cereals: Lessons from barley - a review. *Journal of Advanced Research*, *22*, 119–135. https://doi.org/10.1016/j.jare.2019.10.013

Bagherian, M., Harris, G., Sathishkumar, P., & Lloyd, J. P. B. (2025). Start right to end right: Authentic open reading frame selection matters for nonsense-mediated decay target identification. *Genes*, *16*. https://doi.org/10.3390/genes16111297

Barkan, A. (2011). Expression of plastid genes: Organelle-specific elaborations on a prokaryotic scaffold. *Plant Physiology*, *155*, 1520–32. https://doi.org/10.1104/pp.110.171231

Bartlett, J. G., Alves, S. C., Smedley, M., Snape, J. W., & Harwood, W. A. (2008). High-throughput *Agrobacterium*-mediated barley transformation. *Plant Methods*, *4*, 22. https://doi.org/10.1186/1746-4811-4-22

Belhaj, K., Chaparro-Garcia, A., Kamoun, S., Patron, N. J., & Nekrasov, V. (2015). Editing plant genomes with CRISPR/Cas9. *Current Opinion in Biotechnology*, *32*, 76–84. https://doi.org/10.1016/j.copbio.2014.11.007

Bock, R. (2007). Structure, function, and inheritance of plastid genomes. In *Cell and molecular biology of plastids* (pp. 29–63). Springer. https://doi.org/10.1007/4735_2007_0223

Bohne, A. V. (2014). The nucleoid as a site of rRNA processing and ribosome assembly. *Frontiers in Plant Science*, *5*, 257. https://doi.org/10.3389/fpls.2014.00257

Brinkman, E. K., Chen, T., Amendola, M., & van Steensel, B. (2014). Easy quantitative assessment of genome editing by sequence trace decomposition. *Nucleic Acids Research*, *42*, e168–e168. https://doi.org/10.1093/nar/gku936

Bunce, J. A. (2021). Three new methods indicate that CO_2 concentration affects plant respiration in the range relevant to global change. *AoB Plants*, *13*, plab004. https://doi.org/10.1093/aobpla/plab004

Bünger, W., & Feierabend, J. (1980). Capacity for RNA synthesis in 70S ribosome-deficient plastids of heat-bleached rye leaves. *Planta*, *149*, 163–169. https://doi.org/https://doi.org/10.1007/BF00380878

Burger, W. C. (1965). Effect of light on the germination of barley and its relation to dormancy. *Journal of the Institute of Brewing*, *71*, 244–250. https://doi.org/10.1002/j.2050-0416.1965.tb02053.x

Burgess, A. J. (2023). Breath of green life: Reduction in plant day and night respiration under elevated CO_2. *Plant Physiology*, *192*, 31–33. https://doi.org/10.1093/plphys/kiad087

Cai, Q., Guo, L., Shen, Z. R., Wang, D. Y., Zhang, Q., & Sodmergen. (2015). Elevation of pollen mitochondrial DNA copy number by WHIRLY2: Altered respiration and pollen tube growth in *Arabidopsis*. *Plant Physiology*, *169*, 660–73. https://doi.org/10.1104/pp.15.00437

Cappadocia, L., Marechal, A., Parent, J. S., Lepage, E., Sygusch, J., & Brisson, N. (2010). Crystal structures of DNA-Whirly complexes and their role in *Arabidopsis* organelle genome repair. *The Plant Cell*, *22*, 1849–67. https://doi.org/10.1105/tpc.109.071399

Cappadocia, L., Parent, J.-S., Zampini, É., Lepage, É., Sygusch, J., & Brisson, N. (2012). A conserved lysine residue of plant Whirly proteins is necessary for higher order protein assembly and protection against DNA damage. *Nucleic Acids Research*, *40*, 258–269. https://doi.org/10.1093/nar/gkr740

Chan, K. X., Phua, S. Y., Crisp, P., McQuinn, R., & Pogson, B. J. (2016). Learning the languages of the chloroplast: Retrograde signaling and beyond. *Annual Review of Plant Biology*, *67*, 25–53. https://doi.org/10.1146/annurev-arplant-043015-111854

Chaves, M. M., Flexas, J., & Pinheiro, C. (2009). Photosynthesis under drought and salt stress: Regulation mechanisms from whole plant to cell. *Annals of Botany*, *103*, 551–560. https://doi.org/10.1093/aob/mcn125

Chen, K., & Gao, C. (2020). Genome-edited crops: How to move them from laboratory to market. *Frontiers of Agricultural Science and Engineering*, *7*. https://doi.org/10.15302/j-fase-2020332

Comadira, G., Rasool, B., Kaprinska, B., Garcia, B. M., Morris, J., Verrall, S. R., Bayer, M., Hedley, P. E., Hancock, R. D., & Foyer, C. H. (2015). WHIRLY1 functions in the control of responses to nitrogen deficiency but not aphid infestation in barley. *Plant Physiology*, *168*, 1140–51. https://doi.org/10.1104/pp.15.00580

Concordet, J.-P., & Haeussler, M. (2018). CRISPOR: Intuitive guide selection for CRISPR/-Cas9 genome editing experiments and screens. *Nucleic Acids Research*, *46*, W242–W245. https://doi.org/10.1093/nar/gky354

Crawford, T., Lehotai, N., & Strand, A. (2018). The role of retrograde signals during plant stress responses. *Journal of Experimental Botany*, *69*, 2783–2795. https://doi.org/10.1093/jxb/erx481

De Clercq, I., Vermeirssen, V., Van Aken, O., Vandepoele, K., Murcha, M. W., Law, S. R., Inze, A., Ng, S., Ivanova, A., Rombaut, D., van de Cotte, B., Jaspers, P., Van de Peer, Y., Kangasjarvi, J., Whelan, J., & Van Breusegem, F. (2013). The membrane-bound NAC transcription factor ANAC013 functions in mitochondrial retrograde regulation of the oxidative stress response in *Arabidopsis*. *The Plant Cell*, *25*, 3472–90. https://doi.org/10.1105/tpc.113.117168

Den Dunnen, J. T., Dalgleish, R., Maglott, D. R., Hart, R. K., Greenblatt, M. S., McGowan-Jordan, J., Roux, A.-F., Smith, T., Antonarakis, S. E., Taschner, P. E., et al. (2016). HGVS recommendations for the description of sequence variants: 2016 update. *Human Mutation*, *37*, 564–569. https://doi.org/10.1002/humu.2298

Desveaux, D., Allard, J., Brisson, N., & Sygusch, J. (2002). A new family of plant transcription factors displays a novel ssDNA-binding surface. *Nature Structural Biology*, *9*, 512–7. https://doi.org/10.1038/nsb814

Desveaux, D., Marechal, A., & Brisson, N. (2005). Whirly transcription factors: Defense gene regulation and beyond. *Trends in Plant Science*, *10*, 95–102. https://doi.org/10.1016/j.tplants.2004.12.008

Desveaux, D., Després, C., Joyeux, A., Subramaniam, R., & Brisson, N. (2000). PBF-2 is a novel single-stranded DNA binding factor implicated in *PR-10a* gene activation in potato. *The Plant Cell*, *12*, 1477–1489. https://doi.org/10.1105/tpc.12.8.1477

Desveaux, D., Subramaniam, R., Després, C., Mess, J.-N., Lévesque, C., Fobert, P. R., Dangl, J. L., & Brisson, N. (2004). A "Whirly" transcription factor is required for salicylic acid-dependent disease resistance in *Arabidopsis*. *Developmental Cell*, *6*, 229–240. https://doi.org/10.1016/S1534-5807(04)00028-0

Didaran, F., Kordrostami, M., Ghasemi-Soloklui, A. A., Pashkovskiy, P., Kreslavski, V., Kuznetsov, V., & Allakhverdiev, S. I. (2024). The mechanisms of photoinhibition and repair in plants under high light conditions and interplay with abiotic stressors. *Journal of Photochemistry and Photobiology B: Biology*, *259*, 113004. https://doi.org/10.1016/j.jphotobiol.2024.113004

Dietz, K. J., Turkan, I., & Krieger-Liszkay, A. (2016). Redox- and reactive oxygen species-dependent signaling into and out of the photosynthesizing chloroplast. *Plant Physiology*, *171*, 1541–50. https://doi.org/10.1104/pp.16.00375

Dogra, V., Li, M., Singh, S., Li, M., & Kim, C. (2019). Oxidative post-translational modification of EXECUTER1 is required for singlet oxygen sensing in plastids. *Nature Communications*, *10*, 2834. https://doi.org/10.1038/s41467-019-10760-6

Doudna, J. A., & Charpentier, E. (2014). Genome editing. The new frontier of genome engineering with CRISPR-Cas9. *Science*, *346*, 1258096. https://doi.org/10.1126/science.1258096

Duan, L., Perez-Ruiz, J. M., Cejudo, F. J., & Dinneny, J. R. (2021). Characterization of CYCLOPHILLIN38 shows that a photosynthesis-derived systemic signal controls lateral root emergence. *Plant Physiology*, *185*, 503–518. https://doi.org/10.1093/plphys/kiaa032

Dubreuil, C., Jin, X., Barajas-Lopez, J. D., Hewitt, T. C., Tanz, S. K., Dobrenel, T., Schroder, W. P., Hanson, J., Pesquet, E., Gronlund, A., Small, I., & Strand, A. (2018). Establishment of photosynthesis through chloroplast development is controlled by two distinct regulatory phases. *Plant Physiology*, *176*, 1199–1214. https://doi.org/10.1104/pp.17.00435

Dusenge, M. E., Duarte, A. G., & Way, D. A. (2019). Plant carbon metabolism and climate change: Elevated CO_2 and temperature impacts on photosynthesis, photo-

respiration and respiration. *New Phytologist*, *221*, 32–49. https://doi.org/10.1111/nph.15283

Edwards, K., Johnstone, C., & Thompson, C. (1991). A simple and rapid method for the preparation of plant genomic DNA for PCR analysis. *Nucleic Acids Research*, *19*, 1349. https://doi.org/10.1093/nar/19.6.1349

Electroblotting of multiple gels: A simple apparatus without buffer tank for rapid transfer of proteins from polycrylamide to nitrocellulose. (1984). *Journal of Biochemical and Biophysical Methods*, *10*, 203–209. https://doi.org/10.1016/0165-022X(84)90040-X

Estavillo, G. M., Crisp, P. A., Pornsiriwong, W., Wirtz, M., Collinge, D., Carrie, C., Giraud, E., Whelan, J., David, P., Javot, H., Brearley, C., Hell, R., Marin, E., & Pogson, B. J. (2011). Evidence for a SAL1-PAP chloroplast retrograde pathway that functions in drought and high light signaling in *Arabidopsis*. *The Plant Cell*, *23*, 3992–4012. https://doi.org/10.1105/tpc.111.091033

Estrada-Melo, A. C., Reid, M. S., Jiang, C.-Z., et al. (2015). Overexpression of an ABA biosynthesis gene using a stress-inducible promoter enhances drought resistance in petunia. *Horticulture Research*, *2*. https://doi.org/10.1038/hortres.2015.13

Feierabend, J., & Mikus, M. (1977). Occurrence of a high temperature sensitivity of chloroplast ribosome formation in several higher plants. *Plant Physiology*, *59*, 863–867. https://doi.org/10.1104/pp.59.5.863

Flexas, J., & Medrano, H. (2002). Drought-inhibition of photosynthesis in C_3 plants: Stomatal and non-stomatal limitations revisited. *Annals of Botany*, *89*, 183–9. https://doi.org/10.1093/aob/mcf027

Foyer, C. H., & Hanke, G. (2022). ROS production and signalling in chloroplasts: Cornerstones and evolving concepts. *The Plant Journal*, *111*, 642–661. https://doi.org/10.1111/tpj.15856

Foyer, C. H., Karpinska, B., & Krupinska, K. (2014). The functions of WHIRLY1 and REDOX-RESPONSIVE TRANSCRIPTION FACTOR 1 in cross tolerance responses in plants: A hypothesis. *Philosophical Transactions of the Royal Society B: Biological Sciences*, *369*. https://doi.org/10.1098/rstb.2013.0226

Frank, S., Saeid Nia, M., Schäfer, A., Desel, C., Mulisch, M., Voigt, U., Nowara, D., Tandron Moya, Y. A., von Wiren, N., Bilger, W., Hensel, G., & Krupinska, K. (2024). Over-

accumulation of chloroplast-nucleus located WHIRLY1 in barley leads to a decrease in growth and an enhanced stress resistance. *The Plant Journal*, *119*, 1210–1225. https://doi.org/https://doi.org/10.1111/tpj.16819

Franklin, K. A. (2009). Light and temperature signal crosstalk in plant development. *Current Opinion in Plant Biology*, *12*, 63–8. https://doi.org/10.1016/j.pbi.2008.09.007

Galli, M., Martiny, E., Imani, J., Kumar, N., Koch, A., Steinbrenner, J., & Kogel, K. H. (2022). CRISPR/SpCas9-mediated double knockout of barley Microrchidia MORC1 and MORC6a reveals their strong involvement in plant immunity, transcriptional gene silencing and plant growth. *Plant Biotechnology Journal*, *20*, 89–102. https://doi.org/10.1111/pbi.13697

Garcia-Gimenez, G., Barakate, A., Smith, P., Stephens, J., Khor, S. F., Doblin, M. S., Hao, P., Bacic, A., Fincher, G. B., Burton, R. A., Waugh, R., Tucker, M. R., & Houston, K. (2020). Targeted mutation of barley (1,3;1,4)-beta-glucan synthases reveals complex relationships between the storage and cell wall polysaccharide content. *The Plant Journal*, *104*, 1009–1022. https://doi.org/10.1111/tpj.14977

Gasparis, S., Kala, M., Przyborowski, M., Lyznik, L. A., Orczyk, W., & Nadolska-Orczyk, A. (2018). A simple and efficient CRISPR/Cas9 platform for induction of single and multiple, heritable mutations in barley (*Hordeum vulgare* L.). *Plant Methods*, *14*, 111. https://doi.org/10.1186/s13007-018-0382-8

Godfrey, D., Bohlenius, H., Pedersen, C., Zhang, Z., Emmersen, J., & Thordal-Christensen, H. (2010). Powdery mildew fungal effector candidates share N-terminal Y/F/WxC-motif. *BMC Genomics*, *11*, 317. https://doi.org/10.1186/1471-2164-11-317

Golin, S., Negroni, Y. L., Bennewitz, B., Klosgen, R. B., Mulisch, M., La Rocca, N., Cantele, F., Vigani, G., Lo Schiavo, F., Krupinska, K., & Zottini, M. (2020). WHIRLY2 plays a key role in mitochondria morphology, dynamics, and functionality in *Arabidopsis thaliana*. *Plant Direct*, *4*, e00229. https://doi.org/10.1002/pld3.229

Grabowski, E. (2008). Isolierung, Charakterisierung und funktionelle Analyse der Whirly-Proteine der Gerste (*Hordeum vulgare* L.). [Doctoral dissertation, Mathematisch-Naturwissenschaftliche Fakultät, Christian-Albrechts-Universität zu Kiel].

Grabowski, E., Miao, Y., Mulisch, M., & Krupinska, K. (2008). Single-stranded DNA-binding protein WHIRLY1 in barley leaves is located in plastids and the nucleus of the same cell. *Plant Physiology*, *147*, 1800–4. https://doi.org/10.1104/pp.108.122796

Granier, C., Massonnet, C., Turc, O., Muller, B., Chenu, K., & Tardieu, F. (2002). Individual leaf development in *Arabidopsis thaliana*: A stable thermal-time-based programme. *Annals of Botany*, *89*, 595–604. https://doi.org/10.1093/aob/mcf085

Gubler, F., Hughes, T., Waterhouse, P., & Jacobsen, J. (2008). Regulation of dormancy in barley by blue light and after-ripening: Effects on abscisic acid and gibberellin metabolism. *Plant Physiology*, *147*, 886–96. https://doi.org/10.1104/pp.107.115469

Haeussler, M., Schönig, K., Eckert, H., Eschstruth, A., Mianné, J., Renaud, J. B., Schneider-Maunoury, S., Shkumatava, A., Teboul, L., Kent, J., Joly, J. S., & Concordet, J. P. (2016). Evaluation of off-target and on-target scoring algorithms and integration into the guide RNA selection tool CRISPOR. *Genome Biology*, *17*, 148. https://doi.org/10.1186/s13059-016-1012-2

Hensel, G., Valkov, V., Middlefell-Williams, J., & Kumlehn, J. (2008). Efficient generation of transgenic barley: The way forward to modulate plant-microbe interactions. *Journal of Plant Physiology*, *165*, 71–82. https://doi.org/10.1016/j.jplph.2007.06.015

Herrmann, R. G., & Feierabend, J. (1980). The presence of DNA in ribosome-deficient plastids of heat-bleached rye leaves. *European Journal of Biochemistry*, *104*, 603–609. https://doi.org/10.1111/j.1432-1033.1980.tb04464.x

Hinchliffe, A., & Harwood, W. A. (2019). *Agrobacterium*-mediated transformation of barley immature embryos. *Methods in Molecular Biology*, *1900*, 115–126. https://doi.org/10.1007/978-1-4939-8944-7_8

Hoang, H. H., Sechet, J., Bailly, C., Leymarie, J., & Corbineau, F. (2014). Inhibition of germination of dormant barley (*Hordeum vulgare* L.) grains by blue light as related to oxygen and hormonal regulation. *Plant, Cell & Environment*, *37*, 1393–403. https://doi.org/10.1111/pce.12239

Hofacker, I. L., Fontana, W., Stadler, P. F., Bonhoeffer, L. S., Tacker, M., & Schuster, P. (1994). Fast folding and comparison of RNA secondary structures. *Monatshefte*

für Chemie / Chemical Monthly, *125*, 167–188. https://doi.org/10.1007/BF00818163

Hoffie, I. (2023). Entwicklung des modularen CasCADE-Vektorsystems und dessen Verwendung zur gezielten Mutagenese der *Stp13*-Orthologe von Weizen und Gerste für die Etablierung dauerhafter Resistenz gegen Rost- und Mehltaupilze. [Doctoral dissertation, Naturwissenschaftliche Fakultät, Gottfried Wilhelm Leibniz Universität Hannover].

Hu, Y., & Shu, B. (2021). Identifying strawberry Whirly family transcription factors and their expressions in response to crown rot. *Notulae Botanicae Horti Agrobotanici Cluj-Napoca*, *49*. https://doi.org/10.15835/nbha49212323

Huang, C., Yu, J., Cai, Q., Chen, Y., Li, Y., Ren, Y., & Miao, Y. (2020). Triple-localized WHIRLY2 influences leaf senescence and silique development via carbon allocation. *Plant Physiology*, *184*, 1348–1362. https://doi.org/10.1104/pp.20.00832

Impens, L., Jacobs, T. B., Nelissen, H., Inze, D., & Pauwels, L. (2022). Mini-review: Transgenerational CRISPR/Cas9 gene editing in plants. *Frontiers in Genome Editing*, *4*, 825042. https://doi.org/10.3389/fgeed.2022.825042

Isemer, R., Krause, K., Grabe, N., Kitahata, N., Asami, T., & Krupinska, K. (2012a). Plastid located WHIRLY1 enhances the responsiveness of *Arabidopsis* seedlings toward abscisic acid. *Frontiers in Plant Science*, *3*, 283. https://doi.org/10.3389/fpls.2012.00283

Isemer, R., Mulisch, M., Schafer, A., Kirchner, S., Koop, H. U., & Krupinska, K. (2012b). Recombinant WHIRLY1 translocates from transplastomic chloroplasts to the nucleus. *FEBS Letters*, *586*, 85–8. https://doi.org/10.1016/j.febslet.2011.11.029

Janack, B., Sosoi, P., Krupinska, K., & Humbeck, K. (2016). Knockdown of *WHIRLY1* affects drought stress-induced leaf senescence and histone modifications of the senescence-associated gene *HvS40*. *Plants*, *5*. https://doi.org/10.3390/plants5030037

Jang, G., Lee, S., Um, T. Y., Chang, S. H., Lee, H. Y., Chung, P. J., Kim, J.-K., & Do Choi, Y. (2016). Genetic chimerism of CRISPR/Cas9-mediated rice mutants. *Plant Biotechnology Reports*, *10*, 425–435. https://doi.org/10.1007/s11816-016-0414-7

Jarvis, P., & Lopez-Juez, E. (2013). Biogenesis and homeostasis of chloroplasts and other plastids. *Nature Reviews Molecular Cell Biology*, *14*, 787–802. https://doi.org/10.1038/nrm3702

Jeran, N., Mercier, M., Pesaresi, P., & Tadini, L. (2025). Proteostasis and protein quality control in chloroplasts: Mechanisms and novel insights related to protein mislocalization. *Journal of Experimental Botany*, *76*, 4294–4312. https://doi.org/10.1093/jxb/eraf182

Johnson, M. P., & Wientjes, E. (2020). The relevance of dynamic thylakoid organisation to photosynthetic regulation. *Biochimica et Biophysica Acta - Bioenergetics*, *1861*, 148039. https://doi.org/10.1016/j.bbabio.2019.06.011

Kalyna, M., Simpson, C. G., Syed, N. H., Lewandowska, D., Marquez, Y., Kusenda, B., Marshall, J., Fuller, J., Cardle, L., McNicol, J., Dinh, H. Q., Barta, A., & Brown, J. W. (2012). Alternative splicing and nonsense-mediated decay modulate expression of important regulatory genes in *Arabidopsis*. *Nucleic Acids Research*, *40*, 2454–69. https://doi.org/10.1093/nar/gkr932

Karpinska, B., Razak, N., James, E. K., Morris, J. A., Verrall, S. R., Hedley, P. E., Hancock, R. D., & Foyer, C. H. (2022). WHIRLY1 functions in the nucleus to regulate barley leaf development and associated metabolite profiles. *Biochemical Journal*, *479*, 641–659.

Kircher, S., & Schopfer, P. (2012). Photosynthetic sucrose acts as cotyledon-derived long-distance signal to control root growth during early seedling development in *Arabidopsis*. *Proceedings of the National Academy of Sciences*, *109*, 11217–21. https://doi.org/10.1073/pnas.1203746109

Kralova, M., Kubalova, I., Hajny, J., Kubiasova, K., Vagaska, K., Ge, Z., Gallei, M., Semeradova, H., Kucharova, A., Honig, M., Monzer, A., Kovacik, M., Friml, J., Novak, O., Benkova, E., Ikeda, Y., & Zalabak, D. (2024). A decoy receptor derived from alternative splicing fine-tunes cytokinin signaling in *Arabidopsis*. *Molecular Plant*, *17*, 1850–1865. https://doi.org/10.1016/j.molp.2024.11.001

Krause, K., Kilbienski, I., Mulisch, M., Rodiger, A., Schafer, A., & Krupinska, K. (2005). DNA-binding proteins of the Whirly family in *Arabidopsis thaliana* are targeted to the organelles. *FEBS Letters*, *579*, 3707–12. https://doi.org/10.1016/j.febslet.2005.05.059

Krause, K., & Krupinska, K. (2009). Nuclear regulators with a second home in organelles. *Trends in Plant Science*, *14*, 194–9. https://doi.org/10.1016/j.tplants.2009.01.005

Krause, K., Oetke, S., & Krupinska, K. (2012). Dual targeting and retrograde translocation: Regulators of plant nuclear gene expression can be sequestered by plastids. *International Journal of Molecular Sciences*, *13*, 11085–11101. https://doi.org/10.3390/ijms130911085

Krupinska, K., Blanco, N. E., Oetke, S., & Zottini, M. (2020). Genome communication in plants mediated by organelle-nucleus-located proteins. *Philosophical Transactions of the Royal Society B: Biological Sciences*, *375*, 20190397. https://doi.org/10.1098/rstb.2019.0397

Krupinska, K., Braun, S., Nia, M. S., Schafer, A., Hensel, G., & Bilger, W. (2019). The nucleoid-associated protein WHIRLY1 is required for the coordinate assembly of plastid and nucleus-encoded proteins during chloroplast development. *Planta*, *249*, 1337–1347. https://doi.org/10.1007/s00425-018-03085-z

Krupinska, K., Desel, C., Frank, S., & Hensel, G. (2022). WHIRLIES are multifunctional DNA-binding proteins with impact on plant development and stress resistance. *Frontiers in Plant Science*, *13*, 880423. https://doi.org/10.3389/fpls.2022.880423

Krupinska, K., Frank, S., Boschian, L., Saeid Nia, M., Braun, S., Schafer, A., Voigt, U., Niewiadomska, E., Hause, B., Hensel, G., & Bilger, W. (2025). Iron allocation to chloroplast proteins depends on the DNA-binding protein WHIRLY1. *Planta*, *262*, 32. https://doi.org/10.1007/s00425-025-04736-8

Krupinska, K., Oetke, S., Desel, C., Mulisch, M., Schafer, A., Hollmann, J., Kumlehn, J., & Hensel, G. (2014a). WHIRLY1 is a major organizer of chloroplast nucleoids. *Frontiers in Plant Science*, *5*, 432. https://doi.org/10.3389/fpls.2014.00432

Krupinska, K., Dähnhardt, D., Fischer-Kilbienski, I., Kucharewicz, W., Scharrenberg, C., Trösch, M., & Buck, F. (2014b). Identification of WHIRLY1 as a factor binding to the promoter of the stress- and senescence-associated gene *HvS40*. *Journal of Plant Growth Regulation*, *33*, 91–105. https://doi.org/10.1007/s00344-013-9378-9

Krupinska, K., Eirich, J., Repnik, U., Desel, C., Nia, M. S., Schäfer, A., Voigt, U., Bennewitz, B., Bilger, W., Finkemeier, I., & Hensel, G. (2024). The major nucleoid-associated protein WHIRLY1 promotes chloroplast development in barley. https://doi.org/10.1101/2024.05.06.592765

Krzyszton, M., Kufel, J., & Zakrzewska-Placzek, M. (2025). RNA interference and turnover in plants - a complex partnership. *Frontiers in Plant Science*, *16*, 1608888. https://doi.org/10.3389/fpls.2025.1608888

Kucharewicz, W., Distelfeld, A., Bilger, W., Muller, M., Munne-Bosch, S., Hensel, G., & Krupinska, K. (2017). Acceleration of leaf senescence is slowed down in transgenic barley plants deficient in the DNA/RNA-binding protein WHIRLY1. *Journal of Experimental Botany*, *68*, 983–996. https://doi.org/10.1093/jxb/erw501

Kumlehn, J., Hensel, G., ouml, & tz. (2009). Genetic transformation technology in the Triticeae. *Breeding Science*, *59*, 553–560. https://doi.org/10.1270/jsbbs.59.553

Lancashire, P. D., Bleiholder, H., Boom, T. v. d., Langelüddeke, P., Stauss, R., Weber, E., & Witzenberger, A. (1991). A uniform decimal code for growth stages of crops and weeds. *Annals of Applied Biology*, *119*, 561–601. https://doi.org/https://doi.org/10.1111/j.1744-7348.1991.tb04895.x

Lee, D. W., Jung, C., & Hwang, I. (2013). Cytosolic events involved in chloroplast protein targeting. *Biochimica et Biophysica Acta*, *1833*, 245–52. https://doi.org/10.1016/j.bbamcr.2012.03.006

Lee, K. P., Kim, C., Landgraf, F., & Apel, K. (2007). EXECUTER1- and EXECUTER2-dependent transfer of stress-related signals from the plastid to the nucleus of *Arabidopsis thaliana*. *Proceedings of the National Academy of Sciences*, *104*, 10270–5. https://doi.org/10.1073/pnas.0702061104

Lee, S., Lee, D. W., Lee, Y., Mayer, U., Stierhof, Y. D., Lee, S., Jurgens, G., & Hwang, I. (2009). Heat shock protein cognate 70-4 and an E3 ubiquitin ligase, CHIP, mediate plastid-destined precursor degradation through the ubiquitin-26S proteasome system in *Arabidopsis*. *The Plant Cell*, *21*, 3984–4001. https://doi.org/10.1105/tpc.109.071548

Lepage, E., Zampini, E., & Brisson, N. (2013). Plastid genome instability leads to reactive oxygen species production and plastid-to-nucleus retrograde signaling in *Arabidopsis*. *Plant Physiology*, *163*, 867–81. https://doi.org/10.1104/pp.113.223560

Li, Y., Liu, H., Ma, T., Li, J., Yuan, J., Xu, Y. C., Sun, R., Zhang, X., Jing, Y., Guo, Y. L., & Lin, R. (2023). *Arabidopsis* EXECUTER1 interacts with WRKY transcription factors to mediate plastid-to-nucleus singlet oxygen signaling. *The Plant Cell*, *35*, 827–851. https://doi.org/10.1093/plcell/koac330

Liang, J., Ji, F., Zhou, Q., & He, D. (2025a). Optimizing LED light intensity and photoperiod to promote growth and rooting of medicinal cannabis in photoautotrophic micropropagation. *Biology*, *14*. https://doi.org/10.3390/biology14060706

Liang, X., Zhu, W., Xu, W., & Liang, J. (2025b). CPK2 enhances ABA sensitivity in seed germination and root growth by promoting ABA-induced ABI5 expression and ABI5 protein stability. *Plants*, *14*. https://doi.org/10.3390/plants14172671

Liu, H., Wang, X., Yang, W., Liu, W., Wang, Y., Wang, Q., & Zhao, Y. (2023). Identification of Whirly transcription factors in Triticeae species and functional analysis of TaWHY1-7D in response to osmotic stress. *Frontiers in Plant Science*, *14*, 1297228. https://doi.org/10.3389/fpls.2023.1297228

Llamas, E., & Pulido, P. (2022). A proteostasis network safeguards the chloroplast proteome. *Essays in Biochemistry*, *66*, 219–228. https://doi.org/10.1042/EBC20210058

Lopez-Bucio, J., Cruz-Ramirez, A., & Herrera-Estrella, L. (2003). The role of nutrient availability in regulating root architecture. *Current Opinion in Plant Biology*, *6*, 280–7. https://doi.org/10.1016/s1369-5266(03)00035-9

Lorenz, R., Bernhart, S. H., Honer Zu Siederdissen, C., Tafer, H., Flamm, C., Stadler, P. F., & Hofacker, I. L. (2011). ViennaRNA package 2.0. *Algorithms for Molecular Biology*, *6*, 26. https://doi.org/10.1186/1748-7188-6-26

Lück, S., Bourras, S., & Douchkov, D. (2025). Deep phenotyping platform for microscopic plant-pathogen interactions. *Frontiers in Plant Science*, *16*. https://doi.org/10.3389/fpls.2025.1462694

Lynch, J. P. (2022). Edaphic stress interactions: Important yet poorly understood drivers of plant production in future climates. *Field Crops Research*, *283*. https://doi.org/10.1016/j.fcr.2022.108547

Ma, H., Tu, L. C., Naseri, A., Huisman, M., Zhang, S., Grunwald, D., & Pederson, T. (2016). Multiplexed labeling of genomic loci with dCas9 and engineered sgRNAs using

CRISPRainbow. *Nature Biotechnology*, *34*, 528–30. https://doi.org/10.1038/nbt.3526

Madeira, F., Madhusoodanan, N., Lee, J., Eusebi, A., Niewielska, A., Tivey, A. R. N., Lopez, R., & Butcher, S. (2024). The EMBL-EBI Job Dispatcher sequence analysis tools framework in 2024. *Nucleic Acids Research*, *52*, W521–W525. https://doi.org/10.1093/nar/gkae241

Majeran, W., Friso, G., Asakura, Y., Qu, X., Huang, M., Ponnala, L., Watkins, K. P., Barkan, A., & van Wijk, K. J. (2012). Nucleoid-enriched proteomes in developing plastids and chloroplasts from maize leaves: A new conceptual framework for nucleoid functions. *Plant Physiology*, *158*, 156–89. https://doi.org/10.1104/pp.111.188474

Manh, M. B., Ost, C., Peiter, E., Hause, B., Krupinska, K., & Humbeck, K. (2023). WHIRLY1 acts upstream of ABA-related reprogramming of drought-induced gene expression in barley and affects stress-related histone modifications. *International Journal of Molecular Sciences*, *24*. https://doi.org/10.3390/ijms24076326

Maréchal, A., Parent, J.-S., Sabar, M., Véronneau-Lafortune, F., Abou-Rached, C., & Brisson, N. (2008). Overexpression of mtDNA-associated *AtWhy2* compromises mitochondrial function. *BMC Plant Biology*, *8*, 42. https://doi.org/10.1186/1471-2229-8-42

Maréchal, A., Parent, J.-S., Véronneau-Lafortune, F., Joyeux, A., Lang, B. F., & Brisson, N. (2009). Whirly proteins maintain plastid genome stability in *Arabidopsis*. *Proceedings of the National Academy of Sciences*, *106*, 14693–14698. https://doi.org/doi:10.1073/pnas.0901710106

Marthe, C., Kumlehn, J., & Hensel, G. (2015). Barley (*Hordeum vulgare* L.) transformation using immature embryos. *Methods in Molecular Biology*, *1223*, 71–83. https://doi.org/10.1007/978-1-4939-1695-5_6

Melonek, J., Mulisch, M., Schmitz-Linneweber, C., Grabowski, E., Hensel, G., & Krupinska, K. (2010). WHIRLY1 in chloroplasts associates with intron containing RNAs and rarely co-localizes with nucleoids. *Planta*, *232*, 471–81. https://doi.org/10.1007/s00425-010-1183-0

Meng, C., Yang, M., Wang, Y., Chen, C., Sui, N., Meng, Q., Zhuang, K., & Lv, W. (2020). SlWHY2 interacts with SlRECA2 to maintain mitochondrial function under drought stress

in tomato. *Plant Science*, *301*, 110674. https://doi.org/10.1016/j.plantsci.2020.110674

Montecillo, J. A. V., Chu, L. L., & Bae, H. (2020). CRISPR-Cas9 system for plant genome editing: Current approaches and emerging developments. *Agronomy*, *10*. https://doi.org/10.3390/agronomy10071033

Nakai, M. (2018). New perspectives on chloroplast protein import. *Plant and Cell Physiology*, *59*, 1111–1119. https://doi.org/10.1093/pcp/pcy083

Nakata, M. T., Sato, M., Wakazaki, M., Sato, N., Kojima, K., Sekine, A., Nakamura, S., Shikanai, T., Toyooka, K., Tsukaya, H., & Horiguchi, G. (2018). Plastid translation is essential for lateral root stem cell patterning in *Arabidopsis thaliana*. *Biology Open*, *7*. https://doi.org/10.1242/bio.028175

Negroni, Y. L., Doro, I., Tamborrino, A., Luzzi, I., Fortunato, S., Hensel, G., Khosravi, S., Maretto, L., Stevanato, P., Lo Schiavo, F., de Pinto, M. C., Krupinska, K., & Zottini, M. (2024). The *Arabidopsis* mitochondrial nucleoid-associated protein WHIRLY2 is required for a proper response to salt stress. *Plant and Cell Physiology*, *65*, 576–589. https://doi.org/10.1093/pcp/pcae025

Ng, S., Ivanova, A., Duncan, O., Law, S. R., Van Aken, O., De Clercq, I., Wang, Y., Carrie, C., Xu, L., Kmiec, B., Walker, H., Van Breusegem, F., Whelan, J., & Giraud, E. (2013). A membrane-bound NAC transcription factor, ANAC017, mediates mitochondrial retrograde signaling in *Arabidopsis*. *The Plant Cell*, *25*, 3450–71. https://doi.org/10.1105/tpc.113.113985

Nguyen, T. L. (2023). Investigations of *Arabidopsis thaliana* WHIRLY1 function in early seedling development. [Doctoral dissertation, Faculty of Natural Sciences, Martin Luther University Halle-Wittenberg].

Nyiko, T., Kerenyi, F., Szabadkai, L., Benkovics, A. H., Major, P., Sonkoly, B., Merai, Z., Barta, E., Niemiec, E., Kufel, J., & Silhavy, D. (2013). Plant nonsense-mediated mRNA decay is controlled by different autoregulatory circuits and can be induced by an EJC-like complex. *Nucleic Acids Research*, *41*, 6715–28. https://doi.org/10.1093/nar/gkt366

Oetke, S., Scheidig, A. J., & Krupinska, K. (2022). WHIRLY1 of barley and maize share a PRAPP motif conferring nucleoid compaction. *Plant and Cell Physiology*, *63*, 234–247. https://doi.org/10.1093/pcp/pcab164

Orton, E. S., & Brown, J. K. (2016). Reduction of growth and reproduction of the biotrophic fungus *Blumeria graminis* in the presence of a necrotrophic pathogen. *Frontiers in Plant Science*, *7*, 742. https://doi.org/10.3389/fpls.2016.00742

Pfalz, J., Liebers, M., Hirth, M., Grubler, B., Holtzegel, U., Schroter, Y., Dietzel, L., & Pfannschmidt, T. (2012). Environmental control of plant nuclear gene expression by chloroplast redox signals. *Frontiers in Plant Science*, *3*, 257. https://doi.org/10.3389/fpls.2012.00257

Pfalz, J., Liere, K., Kandlbinder, A., Dietz, K.-J., & Oelmüller, R. (2006). pTAC2, -6, and -12 are components of the transcriptionally active plastid chromosome that are required for plastid gene expression. *The Plant Cell*, *18*, 176–197. https://doi.org/10.1105/tpc.105.036392.

Pfannschmidt, T., Terry, M. J., Van Aken, O., & Quiros, P. M. (2020). Retrograde signals from endosymbiotic organelles: A common control principle in eukaryotic cells. *Philosophical Transactions of the Royal Society B: Biological Sciences*, *375*, 20190396. https://doi.org/10.1098/rstb.2019.0396

Pipitone, R., Eicke, S., Pfister, B., Glauser, G., Falconet, D., Uwizeye, C., Pralon, T., Zeeman, S. C., Kessler, F., & Demarsy, E. (2021). A multifaceted analysis reveals two distinct phases of chloroplast biogenesis during de-etiolation in *Arabidopsis*. *eLife*, *10*. https://doi.org/10.7554/eLife.62709

Pogson, B. J., Ganguly, D., & Albrecht-Borth, V. (2015). Insights into chloroplast biogenesis and development. *Biochimica et Biophysica Acta*, *1847*, 1017–24. https://doi.org/10.1016/j.bbabio.2015.02.003

Powikrowska, M., Oetke, S., Jensen, P. E., & Krupinska, K. (2014). Dynamic composition, shaping and organization of plastid nucleoids. *Frontiers in Plant Science*, *5*, 424. https://doi.org/10.3389/fpls.2014.00424

Prikryl, J., Watkins, K. P., Friso, G., van Wijk, K. J., & Barkan, A. (2008). A member of the Whirly family is a multifunctional RNA- and DNA-binding protein that is essential for chloroplast biogenesis. *Nucleic Acids Research*, *36*, 5152–65. https://doi.org/10.1093/nar/gkn492

Qiu, Z., Chen, D., Teng, L., Guan, P., Yu, G., Zhang, P., Song, J., Zeng, Q., & Zhu, L. (2022). OsWHY1 interacts with OsTRX z and is essential for early chloroplast development in rice. *Rice*, *15*, 50. https://doi.org/10.1186/s12284-022-00596-y

Ren, Y., Li, Y., Jiang, Y., Wu, B., & Miao, Y. (2017). Phosphorylation of WHIRLY1 by CIPK14 shifts its localization and dual functions in *Arabidopsis*. *Molecular Plant*, *10*, 749–763. https://doi.org/10.1016/j.molp.2017.03.011

Richardson, L. G. L., & Schnell, D. J. (2020). Origins, function, and regulation of the TOC-TIC general protein import machinery of plastids. *Journal of Experimental Botany*, *71*, 1226–1238. https://doi.org/10.1093/jxb/erz517

Roth-Bejerano, N., Van der Meulen, R. M., & Wang, M. (2008). Inhibition of barley grain germination by light. *Seed Science Research*, *6*, 137–141. https://doi.org/10.1017/s0960258500003159

Saeid Nia, M., Repnik, U., Krupinska, K., & Bilger, W. (2022). The plastid-nucleus localized DNA-binding protein WHIRLY1 is required for acclimation of barley leaves to high light. *Planta*, *255*, 84. https://doi.org/10.1007/s00425-022-03854-x

Sambrook, J., Fritsch, E. F., & Maniatis, T. (1989). *Molecular cloning: A laboratory manual*.

Sato, N. (2001). Was the evolution of plastid genetic machinery discontinuous? *Trends in Plant Science*, *6*, 151–155. https://doi.org/10.1016/S1360-1385(01)01888-X

Schneider, C. A., Rasband, W. S., & Eliceiri, K. W. (2012). NIH Image to ImageJ: 25 years of image analysis. *Nature Methods*, *9*, 671–5. https://doi.org/10.1038/nmeth.2089

Schreiber, M., Mascher, M., Wright, J., Padmarasu, S., Himmelbach, A., Heavens, D., Milne, L., Clavijo, B. J., Stein, N., & Waugh, R. (2020). A genome assembly of the barley 'transformation reference' cultivar Golden Promise. *G3: Genes, Genomes, Genetics*, *10*, 1823–1827. https://doi.org/10.1534/g3.119.401010

Sharma, N., Nagar, S., Thakur, M., Suriyakumar, P., Kataria, S., Shanker, A. K., Landi, M., & Anand, A. (2023). Photosystems under high light stress: Throwing light on mechanism and adaptation. *Photosynthetica*, *61*, 250–263. https://doi.org/10.32615/ps.2023.021

Shi, Y., Ke, X., Yang, X., Liu, Y., & Hou, X. (2022). Plants response to light stress. *Journal of Genetics and Genomics*, *49*, 735–747. https://doi.org/10.1016/j.jgg.2022.04.017

Sievers, F., Wilm, A., Dineen, D., Gibson, T. J., Karplus, K., Li, W., Lopez, R., McWilliam, H., Remmert, M., Söding, J., et al. (2011). Fast, scalable generation of high-quality protein multiple sequence alignments using clustal omega. *Molecular systems biology*, *7*, 539. https://doi.org/10.1038/msb.2011.75

Stern, D. B., Goldschmidt-Clermont, M., & Hanson, M. R. (2010). Chloroplast RNA metabolism. *Annual Review of Plant Biology*, *61*, 125–155. https://doi.org/https://doi.org/10.1146/annurev-arplant-042809-112242

Studies on transformation of *Escherichia coli* with plasmids. (1983). *Journal of Molecular Biology*, *166*, 557–580. https://doi.org/10.1016/S0022-2836(83)80284-8

Sun, K., Wolters, A. M., Vossen, J. H., Rouwet, M. E., Loonen, A. E., Jacobsen, E., Visser, R. G., & Bai, Y. (2016). Silencing of six susceptibility genes results in potato late blight resistance. *Transgenic Research*, *25*, 731–42. https://doi.org/10.1007/s11248-016-9964-2

Sun, X., Singla-Rastogi, M., Wang, J., Zhao, C., Wang, X., & Li, P. (2024). The uS10c-BPG2 module mediates ribosomal RNA processing in chloroplast nucleoids. *Nucleic Acids Research*, *52*, 7893–7909. https://doi.org/10.1093/nar/gkae339

Świda-Barteczka, A., Krieger-Liszkay, A., Bilger, W., Voigt, U., Hensel, G., Szweykowska-Kulinska, Z., & Krupinska, K. (2018). The plastid-nucleus located DNA/RNA binding protein WHIRLY1 regulates microRNA-levels during stress in barley (*Hordeum vulgare* L.) *RNA Biology*, *15*, 886–891. https://doi.org/10.1080/15476286.2018.1481695

Taylor, R. E., West, C. E., & Foyer, C. H. (2022). Whirly protein functions in plants. *Food and Energy Security*, *12*, e379. https://doi.org/10.1002/fes3.379

Tingay, S., McElroy, D., Kalla, R., Fieg, S., Wang, M., Thornton, S., & Brettell, R. (1997). *Agrobacterium tumefaciens*-mediated barley transformation. *The Plant Journal*, *11*, 1369–1376. https://doi.org/10.1046/j.1365-313X.1997.11061369.x

Tuan, P. A., Kumar, R., Rehal, P. K., Toora, P. K., & Ayele, B. T. (2018). Molecular mechanisms underlying abscisic acid/gibberellin balance in the control of seed dormancy and germination in cereals. *Frontiers in Plant Science*, *9*, 668. https://doi.org/10.3389/fpls.2018.00668

Ullah, A., Sadaf, S., Ullah, S., Alshaya, H., Okla, M. K., Alwasel, Y. A., & Tariq, A. (2022). Using halothermal time model to describe barley (*Hordeum vulgare* L.) seed germination response to water potential and temperature. *Life*, *12*. https://doi.org/10.3390/life12020209

Urquidi Camacho, R. A., Lokdarshi, A., & von Arnim, A. G. (2020). Translational gene regulation in plants: A green new deal. *Wiley Interdisciplinary Reviews: RNA*, *11*, e1597. https://doi.org/10.1002/wrna.1597

Velez-Ramirez, A. I., van Ieperen, W., Vreugdenhil, D., van Poppel, P. M., Heuvelink, E., & Millenaar, F. F. (2014). A single locus confers tolerance to continuous light and allows substantial yield increase in tomato. *Nature Communications*, *5*, 4549. ht tps://doi.org/10.1038/ncomms5549

Wang, L., Kim, C., Xu, X., Piskurewicz, U., Dogra, V., Singh, S., Mahler, H., & Apel, K. (2016). Singlet oxygen- and EXECUTER1-mediated signaling is initiated in grana margins and depends on the protease FtsH2. *Proceedings of the National Academy of Sciences*, *113*, E3792–800. https://doi.org/10.1073/pnas.1603562113

Wang, L., Zhao, Z., Li, H., Pei, D., Ma, Q., Huang, Z., Wang, H., & Xiao, L. (2024). Genome-wide identification and molecular evolutionary history of the Whirly family genes in *Brassica napus*. *Plants*, *13*. https://doi.org/10.3390/plants13162243

Wang, Q. L., Chen, J. H., He, N. Y., & Guo, F. Q. (2018). Metabolic reprogramming in chloroplasts under heat stress in plants. *International Journal of Molecular Sciences*, *19*. https://doi.org/10.3390/ijms19030849

Wang, Y., Selinski, J., Mao, C., Zhu, Y., Berkowitz, O., & Whelan, J. (2020). Linking mitochondrial and chloroplast retrograde signalling in plants. *Philosophical Transactions of the Royal Society B: Biological Sciences*, *375*, 20190410. https://doi.org /10.1098/rstb.2019.0410

Waterhouse, A. M., Procter, J. B., Martin, D. M., Clamp, M., & Barton, G. J. (2009). Jalview version 2–a multiple sequence alignment editor and analysis workbench. *Bioinformatics*, *25*, 1189–91. https://doi.org/10.1093/bioinformatics/btp033

Waters, M. T., & Langdale, J. A. (2009). The making of a chloroplast. *The EMBO Journal*, *28*, 2861–73. https://doi.org/10.1038/emboj.2009.264

Woodson, J. D., & Chory, J. (2008). Coordination of gene expression between organellar and nuclear genomes. *Nature Reviews Genetics*, *9*, 383–95. https://doi.org/10.1 038/nrg2348

Woodson, J. D., Perez-Ruiz, J. M., & Chory, J. (2011). Heme synthesis by plastid ferrochelatase i regulates nuclear gene expression in plants. *Current Biology*, *21*, 897–903. https://doi.org/10.1016/j.cub.2011.04.004

Woodson, J. D., Perez-Ruiz, J. M., Schmitz, R. J., Ecker, J. R., & Chory, J. (2013). Sigma factor-mediated plastid retrograde signals control nuclear gene expression. *The Plant Journal*, *73*, 1–13. https://doi.org/10.1111/tpj.12011

Yoo, H. H., Kwon, C., Lee, M. M., & Chung, I. K. (2007). Single-stranded DNA binding factor AtWHY1 modulates telomere length homeostasis in *Arabidopsis*. *The Plant Journal*, *49*, 442–451. https://doi.org/https://doi.org/10.1111/j.1365-313X.2006.02974.x

Yu, Q. B., Huang, C., & Yang, Z. N. (2014). Nuclear-encoded factors associated with the chloroplast transcription machinery of higher plants. *Frontiers in Plant Science*, *5*, 316. https://doi.org/10.3389/fpls.2014.00316

Yu, Y., Wang, C., Zhang, X., Wang, J., Li, M., Song, T., Liang, D., & Feng, G. (2025). The transcription factor TaWHY2-6A acts as a positive regulator in response to drought tolerance in transgenic plants. *Biochemical and Biophysical Research Communications*, *755*, 151580. https://doi.org/10.1016/j.bbrc.2025.151580

Zhang, Y., Tian, L., & Lu, C. (2023). Chloroplast gene expression: Recent advances and perspectives. *Plant Communications*, *4*, 100611. https://doi.org/10.1016/j.xplc.2023.100611

5 Appendix

5.1 Generation and characterisation of *why1*-complemented variants

Table A1. Segregation analysis of the T_1 *why1* lines complemented with altered sequences of the *WHIRLY1* of barley

Variant	Family	Phenotype	Transgene (*hpt*)		Segregation		Binomial exact test	χ2-value	p-value for χ2-test
			presence	absence	observed	expected			
Control	E01	green	7	4	1.75:1	3:1	0.172	0.758	0.384
	E02	green	8	3	2.67:1	3:1	0.258	0.030	0.862
	E05	green	11	0	1	3:1	0.042	3.667	0.056
	E08	green	6	0	1	3:1	0.178	2.000	0.157
	E09	green	7	4	1.75:1	3:1	0.172	0.758	0.384
	E10A	green	7	4	1.75:2	3:2	0.172	0.758	0.384
	E10B	green	6	3	2.67:1	3:1	0.234	0.333	0.564
	E11A	green	6	2	3:1	3:1	0.311	0.000	1.000
	E11B	green	4	3	1.33:1	3:1	0.173	1.190	0.275
	E12B	green	6	4	1.5:1	3:1	0.146	1.200	0.273
	E12C	green	5	1	5:1	3:1	0.356	0.222	0.637
	E12D	green	2	1	2:1	3:1	0.422	0.111	0.739
△PRAPP	E01A	green	7	4	1.75:1	3:1	0.172	0.758	0.384
	E02	green	5	2	2.25:1	3:1	0.311	0.048	0.827
	E04A	green	9	1	9:1	3:1	0.188	1.200	0.273
	E05A	green	10	1	10:1	3:1	0.155	1.485	0.223
	E06A	green	10	1	10:1	3:1	0.155	1.485	0.223
	E07A	green	10	1	10:1	3:1	0.155	1.485	0.223
	E03	green	6	4	1.5:1	3:1	0.146	1.200	0.273
	E04	green	6	3	2:1	3:1	0.234	0.333	0.564
	E01	green	2	2	1:1	3:1	0.211	1.333	0.248
	E03A	green	6	4	1.5:1	3:1	0.146	1.200	0.273
	E02	green	9	2	4.5:1	3:1	0.258	0.273	0.602
	E04	green	7	4	1.75:1	3:1	0.172	0.758	0.384
	E05	green	4	1	4:1	3:1	0.396	0.067	0.796
	E06	green	11	0	1	3:1	0.042[a]	3.667	0.056
△PTP	E01	white	1	6	1:6	3:1	0.001	13.762	0.000
	E03	white	7	1	7:1	3:1	0.267	0.667	0.414
	E07	white	7	3	2.33:1	3:1	0.250	0.133	0.715
	E08	white	10	1	10:1	3:1	0.155	1.485	0.223
	E02	white	10	1	10:1	3:1	0.155	1.485	0.223
	E03	white	7	4	1.75:1	3:1	0.172	0.758	0.384
	E03	white	6	4	1.5:1	3:1	0.146	1.200	0.273

Continued on next page

Table continued from previous page

Variant	Family	Phenotype	Transgene (*hpt*)		Segregation		Binomial exact test	χ2-value	p-value for χ2-test
			presence	absence	observed	expected			
ΔPTP	E07	white	10	0	1	3:1	0.056	3.333	0.068
	E08	white	9	2	4.5:2	3:1	0.258	0.273	0.602
	E09	white	7	4	1.75:1	3:1	0.172	0.758	0.384
	E10	white	11	0	1	3:1	0.042	3.667	0.056
	E11	white	6	5	1.2:1	3:1	0.080	2.455	0.117
	E13	white	7	4	1.75:1	3:1	0.172	0.758	0.384
	E18	white	7	4	1.75:1	3:1	0.172	0.758	0.384
C165A	E01B	green	8	3	2.67:1	3:1	0.258	0.030	0.862
	E05B	green	8	2	4:1	3:1	0.282	0.133	0.715
	E06C	green	9	0	1	3:1	0.075	3.000	0.083
	E09C	green	11	1	11:1	3:1	0.127	1.778	0.182
	E13B	green	7	3	2.33:1	3:1	0.250	0.133	0.715
	E14B	green	9	3	3:1	3:1	0.258	0.000	1.000
	E15B	green	10	2	5:1	3:1	0.232	0.444	0.505
	E16C	green	9	2	4.5:1	3:1	0.258	0.273	0.602
	E18B	green	9	2	4.5:1	3:1	0.258	0.273	0.602
	E19A	green	6	6	1:1	3:1	0.040	4.000	0.046
	E21	green	8	3	2.67:1	3:1	0.258	0.030	0.862
K97A	E01	green	7	3	2.33:1	3:1	0.250	0.133	0.715
	E02	green	7	5	1.4:1	3:1	0.103	1.778	0.182
	E05	green	5	4	1.25:1	3:1	0.117	1.815	0.178
	E07	green	7	2	3.5:1	3:1	0.300	0.037	0.847
	E09	green	6	4	1.5:1	3:1	0.146	1.200	0.273
	E10	green	7	2	3.5:1	3:1	0.300	0.037	0.847
	E11	green	8	2	4:1	3:1	0.282	0.133	0.715
	E14	green	6	5	1.2:1	3:1	0.080	2.455	0.117
	E17G	green	9	2	4.5:1	3:1	0.258	0.273	0.602
	E18A	green	6	3	2:1	3:1	0.234	0.333	0.564
	E21A	green	10	1	10:1	3:1	0.155	1.485	0.223
	E27A	green	8	2	4:1	3:1	0.282	0.133	0.715
ΔCBM	E16A	white	2	3	1:1.5	3:1	0.088	3.267	0.071
	E16D	white	5	6	1:1.2	3:1	0.027	5.121	0.024
	E30A	white	5	5	1:1	3:1	0.058	3.333	0.068
K97AΔCBM	E24C	white	1	11	1:11	3:1	0.000	28.444	0.000
	E34A	white	4	3	1.33:1	3:1	0.173	1.190	0.275
	E34B	white	7	5	1.4:1	3:1	0.103	1.778	0.182

[a]In red are shown values statistically different from the 3:1 segregation ratio.

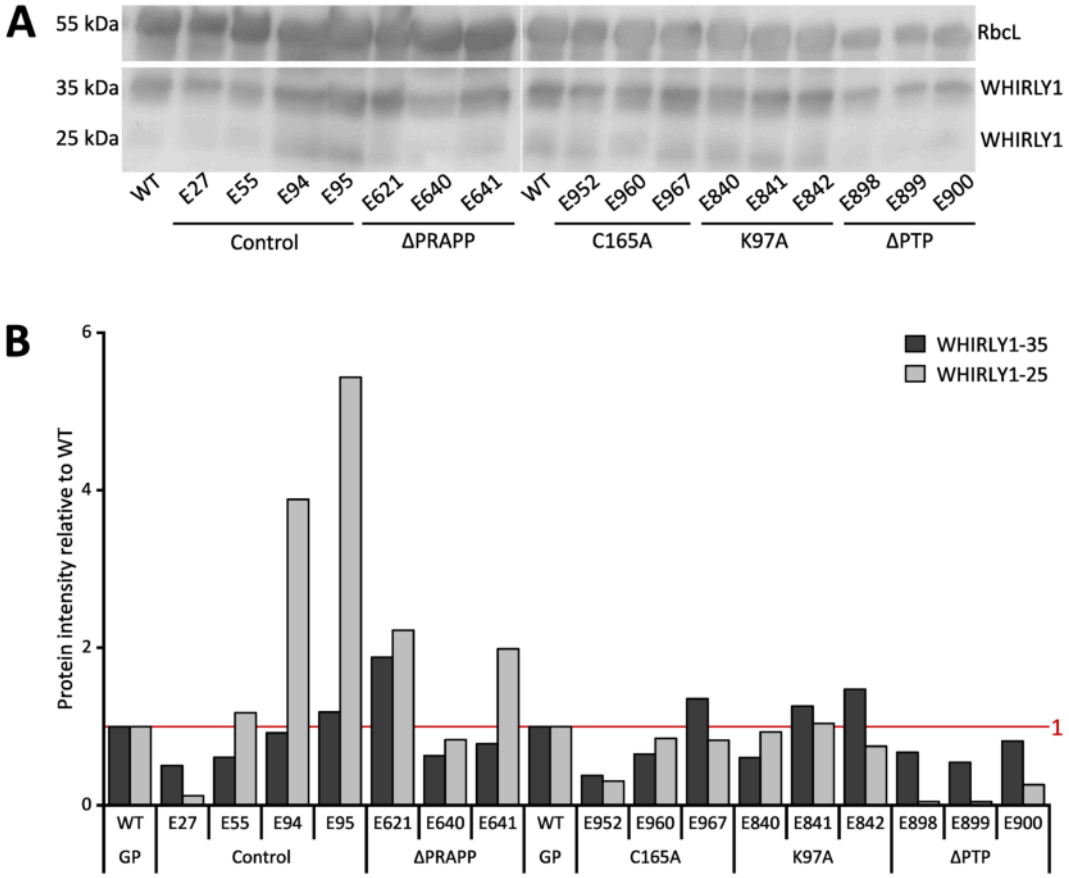

Figure A1. WHIRLY1 protein quantification in *why1*-complemented variants. **(A)** Western blot analysis showing WHIRLY1 protein levels. **(B)** Quantification of WHIRLY1 signal intensities in the *why1*-complemented variants relative to the corresponding wild type. The samples were run on two independent gels. Therefore, both wild-type controls are displayed in the gel image and in the graph. Raw band volumes obtained with GelAnalyzer 23 were first normalized to the respective rbcL loading control, followed by normalization to the WHIRLY1 level of the wild type on each gel. The red line indicates the normalized wild-type reference value. GP, cultivar Golden Promise; WT, wild type; E27 to E900, families of the five respective *why1*-complemented variants.

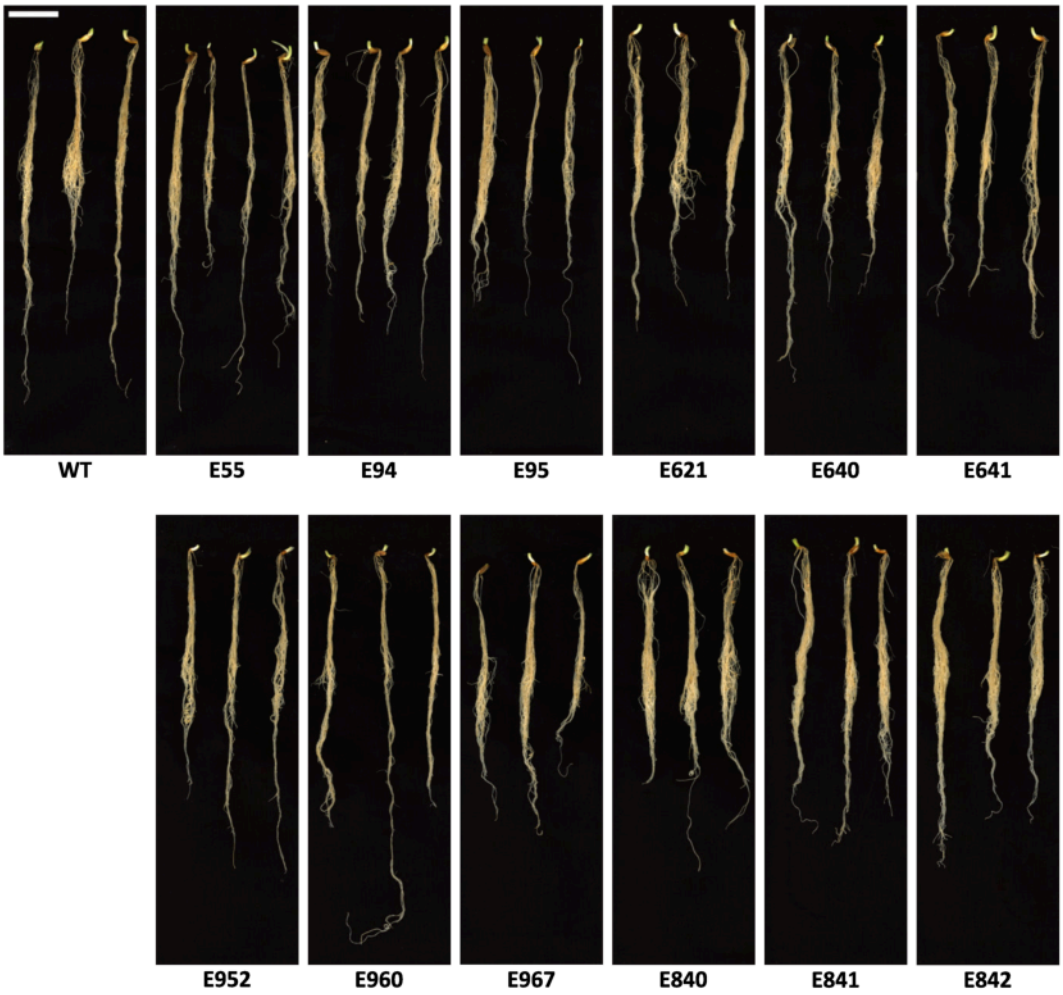

Figure A2. Root images of barley seedlings 14 DAS grown under normal conditions. Upper panel, control and ΔPRAPP variant; lower panel, C165A variant and K97A variant; WT, wild type. Scale bar = 1 cm.

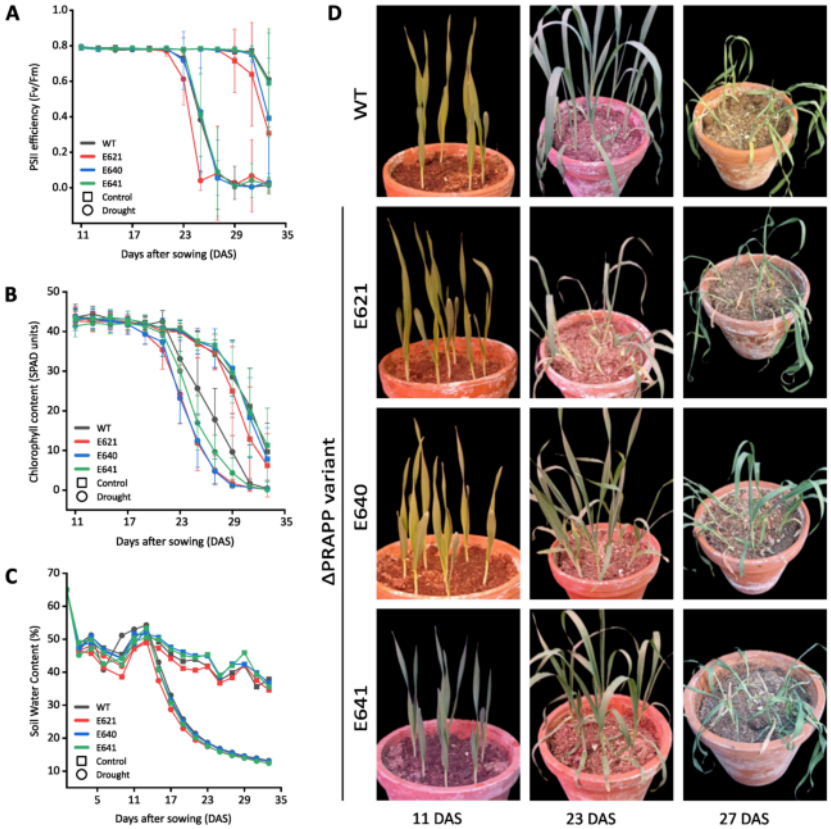

Figure A3. Response of the ΔPRAPP variant to drought. Three independent homozygous families (E621, E640, and E641) were grown under drought and well-watered (control) conditions. **(A)** Maximum quantum efficiency of PSII (F_V/F_M), **(B)** chlorophyll content, and **(C)** soil water content were monitored over time and are shown as mean values ± standard deviation. **(D)** Representative plants grown under drought conditions are shown at three defined time points: 11 DAS, corresponding to the last day of watering; 23 DAS, corresponding to the onset of the decline in PSII efficiency in all plants; and 27 DAS, when PSII efficiency approached zero and remained unchanged thereafter. The experiment was repeated twice, using 3–7 plants per family in each repetition. Occasional instances with only three plants resulted from reduced seedling numbers due to germination failure.

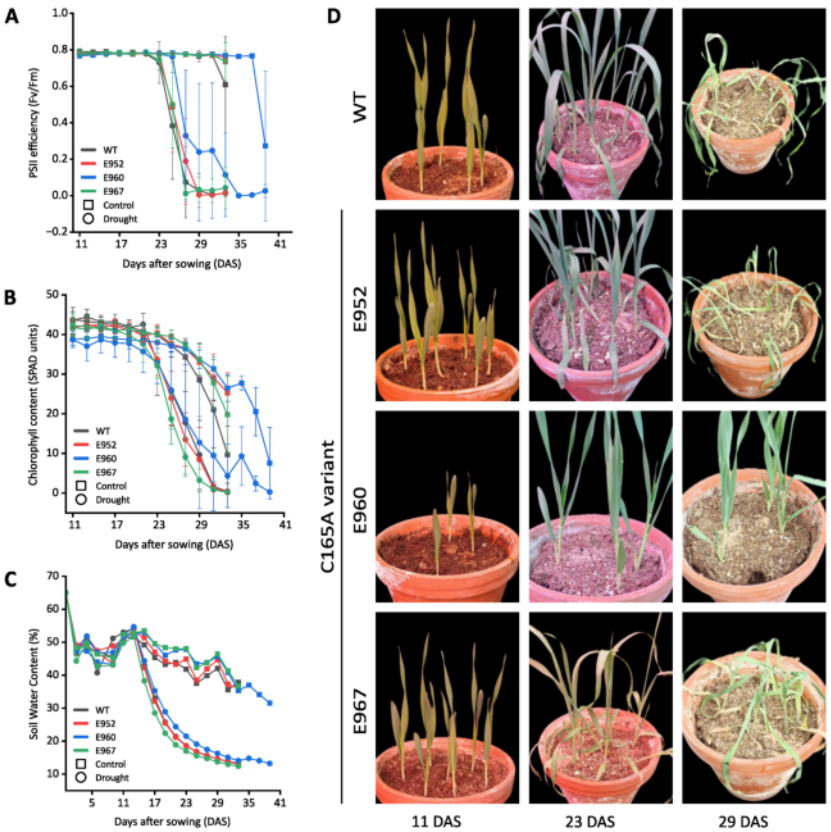

Figure A4. Response of the C165A variant to drought. Three independent homozygous families (E952, E960, and E967) were grown under drought and well-watered (control) conditions. **(A)** Maximum quantum efficiency of PSII (F_V/F_M), **(B)** chlorophyll content, and **(C)** soil water content were monitored over time and are shown as mean values ± standard deviation. **(D)** Representative plants grown under drought conditions are shown at three defined time points: 11 DAS, corresponding to the last day of watering; 23 DAS, corresponding to the onset of the decline in PSII efficiency in all plants; and 29 DAS, when PSII efficiency approached zero and remained unchanged thereafter. The experiment was repeated twice, using 3–7 plants per family in each repetition. Occasional instances with only three plants resulted from reduced seedling numbers due to germination failure.

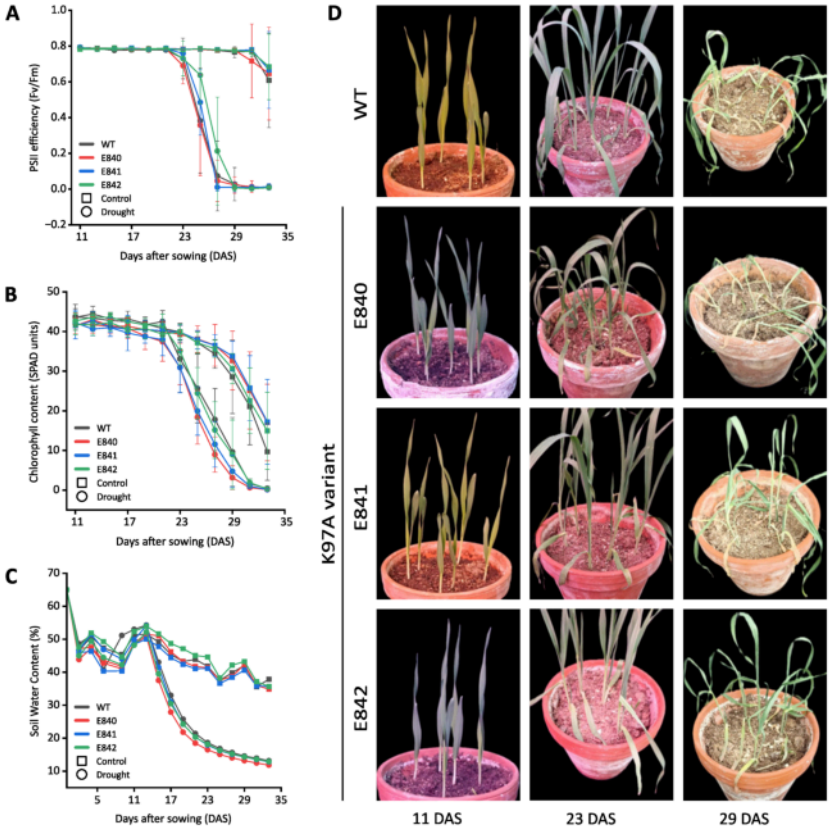

Figure A5. Response of the K97A variant to drought. Three independent homozygous families (E840, E841, and E842) were grown under drought and well-watered (control) conditions. **(A)** Maximum quantum efficiency of PSII (F_V/F_M), **(B)** chlorophyll content, and **(C)** soil water content were monitored over time and are shown as mean values ± standard deviation. **(D)** Representative plants grown under drought conditions are shown at three defined time points: 11 DAS, corresponding to the last day of watering; 23 DAS, corresponding to the onset of the decline in PSII efficiency in all plants; and 29 DAS, when PSII efficiency approached zero and remained unchanged thereafter. The experiment was repeated twice, using 3–7 plants per family in each repetition. Occasional instances with only three plants resulted from reduced seedling numbers due to germination failure.

Table A2. Pairwise comparisons of primary leaf length between genotypes

Genotype 1	Genotype 2	Welch's ANOVA + Games-Howell p-value	Kruskal-Wallis + Dunn's p-value
GP	E27	**0.0064**[a]	**0.0019**
GP	E55	0.1885	0.5621
GP	E95	**0.0345**	0.0940
GP	E621	0.7147	1.0000
GP	E640	0.9496	1.0000
GP	E641	0.4471	1.0000
GP	E952	0.7792	1.0000
GP	E960	1.0000	1.0000
GP	E967	0.4886	1.0000
GP	E840	0.5213	1.0000
GP	E841	0.7794	1.0000
GP	E842	0.5776	1.0000
E27	E55	0.7714	1.0000
E27	E95	0.9044	1.0000
E27	E621	0.6021	1.0000
E27	E640	0.1460	0.3922
E27	E641	0.2474	1.0000
E27	E952	0.5297	1.0000
E27	E960	**0.0113**	**0.0497**
E27	E967	0.7829	1.0000
E27	E840	0.6880	1.0000
E27	E841	0.2499	0.9371
E27	E842	0.3071	1.0000
E55	E95	1.0000	1.0000
E55	E621	1.0000	1.0000
E55	E640	0.9723	1.0000
E55	E641	0.9992	1.0000
E55	E952	1.0000	1.0000
E55	E960	0.2851	1.0000
E55	E967	1.0000	1.0000
E55	E840	1.0000	1.0000
E55	E841	0.9978	1.0000
E55	E842	0.9997	1.0000
E95	E621	0.9993	1.0000
E95	E640	0.7893	1.0000
E95	E641	0.9535	1.0000
E95	E952	0.9970	1.0000
E95	E960	0.0810	0.8649
E95	E967	1.0000	1.0000
E95	E840	0.9999	1.0000
E95	E841	0.9414	1.0000

Continued on next page

Table continued from previous page

Genotype 1	Genotype 2	Welch's ANOVA + Games-Howell p-value	Kruskal-Wallis + Dunn's p-value
E95	E842	0.9749	1.0000
E621	E640	0.9999	1.0000
E621	E641	1.0000	1.0000
E621	E952	1.0000	1.0000
E621	E960	0.7946	1.0000
E621	E967	1.0000	1.0000
E621	E840	1.0000	1.0000
E621	E841	1.0000	1.0000
E621	E842	1.0000	1.0000
E640	E641	1.0000	1.0000
E640	E952	1.0000	1.0000
E640	E960	0.9754	1.0000
E640	E967	0.9965	1.0000
E640	E840	0.9988	1.0000
E640	E841	1.0000	1.0000
E640	E842	1.0000	1.0000
E641	E952	1.0000	1.0000
E641	E960	0.6050	1.0000
E641	E967	1.0000	1.0000
E641	E840	1.0000	1.0000
E641	E841	1.0000	1.0000
E641	E842	1.0000	1.0000
E952	E960	0.8472	1.0000
E952	E967	1.0000	1.0000
E952	E840	1.0000	1.0000
E952	E841	1.0000	1.0000
E952	E842	1.0000	1.0000
E960	E967	0.5805	1.0000
E960	E840	0.6207	1.0000
E960	E841	0.8626	1.0000
E960	E842	0.7039	1.0000
E967	E840	1.0000	1.0000
E967	E841	0.9999	1.0000
E967	E842	1.0000	1.0000
E840	E841	1.0000	1.0000
E840	E842	1.0000	1.0000
E841	E842	1.0000	1.0000

[a]The p-values in bold show the significant differences in primary leaf length between the different genotypes.

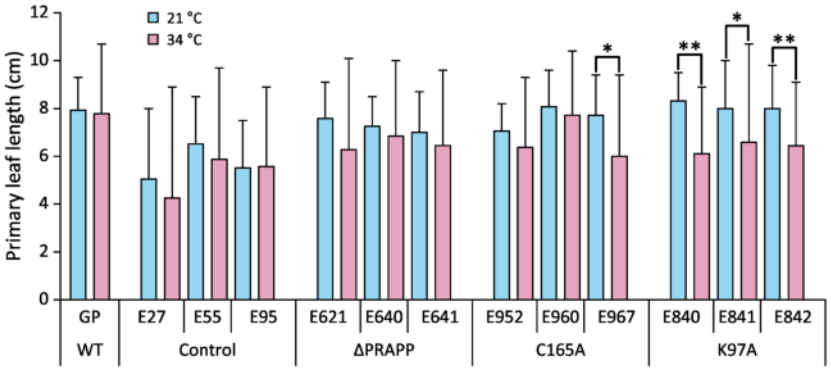

Figure A6. Comparison of the primary leaf lengths of *why1*-complemented plants under normal temperature and light conditions and high temperature and normal continuous light conditions. Statistical analysis was performed using independent two-sample t-test with Welch's correction for unequal variances ($\alpha = 0.05$). Significance levels were indicated as follows: $p \leq 0.05$ (*), $p \leq 0.01$ (**), and $p \leq 0.001$ (***). Data were collected from 12 plants per family per experiment, with two experimental replicates 14 DAS.

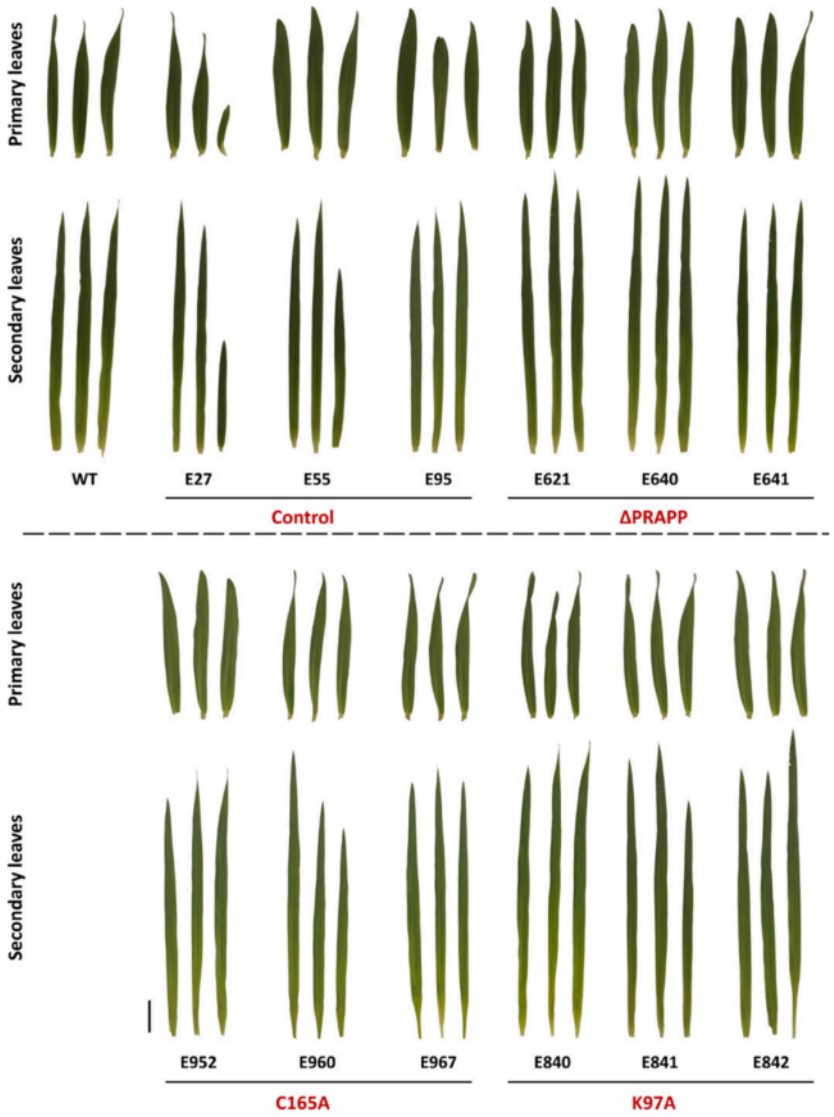

Figure A7. Primary leaf greenness of *why1*-complemented variants under normal light and temperature conditions. Images were taken 14 DAS. Three representative leaves of each of three families of the Control, ΔPRAPP, C165A, and K97A variants are shown, as well as three representative leaves of the wild-type plants (WT). Data were collected from 12 plants per family per experiment, with two experimental replicates. Scale bar = 2 cm.

5.2 Generation of *why2* mutants

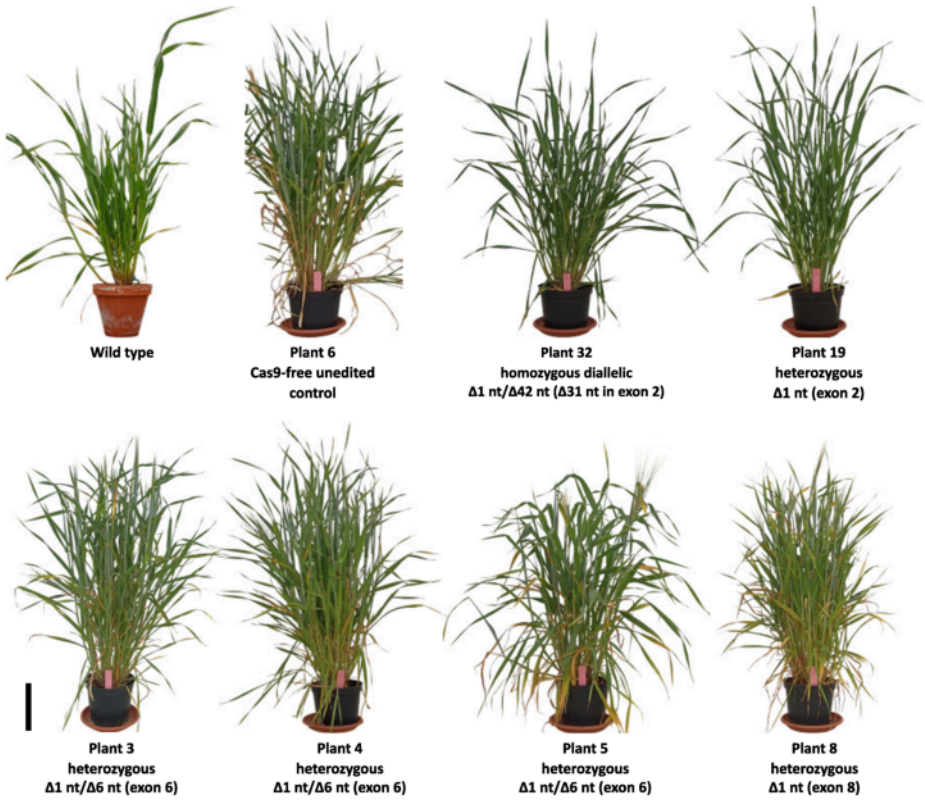

Figure A8. Representative M_0 *why2* mutant heterozygous and homozygous diallelic plants showing normal greenness under standard growth conditions. The wild-type plant is 2 months old; all other plants are 3 months old. Scale bar = 15 cm.

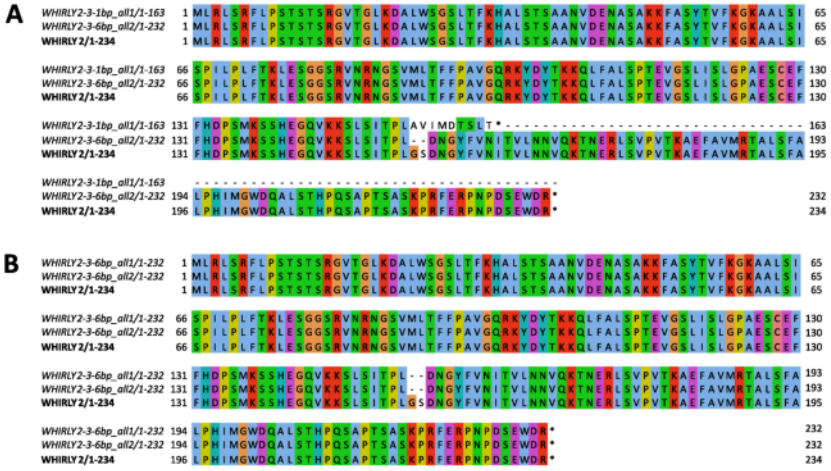

Figure A9. Predicted protein alignments for *why2* mutant homozygous and heterozygous biallelic plants. **(A)** A homozygous biallelic *why2* mutant plant, with one allele carrying a single-nucleotide deletion resulting in a nonsense mutation, and the other allele carrying an in-frame six-nucleotide deletion in exon 6. **(B)** A homozygous *why2* mutant plant with an in-frame six-nucleotide deletion in exon 6 of the *WHIRLY2* gene. In bold is shown the wild-type sequence of WHIRLY1. Protein alignments were generated using Clustal Omega (Sievers et al., 2011) and visualized with Jalview 2.11.4.1. Amino acid colouring follows the Clustal scheme.

Table A3. Off-target analysis for the guide sequences targeting *WHIRLY2*

	Sequence + PAM	Genomic position	Strand
gRNA 1	CTCAAAGATGCTCTCTGGAGCGG	CABVVH010000006.1:72676956-72676978	+
off-target 1	CTCAAAAACTCTTTCTGGAGAGG	CABVVH010000002.1:239643494-239643516	+
off-target 2	GACAAAGGCGCTCTCTGGAGTGG	CABVVH010000001.1:152052735-152052757	–
off-target 3	CTCAAGAATGATCTCAGGAGTGG	CABVVH010000005.1:530961790-530961812	–
off-target 4	CTCAAAAGTTCTTTCTGGAGAGG	CABVVH010000001.1:383598877-383598899	–
off-target 5	AACAAAGATGCGCTCAGGAGTGG	CABVVH010000004.1:347945218-347945240	–
off-target 6	GTCAAAGACGCACTCTGGTGTGG	CABVVH010000003.1:452663099-452663121	+
off-target 7	TTTAAAGATGATTTCTGGAGTGG	CABVVH010000004.1:226723820-226723842	+
off-target 8	CTCAAAAGTGCTTTCTGGATAGG	CABVVH010000006.1:132581421-132581443	–
off-target 9	TTGAAAAATGCTTTCTGGAGCGG	CABVVH010000006.1:728456-728478	+
off-target 10	TTCAGTGATGCTCACTGGAGTGG	CABVVH010000002.1:558868374-558868396	+
gRNA 2	TCTTCCCGGCAGTTGGACAAAGG	CABVVH010000006.1:72676630-72676652	+
off-target 1	ACTTCTCGGCAGATGAACAACGG	CABVVH010000006.1:5956165-5956187	+
off-target 2	TTTTCCCGACAGCTAGACAAAGG	CABVVH010000003.1:187625674-187625696	+
off-target 3	TCTTGCAGGCAATTGGACAGCGG	CABVVH010000001.1:400850443-400850465	–
off-target 4	TCTTCTTGGCAGTAGGACGAGGG	CABVVH010000004.1:216392394-216392416	+
off-target 5	TCTGCCTGGCAGTTGGACTTGGG	CABVVH010000001.1:318249063-318249085	–
off-target 6	TCTGCTAGGCAGTTGGACGAAGG	CABVVH010000002.1:442150044-442150066	–
off-target 7	TCTGCCTGGCCGTTGGACAGGGG	CABVVH010000006.1:368782959-368782981	+
off-target 8	TCTTCTTGGCAGTTGGAAGAGGG	CABVVH010000004.1:230543192-230543214	–
off-target 9	TCTTCCTGGCCGTTGGACTGGGG	CABVVH010000004.1:491969658-491969680	+
off-target 10	TCGGCGCGGCAGCTGGACAAGGG	CABVVH010000004.1:31160504-31160526	+
gRNA 3	TATCCATTATCACTGCCAAGAGG	CABVVH010000006.1:72675762-72675784	–
off-target 1	TCTACATTTTCACTGCCAAACGG	CABVVH010000003.1:521438231-521438253	+
off-target 2	TAGCCACTATCATTGACAAGTGG	CABVVH010000003.1:255018421-255018443	+
off-target 3	TAGCCACTATCATTGACAAGTGG	CABVVH010000004.1:161471638-161471660	+
off-target 4	TCTCGATTATCACTGCAAAATGG	CABVVH010000007.1:207052292-207052314	+
off-target 5	TCTCGATTATCACTGCAAAATGG	CABVVH010000007.1:207045041-207045063	+
off-target 6	TAGCCATCATCAATGACAAGTGG	CABVVH010000004.1:228991749-228991771	–
off-target 7	GATCCAATTTCACTGCCAGGAGG	CABVVH010000006.1:370050126-370050148	–
off-target 8	TCTACATTATCAATGCCAATTGG	CABVVH010000001.1:410520065-410520087	–
off-target 9	TTTTCATTATGACTACCAAGAGG	CABVVH010000007.1:382990500-382990522	+
off-target 10	TATCCAATATGACAGACAAGTGG	CABVVH010000003.1:314280923-314280945	–
gRNA 4	GCACATCATGGGCTGGGACCAGG	CABVVH010000006.1:72673916-72673938	+
off-target 1	GAACATTAAGGACTGGGACCAGG	CABVVH010000002.1:133431433-133431455	+
off-target 2	GCTCACCATGGGCAGAGACCAGG	CABVVH010000004.1:190790228-190790250	+
off-target 3	TCTCGTCATGGGCTGGGATCCGG	CABVVH010000001.1:183953243-183953265	–
off-target 4	GCTCATCATGAGCAGGGACAGGG	CABVVH010000003.1:565847126-565847148	+
off-target 5	CCACATCATAGGCTGACACCCGG	CABVVH010000007.1:14037485-14037507	+
off-target 6	GCACATCAATGGCTGGGGCAAGG	CABVVH010000003.1:6442544-6442566	+
off-target 7	GTACGTCATGTCCTGGGACCTGG	CABVVH010000005.1:409246783-409246805	–

Continued on next page

Table continued from previous page

	Sequence + PAM	Genomic position	Strand
off-target 8	ACACATCATGCGCAGGGACACGG	CABVVH010000004.1:304962709-304962731	–
off-target 9	CCACATCATGCAATGGGACCTGG	CABVVH010000004.1:254501711-254501733	+
off-target 10	GCACGTCATGTGTTGGGATCTGG	CABVVH010000005.1:316920857-316920879	+

[a]The first 10 off-targets predicted by CRISPOR (Haeussler et al., 2016; Concordet & Haeussler, 2018) are shown for each guide. The PAM sequence is shown in bold. The seed region is underlined. The mismatches are shown in red.

Table A4. Sequencing analysis of the potential *why2* knockout T_0 regenerants

T_0 plant nr.	Cas9	gRNA 1	gRNA 2	gRNA 3	gRNA 4
1	y	n	n	n	n
2	y	n	n	n	n
3[a]	n	n	n	y	n
4	y	n	n	y	n
5	y	n	n	y	n
6	n	n	n	n	n
7	n	n	n	n	n
8	y	n	n	n	y
9	y	n	n	n	n
10	n	n	n	n	n
11	n	n	n	n	n
12	n	n	n	n	n
13	y	n	n	n	n
14	y	n	n	n	y
15	y	n	n	n	n
16	y	n	n	n	n
17	y	n	n	n	n
18	y	n	n	n	n
19	y	y	n	n	n
20	n	n	n	n	n
21	y	n	n	y	y
22	y	n	n	n	n
23	y	n	n	n	n
24	y	n	n	n	n
25	n	n	n	n	n
26	y	n	n	n	n
27	y	n	n	n	n
28	y	n	n	n	n
29	y	n	n	n	y
30	y	n	n	n	n
31	y	n	n	n	n
32	y	y	n	n	n
33	n	n	n	n	n
34	n	n	n	n	n
35	n	n	n	n	n
36	y	n	n	y	n
37			did not survive		
38	y	n	n	y	n
39	n	n	n	n	n
40	y	n	n	y	n
41	y	n	n	n	n

Continued on next page

Table continued from previous page

T_0 plant nr.	Cas9	gRNA 1	gRNA 2	gRNA 3	gRNA 4
42	n	n	n	n	n
43	y	n	n	n	n
44	n	n	n	n	n
45	y	n	n	n	n
46	n	n	n	n	n
47	y	n	n	n	n
48	n	n	n	n	n
49	n	n	n	n	n
50	n	n	n	n	n
51	n	n	n	n	n
52	n	n	n	n	n

[a]Plants carrying indels are shown in bold.

Table A5. Sequencing analysis of T_1 plants deriving from M_0 heterozygous *why2* mutants

M_0 parent plant - gRNA	Plant nr.[a]	Cas9[b]	gRNA 1	gRNA 2	gRNA 3	gRNA 4
19-1	53	n	n	n	n	n
	54	nd	nd	nd	nd	nd
	55	n	y	n	n	n
	56	n	y	n	n	n
	57	n	y	n	n	n
	58	nd	nd	nd	nd	nd
	59	nd	nd	nd	nd	nd
	60	n	y	n	n	n
	61	n	y	n	n	n
	62	nd	nd	nd	nd	nd
	63	nd	nd	nd	nd	nd
	64	nd	nd	nd	nd	nd
	65	y	not sequenced			
	66	no germination				
	67	nd	nd	nd	nd	nd
	68	y	not sequenced			
	69	nd	nd	nd	nd	nd
	70	n	y	n	n	n
	71	nd	nd	nd	nd	nd
	72	n	y	n	n	n
	73	nd	nd	nd	nd	nd
	74	n	y	n	n	n
	75	no germination				
	76	y	not sequenced			
32-1	77	n	n	n	n	n
	78	n	n	n	n	n
	79	y	not sequenced			
	80	n	n	n	n	n
	81	nd	nd	nd	nd	nd
	82	nd	nd	nd	nd	nd
	83	nd	nd	nd	nd	nd
	84	no germination				
	85	n	n	n	n	n
	86	y	not sequenced			
	87	nd	nd	nd	nd	nd
	88	y	not sequenced			
	89	nd	nd	nd	nd	nd
	90	nd	nd	nd	nd	nd
	91	n	n	n	n	n
	92	n	n	n	n	n
	93	n	n	n	n	n

Continued on next page

Table continued from previous page

M_0 parent plant - gRNA	Plant nr.	Cas9	gRNA 1	gRNA 2	gRNA 3	gRNA 4
32-1	94	y	not sequenced			
	95	y	not sequenced			
	96	n	n	n	n	n
	97	nd	nd	nd	nd	nd
	98	nd	nd	nd	nd	nd
	99	nd	nd	nd	nd	nd
	100	n	y	n	n	n
5-3	101	nd	nd	nd	nd	nd
	102	y	not sequenced			
	103	no germination				
	104	no germination				
	105	no germination				
	106	y	not sequenced			
	107	y	not sequenced			
	108	y	not sequenced			
	109	y	not sequenced			
	110	nd	nd	nd	nd	nd
	111	y	not sequenced			
	112	nd	nd	nd	nd	nd
	113	y	not sequenced			
	114	y	not sequenced			
	115	y	not sequenced			
	116	n	n	n	n	n
	117	n	n	n	n	n
	118	y	not sequenced			
	119	y	not sequenced			
	120	y	not sequenced			
	121	y	not sequenced			
	122	y	not sequenced			
	123	y	not sequenced			
	124	no germination				
21-3+4	125	no germination				
	126	nd	nd	nd	nd	nd
	127	y	not sequenced			
	128	y	not sequenced			
	129	y	not sequenced			
	130	y	not sequenced			
	131	n	n	n	y	y
	132	no germination				
	133	no germination				
	134	n	n	n	y	y

Continued on next page

Table continued from previous page

M_0 parent plant - gRNA	Plant nr.	Cas9	gRNA 1	gRNA 2	gRNA 3	gRNA 4
21-3+4	135	no germination				
	136	no germination				
	137	no germination				
	138	n	n	n	y	y
	139	y	not sequenced			
	140	n	n	n	n	y
	141	y	not sequenced			
	142	y	not sequenced			
	143	y	not sequenced			
	144	y	not sequenced			
	145	y	not sequenced			
	146	no germination				
	147	n	n	n	n	y
	148	n	n	y	y	y
38-3	149	y	not sequenced			
	150	n	n	n	n	n
	151	y	not sequenced			
	152	y	not sequenced			
	153	n	n	n	n	n
	154	y	not sequenced			
	155	y	not sequenced			
	156	no germination				
	157	no germination				
	158	y	not sequenced			
	159	no germination				
	160	n	n	n	n	n
	161	n	n	n	y	n
	162	nd	nd	nd	nd	nd
	163	n	n	n	n	n
	164	n	n	n	n	n
	165	n	n	n	n	n
	166	y	not sequenced			
	167	no germination				
	168	no germination				
	169	no germination				
	170	nd	nd	nd	nd	nd
	171	y	not sequenced			
	172	no germination				
40-3	196	y	not sequenced			
	197	y	not sequenced			
	199	y	not sequenced			

Continued on next page

Table continued from previous page

M_0 parent plant - gRNA	Plant nr.	Cas9	gRNA 1	gRNA 2	gRNA 3	gRNA 4
	201	y	not sequenced			
	202	y	not sequenced			
	204	y	not sequenced			
	205	n	n	n	n	n
40-3	206	n	n	n	n	n
	209	y	not sequenced			
	210	y	not sequenced			
	211	n	n	n	n	n
	212	n	n	n	n	n
	215	y	not sequenced			
	216	y	not sequenced			
	217	y	not sequenced			
	218	y	not sequenced			
	219	y	not sequenced			
	220	y	not sequenced			
	221	n	n	n	n	n
	222	n	n	n	y	n
	223	y	not sequenced			
	224	n	y	y	y	y
	225	y	not sequenced			
5-3	**227**	n	n	n	y	n
	228	n	n	n	y	n
	230	y	not sequenced			
	232	y	not sequenced			
	233	y	not sequenced			
	235	n	n	y	y	n
	236	y	not sequenced			
	237	n	n	n	y	n
	238	n	n	n	y	n
	240	n	n	n	y	n
	242	y	not sequenced			
	243	y	not sequenced			
	247	n	n	n	n	n
	249	n	n	n	n	n
	250	n	n	n	n	n
	251	n	n	n	n	n
3-3	253	n	n	n	n	n
	254	n	n	n	n	n
	257	n	n	n	n	n
	259	n	n	n	n	n
	260	n	n	n	n	n

Continued on next page

Table continued from previous page

M_0 parent plant - gRNA	Plant nr.	Cas9	gRNA 1	gRNA 2	gRNA 3	gRNA 4
3-3	261	n	n	n	n	n
	264	n	n	n	n	n
	265	n	n	n	n	n
	267	n	n	n	n	n

[a]Plants carrying indels are shown in bold.
[b]Plants still carrying the Cas9 cassette were not sequenced.

List of Figures

List of Tables

Acknowledgments

This work was possible with the support of many people who I am happy to acknowledge.

First, I want to thank my two supervisors, Dr. Götz Hensel and Prof. Dr. Karin Krupinska, for the role they played in shaping this project. I want to thank Götz for his support, for always keeping the door of his office open whenever I had a question or a doubt, for replying to my emails even on weekends or while travelling, and for the feedback he provided throughout my doctoral research until the very end. I want to thank Karin for her support throughout the duration of my research, for her feedback on this dissertation, for being thorough and tireless even after having retired, and for filling our meetings with laughter. I am in awe of your energy and the love you have for science. I want to thank both of my supervisors, and especially götz, with whom I communicated almost every day, for creating an atmosphere of openness, understanding, and mutual respect. I have learnt a great deal from both of you, and I am most grateful for your work ethic and example.

For generating the *why1*-complemented lines, I want to thank two technicians: Anke Schäfer from the group of Prof. Dr. Krupinska at the Christian Albrecht University of Kiel for cloning the constructs used to transform barley with different WHIRLY1 variants, and Sabine Sommerfeld from the Leibniz Institute of Plant Genetics and Crop Plant Research, IPK, Gatersleben for the *Agrobacterium*-mediated transformation of barley with these constructs.

My thanks also go to Prof. Dr. Andreas P. M. Weber for his invaluable feedback on my research during our TAC and institute meetings, and to appl. Prof. Dr. Jahns for his feedback during our TAC meetings and for allowing me to use his group's resources for the PSII measurements.

I want to thank Dr. Stephanie Bethmann for teaching me how to use the DUAL PAM, how to perform the Western blotting techniques, and for being so generous with her help. I will always cherish our conversations. Danke, Stephi!

I also want to thank Dr. Dimitar Douchkov of the Biotrophy and Immunity group at the Leibniz Institute of Plant Genetics and Crop Plant Research, IPK, Gatersleben, for performing the powdery mildew assay, and Prof. Dr. Holger Gohlke of the Institute for Pharmaceutical and Medicinal Chemistry at Heinrich Heine University Düsseldorf for

the modelling of the two in-frame homozygous *why2* mutants.

Several people made days in the lab and at the institute more enjoyable. I thank my friend Pouneh joon, who was the first to welcome me with open arms and introduce me to the lab. I miss our walks at the Botanical Garden and your joyful dances when you were happy. I thank Hanna Gölmann. Having Bosnian and Albanian coffee with you made me miss home less. Many other colleagues helped along the way, whether by answering a question or showing me how to use a device. I thank you all.

I have a special thank you for the greenhouse gardeners, Anja, Jochen, and Andrea, for the readiness with which they always helped.

My family deserves more thanks than I can put into words. Very little of this would mean anything without you. We do science for people, and you are my most important people. Ju dua shumë.

Finally, I want to thank my first and best friend in Germany, Andrés, for helping me see things more clearly when frustration got in the way. Times were easier because of you.